NRF2 INDUCTION BY CARDIOPLEGIA AND OXIDATIVE STRESS

by

Hongting Diao

A Dissertation Submitted to the Faculty of the

DEPARTMENT OF MEDICAL PHARMACOLOGY

In Partial Fulfillment of the Requirements

For the Degree of

DOCTOR OF PHILOSOPHY

In the Graduate College

THE UNIVERSITY OF ARIZONA

2023

THE UNIVERSITY OF ARIZONA
GRADUATE COLLEGE

As members of the Dissertation Committee, we certify that we have read the dissertation prepared by: Hongting Diao, titled: NRF2 Induction by Cardioplegia and Oxidative Stress and recommend that it be accepted as fulfilling the dissertation requirement for the Degree of Doctor of Philosophy.

[Dr. John Streicher] Date: 5/8/2023

[Dr. Qin Chen] Date: 5/8/2023

[Dr. Raymond Wong] Date: 5/8/2023

[Dr. Nam Lee] Date: 5/8/2023

Final approval and acceptance of this dissertation is contingent upon the candidate's submission of the final copies of the dissertation to the Graduate College.

I hereby certify that I have read this dissertation prepared under my direction and recommend that it be accepted as fulfilling the dissertation requirement.

Date: 5/8/2023

Dr. John Streicher
Dissertation Committee Chair
Department of Pharmacology

ACKNOWLEDGEMENTS

First and foremost I would like to acknowledge my advisor, Dr. Qin Chen. She has been a source of constant encouragement, guidance, and support. I never would have been able to accomplish all that I have without her mentorship and I am very fortunate to have had the opportunity to be a part of her lab. I would also like to acknowledge the contributions of my committee members, Dr. John Streicher, Dr. Nam Lee and Dr. Raymond Wong, for their insight and advice over the years. I am very thankful to have had the opportunity to learn from all of you. In addition, I would like to thank the members of Dr. Chen's lab, Dr. Wujing Dai, Lenee Shrestha and Daniel Wurm, for their contributions and friendship. Finally, I would like to acknowledge my family, especially my mother Yongzhen Wang and my dad Mingzhang Diao, for making me the person I am and putting me in a position to succeed here.

TABLE OF CONTENTS

LIST OF FIGURES 6

LIST OF TABLES 8

ABSTRACT 9

CHAPTER I: INTRODUCTION 10

1.CardioMyocyte Function & Physiology Background 10

2. Cardiovascular Disease (CVD) 14

2.1 Background of CVD 15

2.2 Cardiopulmonary Bypass (CPB) 16

2.3 Cardioplegia: A Short History of Clinical Use 17

3. ROS Production During Open-Heart Surgery 23

3.1. Global Myocardial Ischemic Reperfusion Injury during CPB 23

3.2 Altered Myocardial Metabolism 30

3.3. ROS Production Peri- and Post CPB 31

4. Source of ROS 35

4.1. Biochemical Environment for ROS Generation during Ischemia and Reperfusion 35

4.2. Mitochondria Generation of Superoxide and Hydrogen Peroxide 36

4.3. Xanthine Oxidase (XO) 40

4.4. Nicotinamide Adenine Dinucleotide Phosphate (NADPH) Oxidase (NOX) 42

4.5. Nitric Oxide (NO) 45

5. Nrf2: Master Regulation of Antioxidant Defense 45

5.1. The NRF2 Transcription Factor 45

5.2. Regulation of the KEAP1-NRF2 Pathway by P62/SQATM1 47

5.3. NRF2 Activation via Regulating De Novo NRF2 Protein Translation 48

6. Nrf2 and CPB 49

CHAPTER II: Del NIDO CARDIOPLEGIA OR POTASSIUM IUDUCES NRF2 AND PRPTECTS CARDIOMYOCYTES AGANIST OXIDAITVE STRESS 51

Abstract 51

Introduction 52

Materials and Methods 55

Results 65

Discussion 87

Limitation 91

Chapter III: HYPERKALEMIC OR LOW POTASSIUM CARDIOPLEGIA PROTECTS AGANIST RRDUCTION OF ENERGY METABOLISM BY OXIDATIVE STRESS 92

Abstract 92

Introduction **93**
Material and Methods **95**
Results **99**
Discussion **111**
Limitation **116**
CHAPTER IV: YTH N6-METHYLADENOSINEl RNA BINDING PROTEIN 2 (YTHDF2) PARTICIPATES IN DE NOVO NRF2 PROTEIN TRANSLATION UNDER OXIDATIVE STRESS **117**
Abstract **117**
Introduction **119**
Materials and Methods **123**
Results **131**
Discussion **151**
Limitation **154**
CHAPTER V: SUMMARY STATEMENT **156**
References **160**

LIST OF FIGURES

Figure 1. 1. Typical Ventricular Muscle Cell Action Potential Phases 12

Figure 1. 2. Schematic Diagram..... 14

Figure 1. 3. Cardioplegia History..... 23

Figure 1. 4. Simplified Mechanism of Oxidative Stress..... 26

Figure 1. 5. Mechanisms of Oxidant - Induced NRF2 Activation. 49

Figure 3. 1. Effects of 5 Cardioplegic Solutions on Cellular Metabolism. 101

Figure 3. 2. Metabolites and Metabolic Pathways Altered by HTK and CS. 103

Figure 3. 3. Metabolites and Metabolic Pathways Altered by H2O2 treatment. ... 105

Figure 3. 4. Effect of Cardioplegic Solutions on Metabolites Changed by H_2O_2 Treatment..... 107

Figure 3. 5. HK or LK Protects against H_2O_2 from Inducing Changes in the Metabolites. 109

Figure 3. 6. Effects of Cardioplegic Solutions on Cell Morphology and ROS Generation. 110

Figure 3. 7. Lidocaine Prevents ROS Generation by H_2O_2. 115

Figure 4. 1. H_2O_2 Causes an Increase of YTHD2 in Total Ribosomes. 132

Figure 4. 2. YTHDF2 Distribution in 40/60/80s Ribosome and Polysome Was Enhanced by H_2O_2 Treatment. 134

Figure 4. 3. H_2O_2 Treatment Enhances YTHDF2 Co-localization with Phospho-S6. 135

Figure 4. 4. The Binding Between YTHDF2 and NRF2 5'UTR mRNA Was Increased with H_2O_2 Treatment in A Dose and Time Dependent Manner. 137

Figure 4. 5. YTHD2 Is Required for Nrf2 Protein Induction by H_2O_2. 139

Figure 4. 6. Lack of YTHDF2 Protein Increase in the Cytosol with H_2O_2 Treatment. 140

Figure 4. 7. YTHDF2 Associates with Ribosomes Dependent of RNA Binding. .. 141

Figure 4. 8. Immunoprecipitation of YTHDF2 for Detection of eIFs. 143

Figure 4. 9. H_2O_2 Induces Increase of m^6A in Nrf2 mRNA. 145

Figure 4. 10. METTL3 Is Required for Nrf2 Protein Induction by H_2O_2. 146

Figure 4. 11. METTL3 Binds to Nrf2 5'UTR and Mediates Nrf2 Induction. 148

Figure 4. 12. YTHDF2 Binding Site in Nrf2 5'UTR. 149

LIST OF TABLES

Table 2. 1. Components of Common Cardioplegic Solutions. 66

Table 3. 1. Key Components of Common Cardioplegic Solutions. 99

ABSTRACT

Open heart surgery is often an unavoidable procedure for treatment of cardiovascular disease. Myocardial Ischemia-Reperfusion Injury [1] can occur as a result of cardiopulmonary bypass (CPB), one type of open heart surgery. The multifaceted mechanisms of MIRI involve alteration in metabolism, generation of pro-inflammatory mediators and increases of reactive oxygen species (ROS), ultimately impacting postoperative cardiac performance and complications. Nf-E2 related factor-2 (NRF2), one of the most important regulators for antioxidant response, binds to and activates the Antioxidant Response Element (ARE) in the promoters of many antioxidant and detoxification genes. We addressed whether or not cardioplegic solutions induce the activation of NRF2, therefore serving to protect the myocardium from MIRI. In addition, we also investigated whether cardioplegic solutions affect the baseline cellular metabolism and prevent metabolic reprogramming by oxidative stress. Mechanisms of NRF2 activation involve protein stabilization due to dissociation from KEAP1 or *de novo* protein translation. When severe stress occurs, Nrf2, as a safeguard against MIRI during CPB, can be translated under a stress condition. We have observed that the 5' untranslated region (5'UTR) of Nrf2 mRNA enhances its binding with several RNA binding proteins under oxidative stress. We have discovered YTHD2, a YTH domain containing N(6) methyladenosine (m6A) binding protein, increased its association with Nrf2 mRNA and ribosome promoting translation initiation of Nrf2 protein under oxidative stress.

CHAPTER I: INTRODUCTION

1.CardioMyocyte Function & Physiology Background

Cardiomyocytes, which are the contractile muscle cells, are responsible for pumping the blood throughout the systemic circulation and are contractile unit in the myocardium. In a fully developed heart, cardiomyocytes are densely packed together, shaped like rods with branches, and connect with one another to form elongated fibers featuring gap junctions. These gap junctions are specialized areas of the cell membrane that facilitate direct communication between adjacent cells. Cardiomyocytes exhibit a striped or striated appearance histologically, which is due to their content of myofibrils and concatenated sarcomeres. These structures facilitate the contractile function of the cardiomyocytes.

The sarcoplasmic reticulum, which is responsible for storing and transporting Ca^{2+}, forms an envelop for the myofibrils, while the sarcolemma, also known as the myolemma, contains the cell membrane, which extends inaward in a periodic fashion to form deep invaginations called t-tubules.

The initiation of actin-myosin cross-bridge cycling and subsequent cellular contraction requires an essential component, Ca^{2+}. When Ca^{2+} is present, tropomyosin binds to troponin, which is composed of three subunits: troponin C (TnC), troponin T (TnT),

and troponin I [2]. TnC subunit has a specifical binding site for Ca^{2+}, which allows it to detect the increase in cytoplasmic Ca2+ levels during an action potential. The binding of Ca^{2+} to TnC induces conformational changes in the protein, which results in the pulling away of tropomyosin. This reveals the myosin binding-sites on actin, thus allowing cross bridge cycling to occur when ATP is available. In the absence of Ca^{2+}, the myosin binding sites on actin in thin filaments are covered by tropomyosin such that they are inaccessible to myosin.

Ventricular myocytes are crucial for the pumping of blood throughout systemic and pulmonary circulation. The various phases of a typical ventricular muscle cell action potential and the need for synchronicity as well as the energetic demands are illustrated as below (Figure 1.1). The opening or closing of ion channels, which is crucial for the function of the heart, is a coordinated and sequential process. These changes are triggered by the primary pacemaker cells in the sinoatrial node (SA) and propagated throughout the myocardium via gap junction.

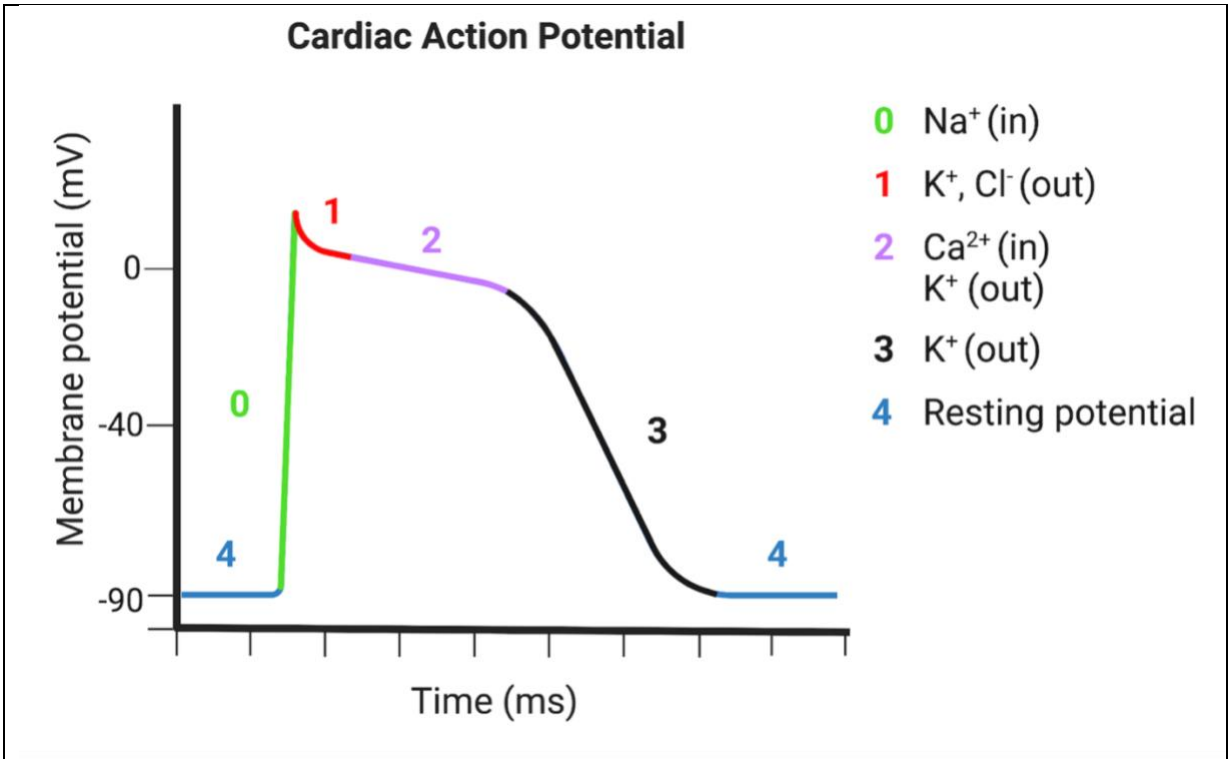

Figure 1. 1. Typical Ventricular Muscle Cell Action Potential Phases

Phase 4 is a resting phase (-90mV) due to ta constant outward leak of K^+ (I_{K1}) through inward rectifier channels. At this time, fast-sodium channels and slow Ca^{2+} L-type channels are closed. An action potential triggered in a neighbouring cardiomyocyte or pacemaker cell causes the membrane potential to rise above -90 mV, causing fast sodium channels start to open one by one and further raising membrane potential up to -70mV, initiating all-or-none depolarization (Phase 0) by inducing large fast sodium channel (I_{Na}) to open and K-leak channels to close. L-type ('long lasting") Ca^{2+} channels (($I_{Ca(L}$) open at -40mV. Phase 1 signifies closing of the fast-sodium channels and opening of a distinct outward K^+ channel (I_{kto}), causing a slight repolarization that appears as a "notch" in the action potential. Phase 2 is driven by sustained opening of L-type Ca^{2+} channels, causing constant inward current of Ca^{2+}, which is balanced by outward current of K^+, creating a plateau in the action potential. Excitation-contraction coupling occurs at this time, as Ca^{2+}-induced Ca^{2+} release from the sarcoplasmic reticulum facilitates actin-myosin crossbridge cycling. L-type Ca^{2+}

channels spontaneously close, K-leak channels reopen, and the cell repolarizes in phase 3.

The figure below (1.2) summarizes the cardiac depolarization, excitation-contraction coupling, and repolarization which rounds out our baseline review of cardiac physiology.

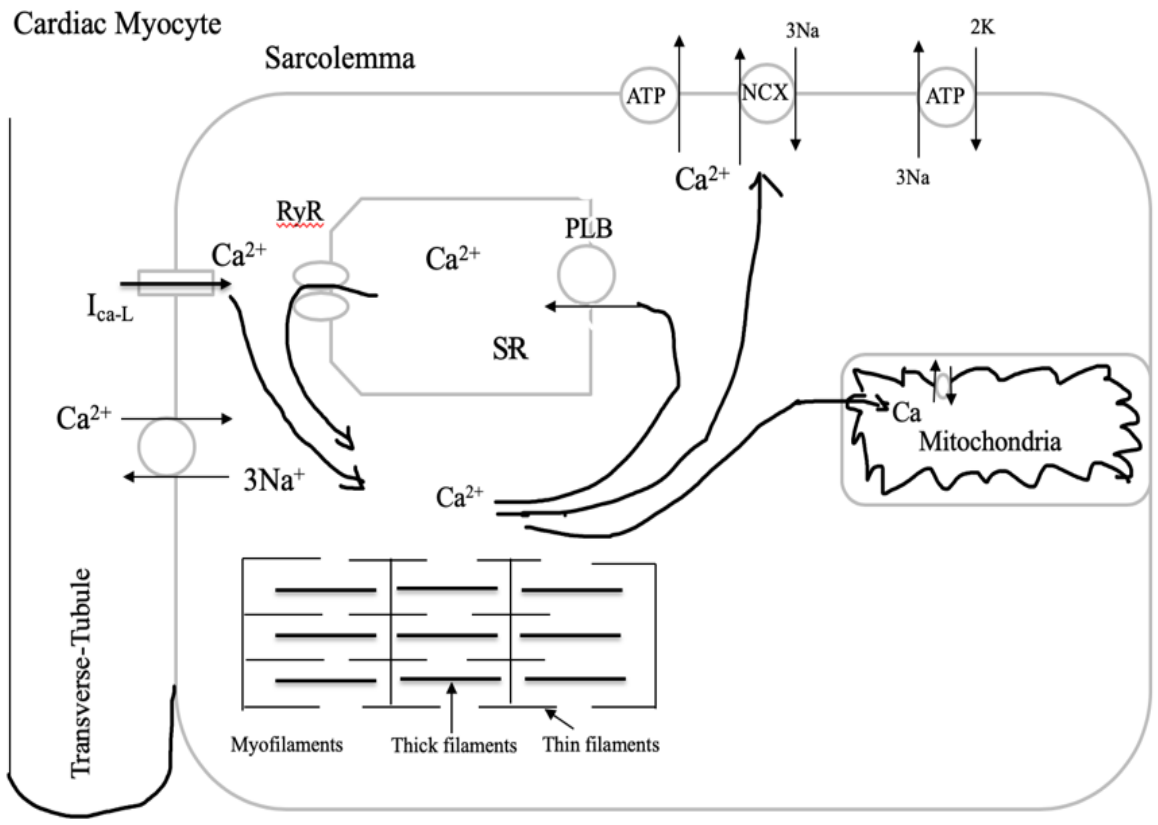

Figure 1. 2. Schematic Diagram.

L-type Ca^{2+} channels open at -40mV. Increased sarcoplasmic Ca^{2+} concentration causes Ca^{2+}-induced Ca^{2+} release from the sarcoplasmic reticulum via RyR (Ryanodine receptor). Massive cytosolic Ca^{2+} binds to troponin C on the thin filaments, moving tropomyosin to reveal myosin binding sites on the actin to permit contraction. Repolarization occurs when ion homeostasis turns re-established via the Sodium-Ca^{2+} exchanger, ATP-dependent Ca^{2+} sequestration through SERCA (Sarco/Endoplasmic Reticulum Ca^{2+} ATPase), and sodium-K^{+} ATPase.

2. Cardiovascular Disease (CVD)

2.1 Background of CVD

Despite being the leading cause of death in the United States, the incidence and mortality rates of cardiovascular disease (CVD) have declined over the past few decades. This decline is due to advances in early diagnosis and treatment, as well as public educational efforts of prevention, aimed at increasing physical activity, controlling obesity and hypertension, and reducing risk factors such as smoking. Despite these gains, cardiovascular disease remains the leading cause of mortality worldwide, responsible for 32% (17.9 million) of global death in 2019[3]. According to the Center for Disease Control and Prevention, the United States spends $229 billion annually from 2017 to 2018[3]. Within the category of cardiovascular disease, coronary heart disease (CHD) is by far the most prevalent cause of death, accounting for nearly half of all cardiovascular disease related deaths, or roughly 1 out of every 6 deaths in the United States [4].

Coronary artery disease is characterized by the accumulation of plaques in the wall of the coronary arteries. With advancements in medical technology, an occluded coronary artery can be re-opened using percutaneous coronary intervention technique. Open-heart surgery remains an option of treatment, particularly for patients with multivessel disease, diffuse or complex coronary disease, with or without valvular disease [5] . The development of cardiopulmonary bypass (CPB) using a heart–lung machine to maintain systematic circulation during operation has revolutionized the field of cardiac surgery and significantly reduced the mortality among patients with coronary artery disease undergoing open-heart surgery.

2.2 Cardiopulmonary Bypass (CPB)

CPB surgery usually requires the perfusion of cardioplegic solution to achieve a relaxed and non-beating heart with a blood-free surgical operation field for operative precision. This is achieved by a controlled global myocardial ischemia via clamping the aorta and directing the blood flow outside the body from superior and inferior vena cava to bypass the heart and lung. Upon completion of the surgical repair on the heart, oxygenated blood is restored to it and the rhythm of myocardial contraction is resumed. Although the benefits exceed the drawback, this artificial myocardial ischemia and reperfusion procedure can cause invisible damage at the cellular level, so called myocardial ischemic reperfusion injury [1]. At the molecular level, MIRI is coupled to increases in oxidative stress, intracellular Ca^{2+} overload, and systemic inflammatory response [6]. These molecular events impair endothelial function for micro circulation, affects myocardial electrophysiology, and undermine muscle contractility, adding to postoperative complications [7]. Hence, it is important to initiate myocardial protection procedures to minimize cellular damage of surgical-induced ischemia during extracorporeal circulation (ECC).

A hypothermic cardioplegic arrest is commonly viewed as a protective method for on-pump cardiac surgery. The low temperature serves to preserve myocardial function

via minimizing myocardial oxygen consumption, therefore preventing ROS generation in theory [8].

The majority of the cardioplegic solutions are hyperkalemic, either as a crystalloid, or mixing with the blood so called blood-based, delivering K+ to reach localized concentration of 12 to 25 mM, to induce depolarized arrest [9]. Supported by over 40 years of clinical practice, these hyperkalemic fluids provide rapid diastolic arrest[10]. By producing abnormally high concentration of K+ to the coronary vasculature, the resting membrane potential of the myocardium changes to -50 mV from -80 mV [11]. This shift locks the transmembrane gradient at a voltage that exceeds the threshold of -70 mV, prohibiting the all-or-nothing response necessary for action potential to propagate [11].

2.3 Cardioplegia: A Short History of Clinical Use

The investigation into the formulation of cardioplegic solution dates back to 1955, when Dennies Melrose introduced elective reversible cardiac arrest by aortic root injection of a high concentration of potassium citrate (over 200 mM) in hypothermic dogs (25°C) at the Postgraduate Medical School in Hammersmith, London. This cardioplegia provided an immediate cardiac arrest, a condition ideal for short-lasting anatomic repair [12]. However, this solution induced refractory ventricular fibrillation, contractile dysfunction and myocardial necrosis[13-18]. These findings resulted in high K^+ cardioplegia being

placed on “clinical hold” for nearly 15 years. Over this time period, topical hypothermia or normothermic ischemia, direct coronary perfusion or intermittent aortic occlusion were tested as a method to protect the heart [19, 20]. Unfortunately, these alternatives failed to provide a better outcome than the “Melrose Technique,” which was highlighted by Cooley as an irreversibly damaged “stone heart” as observed clinically [21].

In the early 1960s, Hoelscher et al. [22], first reported that the damaging effects of the Melrose solution were not due to the potassium ion, but to the calcium- and magnesium chelating property of the citrate. In parallel with Hoelscher’s finding, another German pioneer Bretschneider, et al, developed one of the first crystalloid solution in 1964, known today as HTK. This cardioplegia was low in sodium and free of calcium, inducing cardiac arrest by creating a polarized cell membrane. This solution has since been used routinely with clinical success [23]. However, perfusion of the hearts with an extracellular solution containing zero calcium during ischemia carried a risk “calcium paradox” [24]. During reperfusion with a solution or blood containing calcium, the calcium paradox is a high risk of postoperative myocardial dysfunction.

In the mid-1970s, a second wave of interest in potassium cardioplegia in the form of potassium chloride began to surface [25]. The period from 1970s to 1980s could be termed as The Gold Age of Cardioplegia. Thousands of papers reported many

fundamentals in the technique of cardioplegia, including dosing strategies and solution formulation. Staged administration of cardioplegia, known as multidose strategy, began with all-crystalloid cardioplegia in 1976. That same year, Dr. David Hearse, a biochemist together with a cardiothoracic surgeon, Dr. Mark Braimbridge, developed the extracellular hyperkalemia solution, known today as St. Thomas solution.[26]. This solution was optimized with essential components, having K^+ concentration of 20 mmol/L (No.1 solution), normal ionized Ca^{2+} concentration and Mg^{2+}concentration of 16 mmol/L. St. Thomas solution No.1 was first utilized clinically in 1975[27].

St. Thomas solution No.2 with potassium chloride 16.0 mM, also known as “Plegisol”, was developed in 1981. The main features of No.2 solution, compared with the No.1 solution, include a small decrease in Na^+ or K^+ concentration, a reduction in Ca^{2+} by 50%, and deletion of procaine, but incorporation of a low fraction of bicarbonate, and adjustment of pH to 7.8. No.2 solution was introduced commercially into the United States in 1982 and used worldwide since. In spite of its popularity, hyperkalemia causes Ca^{2+} and Na^+ buildup in cardiac myocytes, because of non-inactivating “window” current induced by 16 mM potassium concentration[11]. As a consequence, abnormal myocardial ionic gradients and a retardation of myocardial recovery may occur.

Glucose-Insulin-potassium cardioplegia, also called GIK, were proposed by Lolley et al[28] to improve anaerobic energy production during ischemia. However, this solution

had a potential risk of calcium paradox because of its zero calcium composition as explained in detail below.

In late 1970s, Kirklin *et al.,* performed randomized clinical studies at the University of Alabama, Birmingham to establish hypothermic potassium cardioplegia as the dominant form of myocardial protection [29]. Within 2-3 years, the use of crystalloid buffer-based cardioplegia became the main cardioprotective technique all over the world, with the St. Thomas being the most widely used crystalloid solution [30]. One year later, Follette and Buckberg in collaboration with colleagues popularized the idea of using blood as a vehicle in a multidose administration protocol [31]. Compared to crystalloid cardioplegia, blood cardioplegia has a number of positive effects, including an ideal oncotic pressure, greater oxygen-supply capacity, better acid-base balance capacity, and the ability for free-radical scavenging by red blood cells and plasma constituents. The blood-based cardioplegia had potent protective effects against myocardial injury during ischemia and reperfusion [32]. Blood cardioplegia is now the predominant form of hyperkalemic cardioplegia[33].

Most early cardiac arrest strategies employed administrating cold dose since hypothemia adds a protective benefit due to its ability to minimize metabolic demand during ischemia[27]. Several downside effects appear to be evident, among which are derangements of pH, activation of platelets or leukocytes, instability of the plasma

membranes, and promotion of edema [34, 35]. As a result, new attention in warm blood cardioplegia took shape in 1983[36].

All blood (miniplegia) had started to gain attention since the 1990s. In addition to popularizing blood cardioplegia, Buckberg and associates [37] also emphasized on the importance of intermittent reinfusion of a cardioplegic solution, reasoned from the washout from noncoronary collateral perfusion. Buckberg also proposed that the myocardium should be kept in a diastolic arrested state with the warm cardioplegic blood during the initial phase of reoxygenation [31] and thereafter recommended warm blood cardioplegia during the induction phase [38].

For a long time, a “dedicated” cardioplegia for infants and pediatric patients was absent. The same cardioplegia for adult surgery was used for infant and pediatric patients, simply by adjusting the dose via volume, flow rate, and pressure [39]. However, the popular crystalloid cardioplegia in the 80’s and early 90’s, for instance, the St Thomas solution, had inconsistent outcome in young patients[2, 40]. Dr. Pedro Del Nido and his team developed Del Nido cardioplegia at the University of Pittsburgh in 1990s. This solution has been widely used for pediatric cardiac surgery in Boston’s Children Hospital and other institutes since 1994 [41].

O'Brien et al.[42] first carried out laboratory research on Del Nido cardioplegia using in vitro isolated rat cardiomyocytes and in vivo pediatric patients undergoing cardiac operations reported in 2009. After exposure primary rat myocytes to Del Nido cardioplegia or adult cardioplegia followed by reperfusion, they found that Del Nido-perfused myocytes had lower diastolic Ca^{2+} during cardioplegia and early reperfusion than with adult cardioplegia. For pediatric patients undergoing cardiac surgey and receiving Del Nido cardioplegia or adult cardioplegia, median serum troponin T level were significantly lower in Del Nido group, which persistented 24 hours postoperatively. In a randomized trial, Del Nido cardioplegia was compared with St Thomas cardioplegia in pediatric patients. It showed that the Del Nido group had a higher cardiac index, lower Mechanical ventilation, and shorter intensive care unit or hospital stay[43]. Since 2003, Del Nido cardioplegia has been successfully used for adult cardiac surgery as well and provided excellent myocardial protection[44-48].

The dilution ratio of cardioplegic solutions has long been a matter of debate. Most commonly used ratio is 4:1 blood to crystalloid dilution, popularized by Buckberg, Gundry, and colleagues. Buckberg translated this formulation into a less dilute 8:1 blood-to-crystalloid dilution. However, it remains inconclusive on whether or not the less diluted solutions have significant benefit over the standard 4:1 diluted cardioplegia[49]. Del Nido employs a more dilute ratio, 1:4 blood to crystalloid, and can produce a long lasting arrest with a bolus administration[44, 50].

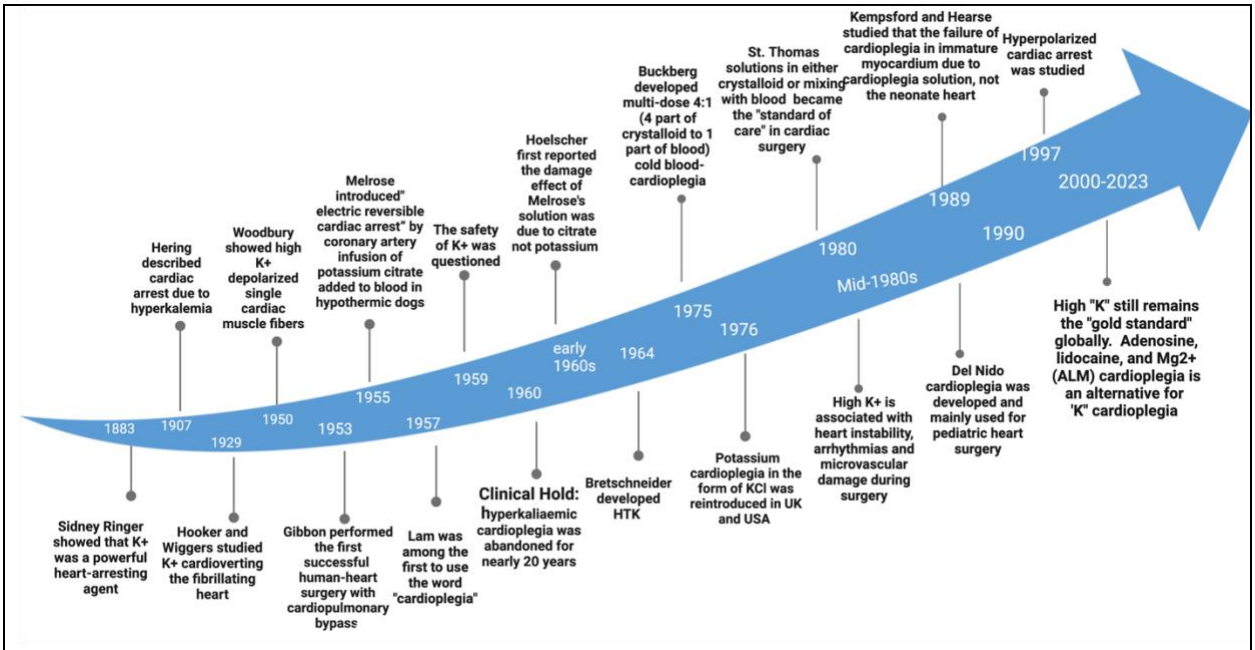

Figure 1. 3. Cardioplegia History

3. ROS Production During Open-Heart Surgery

3.1. Global Myocardial Ischemic Reperfusion Injury during CPB

Numerous of studies demonstrated that a notable proportion of patients may experience impaired cardiac function in the postoperative period. Patients with diabetes,

in particular, are at a higher risk of developing cardiac complications, such as low cardiac output syndrome and have a lower 10-year survival, after undergoing CABG surgery[51]. These patients are also two to five times more likely to develop cardiovascular disease, with estimates suggesting that they may represent up to 30% of cases[52]. Intraoperative ischemia-reperfusion injury is a major factor in the development of transient and prolonged postoperative cardiac dysfunction. Ischemia-reperfusion injury takes place following restoration of blood flow after a period of ischemia. During myocardial reperfusion, the generation of ROS increases significantly, and those molecules play a crucial role as central mediators of ischemia-reperfusion injury.

Oxidative stress, defined as a “disruption of redox balance and control”, can be induced during CPB via over production of reactive oxygen species (ROS) or reduction of antioxidant reservoir due to structural and functional modifications[53]. ROS are highly reactive molecules of oxygen, which harbor one unpaired electron (superoxide anion, hydroxyl radical) or an additional electron pair (H_2O_2) on its valence orbital. Disturbance of the intracellular redox homeostasis can lead to cell death or cell degeneration[54]. ROS exert their damaging effects by attaching to macromolecules, causing (i) lipid peroxidation, (ii) oxidation of proteins or (iii) damage to DNA[55] (**Error! Reference source not found.**). I n addition to ROS, reactive nitrogen species[56] such as nitric oxide (NO), nitrogen dioxide (NO_2-), peroxynitrite (OONO-), dinitrogen trioxide (N_2O_3), and nitrous acid (HNO_2) also contribute to the oxidative stress. The interaction between cellular NO and ROS

leads to the generation of various reactive nitrogen species that play a role in causing oxidative and nitrosative harm.

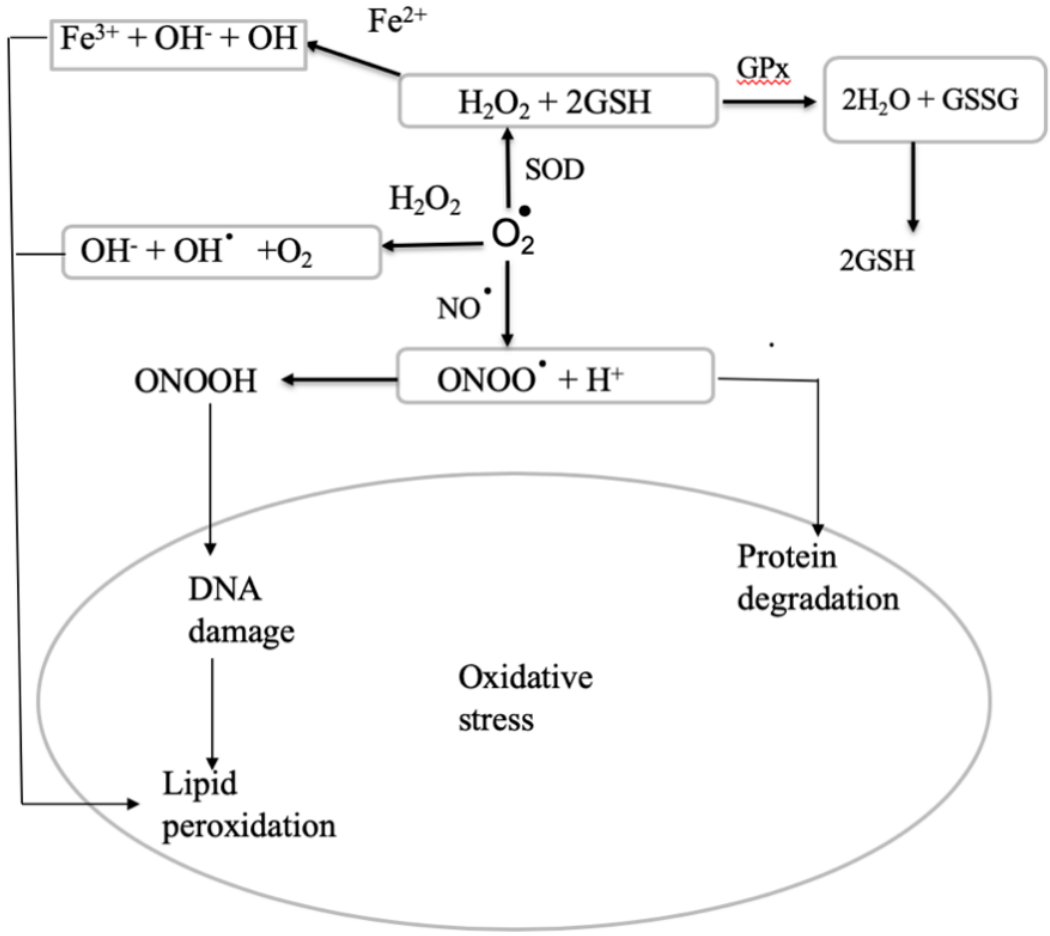

Figure 1. 4. Simplified Mechanism of Oxidative Stress.

cellular RNOS generation and antioxidant action of SOD and GPx.O_2: superoxide radical; H_2O_2: hydrogen peroxide; $ONOO^-$: peroxy radical; OH: hydroxyl radical; NO: nitric radical; SOD: superoxide dismutase; GPx: glutathione peroxidase; GSH: glutathione; GSSH: oxidised glutathione; GSSG-R: glutathione reductase.

During CPB surgery, the blood is routed from the vena cava to the heart-lung machine, the so called cardiopulmonary bypass pump, which facilitates artificial gas exchange and propels oxygenated blood back into the circulation via the aorta. Although the heart-lung machine maintains adequate perfusion by delivering oxygenated blood downstream of the aorta, cardiac perfusion is still tied to the cyclic nature of systole/diastole. Cardioplegic solution is administered via the coronary vasculature during CPB to halt the heart's electrical activity, leading to an inhibition of excitation-contraction. One consequence of such controlled cardiac arrest, in addition to providing a still field for surgical precision, is reducing the heart's demand for energy metabolism. Even with the administration of cardioplegia and cessation of contraction, the myocardium's oxygen consumption persists, although at a reduced rate. The myocardium enters a state of hibernation, but they still requires ATP for essential processes like ion homeostasis. Prolonged oxygen depletion can diminish ATP generation and cause sustained myocardial dysfunction[57].

When the heart is electrically silenced, its oxygen and nutrient demands are decreased, along with the cessation of the blood supply. The resulting ischemia can range in severity from being reversible to fatal. As the duration or severity of ischemia increases, the degree of myocyte injury also escalates[58].

Ischemic injury is a multifaceted phenomenon that extends beyond the depletion of oxygen and ATP, or CO_2 accumulation. Rather, these initial events signify the beginning of ischemia injury, which triggers numerous alternations at the subcellular, cellular, tissue, and organ levels. Upon reperfusion, the provision of adequate oxygen to the ischemic myocardium prompts an acute surge in ROS and RNS. These species can initiate somewhat random, spontaneous, and self-propagating radical reactions with biomolecules. A few consequences include the activation of matrix metalloproteinases or intracellular proteolytic enzymes, and induction of mitochondrial permeability transition.

In a non-ischemic heart, mitochondrial oxidation phosphorylation supplies more than 95% of ATP, with the majority of this energy generated via fatty acid β-oxidation[59]. During ischemia, the reduced blood flow leads to an accumulation of oxidative substrates, causing a decrease in their reductive counterparts and a more than 10-fold increase in the myocardial NADH/NAD^+ ratio[60]. Ischemia has been linked to decreased energy production in mitochondria, which can ultimately cause alterations in intracellular levels of Na^+, Ca^{2+}, and pH[61]. As a response to the energy crisis during ischemia, the heart shifts its main metabolic pathway from β-oxidation towards glycolysis. Glycolysis is a short-term solution to the problem of ischemia because myocardial glycogen stores are limited. Nevertheless, the combination of non-mitochondrial ATP generation during ischemia and accumulation of lactic acid due to glycolysis in ischemic conditions leads to intracellular acidosis[62].

Reperfusion immediately after an episode of ischemia creates an oxidative stress conundrum that initiates a cascade of biochemical events leading to myocardial apoptosis and necrosis[63]. Following reperfusion, a set of ionic and histological distinctions emerged that were not observed during the preceding ischemic phase[64]. Specifically, myocytes exhibited elevated levels of intracellular Na^+, Cl^-, and Ca^{2+}, coupled with reduced levels of intracellular K^+, and their contractile proteins formed distinct bands, while swelling of both mitochondria and cells becomes evident. The main stimulus for the production of ROS in the myocardium is reperfusion injury[65].

Myocardium damage can occur during reperfusion due to mitochondrial dysfunction triggered by ROS production[65]. ROS production-induced opening of the mitochondrial permeability transition pore (mPTP) can cause mitochondrial swelling, damage to the mitochondrial membrane, and ultimately cell death as a result of high level ROS production[66, 67]. In addition, elevated ROS levels exhibit the ability to influence multiple signaling pathways and transcription factors, including MAPK and NF-KB, which can control signaling pathways of inflammation, apoptosis or necrosis[68] .

Although cardiomyocytes are recognized as a significant contributor to the generation of ROS in the damaged myocardium, it should be emphasized that ROS can be produced as well by vascular endothelia cells and activated leukocytes involving

NADPH oxidase and/or xanthine oxidase[69]. The accumulation of activated neutrophils in the myocardium due to ischemic injury can lead to the release of ROS and other proteolytic enzymes. In addition, ROS can be generated by other cell types in the heart including vascular smooth muscle, fibroblast, and lymphocytes leading to peroxidation of membrane lipids, denaturation of proteins and enzymes, damage of nuc[70].

3.2 Altered Myocardial Metabolism

Cardioplegic arrest and aortic cross-clamping leads to anaerobic metabolism in the myocardium due to ischemia, shifting the levels of lactate, citric acid cycle metabolites, purines, nicotinic acid, tyrosine, hyaluronic acid, ketones, fatty acids, and lipid metabolites[71-73]. The persistence of lactate release during ischemia followed by reperfusion indicates that normal aerobic metabolism may take long to recover. The continued production of lactate following reperfusion is a reliable predictor of postoperative ventricular dysfunction, which requires intra-aortic balloon pump support[71].

Following an ischemic episode, the activity of mitochondrial pyruvate dehydrogenase (PDH) is reduced by 40% and remains suppressed for as long as 30 mins after reperfusion[74]. The restoration of myocardial function is dependent on the recovery

of PDH activity[75]. Those findings indicate that prolonged anaerobic metabolism could play an essential role in inadequate postoperative ventricular function, highlighting the importance of enhancing the recovery of aerobic myocardial metabolism during reperfusion as a key target for mitigating reperfusion injury. Interventions such as insulin and adenosine that benefit the shift from anaerobic to aerobic myocardial metabolism can expedite the restoration of left ventricular function in the aftermath of reperfusion[76].

3.3. ROS Production Peri- and Post CPB

Before surgery, individuals with atherosclerotic coronary disease that requires intervention often display indications of oxidative stress and inflammation, which may become significantly pronounced as a result of CPB[77]. Furthermore, many patients undergoing cardiac surgery have coexisting morbidities such as diabetes, kidney and lung diseases, which are associated with abnormal redox state and increased oxidative stress.

CPB requires manipulation of the circulation via several mechanical procedures that ultimately influence the contents of the blood at cellular as well as non-cellular levels. After leaving the body, the blood travels through a series of polyurethane or silicone tubes into a hard-shell reservoir and then a roller or a centrifugal pump before being circulated back to the patient using the same tubing components. The repeated passage of the blood through the nonendothelialised extracorporeal circuit activates polymorphonuclear

leukocytes. The neutrophils are the main polymorphonuclear cell type that's activated as a result of this circuit, and are the primary source of ROS during a cardiothoracic surgical procedure that requires a heart-lung machine. The activation of neutrophils during CPB can be identified through molecular changes, such as the disappearance of L-selectin and increase in CD11b/CD18 (Mac-1) expression[78]. CPB triggers a proinflammatory reaction from neutrophils, which produce an oxidative environment.

Extracorporeal circulation creates an abnormal environment for the red blood cells (RBCs). The prolonged immersion of RBCs in a non-physiological solution, contact with an artificial surface, and turbulence by mechanical pumping induce structural alterations that affect their biophysical, biochemical, and immunological properties[79]. These changes result in a decrease in RBC deformity, which is crucial for maintaining normal microcirculation, as the cells become more rigid and fragile. Furthermore, membrane distortion renders RBCs susceptible to the membrane attack complex (MAC) generated by complement activation, leading to leakage of hemoglobin and substantial increase in the concentration of free hemoglobinHb, which undergoes redox cyclinh and generate peroxides in the presence of H_2O_2[80].

Transfusion of stored blood may contribute to the production of ROS following cardiac surgery. Blood storage alters the erythrocytes, causing the storage defect. Due

to the lack of antioxidant replenishment and exposure to higher levels of oxygen (20%) in the ambient environment, stored blood has an imbalance towards oxidation. The storage defect includes altered cell functions mediated by decreases in ATP and 2,3-diphosphoglycerate levels, modification of nitric oxide-mediated functions, and elevated lipid peroxidation[81]. Clinical research suggests that transfusion of stored blood can lead to additional complications, as alterations in the RBCs' membrane structure during storage render them more susceptible to progressive hemolysis, resulting in the buildup of free hemoglobin and iron in the circulation, as described above[82].

CPB in cardiac surgery has been linked with a broad range of acute lung injuries (AKI), with acute respiratory distress syndrome (ARDS) being one of the most severe manifestations. Although the incidence of ARDS associated with the surgical procedure is low, its potential adverse effects on both morbidity and mortality should not be overlooked. The alteration of the redox status towards oxidative in the lung tissue is believed to be caused by activation of complement and neutrophils, as well as damaged RBCs and reperfusion injury. Analysis of plasma and bronchoalveolar lavage samples from individuals with ARDS after undergoing cardiac surgery has revealed strong indications of severe oxidative stress, such as elevated levels of an inflammatory marker thioredoxin (Trx) and a fatty acid oxidation product 4-hydroxy-2-nonenal chlorotyrosine, nitrotyrosine, and orthotyrosine[83] [84].

The development of acute kidney injury (AKI) following cardiac surgery with CPB can stem from various factors, such as ischemia and reperfusion injury, changes in blood flow patterns, hemolysis, and blood transfusion [85]. Elevated levels of free hemoglobin and plasma myoglobin, both of which possess prooxidant properties, have been demonstrated to be independent predictors of AKI following CPB, due to the associated hemolysis. The depletion of energy in renal epithelial cells during ischemia and reperfusion injury can result in mitochondrial dysfunction, the generation of ROS, and activation of proinflammatory signaling pathways, which can cause cytoskeletal disruption and subsequent tubular cell damage[86]. In addition, these processes occurring within the kidney can lead to active sequestration of neutrophils to renal tissue and further production of ROS[87].

Atrial fibrillation (AF) is a supraventricular tachyarrhythmia characterized by uncoordinated atrial activation with ensuring deterioration of mechanical function[88].There is evidence of an association between postoperative atrial fibrillation (POAF) and ROS generation in the atrium [89]. POAF is a common complication (typically occurring within the first 2-3 days) after cardiac surgery with an occurrence rate that can reach up to 60% depending on the type of surgery, among coronary CABG, valve surgery, or combined procedures[90]. NADPH oxidase, which generates superoxide, is the most significant predictor of developing POAF, according to analysis of right aerial appendage samples from patients undergoing CABG [91]. Association between ROS and POAF consists of a positive feedback loop. As a result of POAFs, atrial tissue gives rise

to an increase of mitochondrial manganese superoxide dismutase activity and mPTP opening sensitivity or frequecy. This opening subsequently increases the outflow of ROS from the mitochondria and the vicious cycle continues[92]. Moreover, the analysis of right atrial tissue indicated that POAF risk was significantly linked to monoamine oxidase (MAO) activity, whereas total glutathione (GSH) levels were inversely associated with POAF[93].

4. Source of ROS

4.1. Biochemical Environment for ROS Generation during Ischemia and Reperfusion

ROS accumulated rapidly at the onset of ischemia in the hearts of experimental rats. Oxygen deprivation, a crucial factor for the production of ATP through oxidative phosphorylation, causes anaerobic metabolism to compensate for ATP production losses, leading to intracellular acidosis and depletion of intracellular creatine phosphate due to a lack of ATP for its synthesis. As intracellular phosphate levels rise, glycolysis and lactate production increase, causing lactic acidosis. The accumulation of lactate and hydrolysis of ATP further lowers intracellular pH by releasing of protons[94]. To counteract the acidosis, cells activate the Na^+/H^+ exchanger (NHE) on the plasma membrane which removes H^+ in exchange for Na^+[95]. The increase of intracellular Na^+ activates the plasma membrane Na^+/Ca^{2+} exchanger (NCX), leading to the extrusion of Na^+ and the influx of Ca^{2+}[96]

Elevated levels of cytoplasmic Ca^{2+} trigger the activation of ryanodine and inositol trisphosphate (IP3) receptors located in the sarcoplasmic reticulum (SR), leading to a further rise in cytosolic Ca^{2+} levels. Once the threshold is met, Ca^{2+} enters the mitochondria and reaches the matrix[97].Its transport is facilitated by the mitochondrial Ca^{2+} uniporter (MCU) and voltage-dependent anion channels (VDACs) present on the inner and outer mitochondrial membrane (IMM and OMM)[98], respectively.

4.2. Mitochondria Generation of Superoxide and Hydrogen Peroxide

To maintain its ability to contract and transport ions, the heart requires substantial quantities of high-energy phosphates, meaning that cardiomyocytes must constantly and rapidly replenish ATP, with over 95% of this process occurring through oxidative substrate utilization from the mitochondria. Given the responsibility of mitochondria in ATP supply, it makes sense that 40% of cell volume is occupied by the mitochondria whereas mitochondria typically take up 25-30% of cell volume in other cell types[99]. The high content of mitochondria makes cardiomyocytes the cell type with the highest mitochondrial content compared to any other cell type in the body. Due to their substantial mitochondrial content, cardiomyocytes are particularly vulnerable to electron transport chain damage and to increased mitochondrial $O_2^{\bullet-}$ generation during ischemia and reperfusion[100].

Mitochondria are the factory of aerobic metabolism. Proper respiratory chain function requires a delicate balance between the pro-oxidant and anti-oxidant system. Importantly, mitochondrial respiration relies in electron transfer and a proton gradient to drive ATP production. Whereas ROS are a natural byproduct of mitochondrial respiration, enhancement of mitoROS production is associated with inflammatory and metabolic disease[101]. MitoROS are generated by multiple mechanisms including but not limited to complexes I-III, within which complex I is the main ROS generator. The complex I serves as an entry site for electrons from NADH into the respiratory chain. Under the condition of high NADH/NAD+ ratio in mitochondrial matrix, O^{2-} is generated through the reaction between O_2 and reduced flavin mononucleotide (FMN), leading to O^{2-} release into the mitochondrial matrix[102]. In addition, O^{2-} also is formed via reverse electron transfer (RET). RET involves a reduced coenzyme Q and a consequent transfer of those electrons back to the complex I.

Complex III is also a source of mitoROS. Although mitochondria produce very low levels of superoxide anion under normal physiological condition, mitoROS are mostly released into the intermembrane space. Complex II may also contribute to ROS production[103]. Complex II produces ROS when both Complex I and Complex I are inhibited, with ROS production believed to occur with the mechanism involving electron transfer from succinate or reduced ubiquinone[103]. In addition to mitochondrial complex I-III, metabolic enzymes such as α-ketoglutarate dehydrogenase and pyruvate

dehydrogenase also contribute to mitoROS generation by both forward electron transfer and RET[104].

Apart from ROS production, impairment of mitoROS scavenging pathways also contributes to ROS accumulation. The predominant ROS buffering systems include glutaredoxin (Grx), glutathione and thioredoxin (Trx) in the mitochondria [105]. The superoxide dismutase family of proteins facilitates the dismutation of superoxide ($O^{2\cdot-}$) into H_2O_2[106].Mitochondrial GSH redox system, comprising glutathione reductase, peroxidase (GPX), and peroxiredoxins (Prdx), is responsible for decomposing H_2O_2 into O_2 and H_2O[107].

The Trx and Grx system also play a prominent role in mitochondrial ROS removal. The Grx family members include Grx2 and Grx5. Under oxidative stress, the ratio of glutathione-to-glutathione disulfide becomes reduced, thus causing proteins to become the substrates. Grx2 regulates O_2^- production from the complex I by catalyzing glutathionylation of two thiol groups; whereas Grx5 regulates iron/sulfur enzymes [108]. In the mitochondrial matrix, SOD2 (MnSOD) is the primary enzyme responsible for dismutation, while SOD1 (Cu, Zn-SOD) carries out dismutation in the intermembrane space.

Thioredoxin-2 (Trx2) was observed in a study where a homozygous KO of Trx2 is embryonically lethal, and heterozygous mice, while viable, show decreased mitochondrial respiratory function and increased mitoROS production[109]. In a similar fashion, mice with cardiac-specific TrxR2 KO display alterations in cardiac structure, dysregulation of autophagy, reduced oxygen consumption, and a shift in their metabolic profile[110]. Our understanding of the regulation of cardiovascular function by Grx and Trx system is limited, yet it is clear that mitochondria play a crucial role in maintaining the delicate balance between oxidant and anti-oxidant systems.

One study showed that ischemia caused a decline in cytochrome c levels within the mitochondrial inner membrane space and led to a rise in the reduction state of the remaining cytochrome c, which correlates with heightened mitochondrial H_2O_2 production that can be alleviated through the administration of exogenous cytochrome c[111]. These experiments indicated that the antioxidant defense and the functional inhibition of cytochrome oxidase dimers is abolished during ischemia. The gradual decline in the availability of functional cytochrome c oxidase, which is needed to replenish oxidized cytochrome c during prolonged ischemia, results in a buildup of reduced cytochrome c that is unable to eliminate $O_2^{\bullet-}$. The ischemic loss of cytochrome c from the intermembrane space caused by outer membrane permeabilization exacerbates this issue, leading to a higher proportion of $O_2^{\bullet-}$ interacting with superoxide dismutase and resulting in an elevation level of H_2O_2 [112].

4.3. Xanthine Oxidase (XO)

Xanthine oxidase (XO) is activated as a result of ischemic reperfusion. This enzyme or technically xanthine oxidoreductase (XOR), converts hypoxanthine to xanthine and the latter to uric acid, whie generating H2O2. XOR is known to exist in two interconvertible forms, with about 80% existing as Xanthine dehydrogenase (XDH) and the remainder as xanthine oxidase (XO). XDH is commonly detected in healthy tissues whereas XO protein expression and activity increased significantly in humans following ischemic reperfusion and a mouse model of myocardial infarction[113]. The transition between XDH and XO may occur either irreversibly, by limited proteolysis, or reversibly by oxidation of thiol groups. It is interesting to note that XDH can in theory produce more superoxide per mole of oxygen during NADH oxidization than XO. Along with NADPH oxidase, it is a major generator of ROS in humans.

XOR is mainly produced by epithelial cells, and it is localized primarily in the cytoplasm. It has transcriptional and posttranscriptional regulations downstream of a signaling pathway. It has been shown that XOR derived ROS in the myocardium during ischemic reperfusion via the activation of Hypoxia-Inducible Factor-2α (HIF-2a), phospholipase A2, TNF-α, IL-1β, INF-γ, angiotension II and vascular peroxidase 1 (VPO1) [114-117]. Hypoxia is the most studied factor that regulates the expression and activity of XOR. In general, under the conditions of excessive oxygen, XOR enzymatic activity is suppressed, whereas in endothelial cells, both transcriptional and posttranslational

regulation of XOR expression were observed to gradually increase in response to hypoxia[118]. Activation of XOR under hypoxic or stress condition may be attributed to the crucial role of p38 MAPK, which has been documented to activate XOR[119].

Pharmacological inhibition of ROS production from purine metabolism has been reported in previous studies but the myocardial benefit effect of XO inhibitors has been a matter of debate. Zhang, *et al.,* observed a decrease in XO activity and XO-derived products, i.e. H_2O_2 and uric acid, in both a rat heart model of myocardial I/R and a cardiac cell model of hypoxia/reoxygenation (H/R) after administration of allopurinol[120]. Huang, *et al.,* discovered a reduction of markers of oxidative stress, malondialdehyde (MDA), oxidized LDL and TNF-α[121]. However, inconsistent results have been reported in the blockade of XO to prevent ROS production[122, 123]. One possible explanation is the pharmacological inhibitor itself may exert antioxidative effect, independent of XO inhibition[124]. In addition, XO exhibits several functions, including nitrite reductase activity, which increases nitric oxide formation[125]. The production of nitric oxide can ameliorate the consequences of MIRI by stimulating vasodilation and inhibiting inflammatory response.

The expression of human XOR protein is regulated at both transcriptional and post-translational levels. The human XOR protein is expressed at a low level because the

basal activity of the human XOR gene (*hXOR*) promoter is minimal when compared with other mammals. The highest expression of hXOR gene is in the liver, followed by the lung, gut, heart, kidney and lactating mammary gland epithelial cells and vascular endothelial cells[126]. Animal studies have demonstrated that during ischemia, there is an accumulation of hypoxanthine, which fuels the production of ROS upon reperfusion due to the conversion of XDH to XO. This contributes to a significant rise in H_2O_2 levels in the myocardium of experimental animals upon reperfusion[127].

4.4. Nicotinamide Adenine Dinucleotide Phosphate (NADPH) Oxidase (NOX)

The NADPH oxidase (NOX) is a transmembrane enzyme that produces O_2^- and H_2O_2 from molecular oxygen, using NADPH or NADH as an electron donor[128]. NOXs are present in many cell types, including cardiomyocytes. The NOX family consists of seven members, NOX 1-5 and the dual oxidases, Duox1 and -2[129], of which Nox2 and Nox4 are main isoforms found in the myocardium[130]. A long list of studies have demonstrated the detrimental role of Nox2/4 due to ROS generation in response to a variety of cardiovascular diseases, including MIRI[131]. Nevertheless, a recent report showed that NOX4 exerts a beneficial effect in the cardiac and vascular systems during chronic hemodynamic stress[132].

Nox2 and Nox4 are abundantly expressed in cardiomyocytes and participate in the response to cardiac injury and cardiac remodeling[133]. NOX2 is mainly located in the

plasma membrane and is activated largely by cytosolic factors, such as Rac1 through its transmembrane loops, $p47^{phox,}$ $P67^{phox}$ and $P40^{phox}$, although the mechanism of interaction between Rac1 and NOX2 remains unknown. Unlike Nox2, Nox4 is predominantly localized on the membranes of subcellular organelles, including endoplasmic reticulum (EM), nucleus, and mitochondria. Nox4 differs from Nox2 and other Nox enzymes by regulation through expression level and does not require agonists[134].

The functional significance of endogenous Nox2 and Nox4 in MIRI has been investigated using Nox isoform-specific KO mice. One study compared the myocardial infarct size after I/R between wild-type mice and Nox2 or Nox4 KO mice. Unexpectedly, the Nox2 but Nox4 KO mice had reduced infarct size compared to their wild type counterpart[131]. Another study did not find attenuation of MIRI by systemic Nox2 KO in mice[135]. Several studies using Nox2-null mice and other models showed that Nox2 in the heart is involved in the development of cardiac hypertrophy and contractile dysfunction following myocardial infarction, pressure overload, or angiotensin II administration[136, 137]. However, other studies suggest that there is a causative relationship between Nox and I/R injury. Indeed, a study demonstrated both systemic Nox2 KO and cardiac specific Nox4 KO resulted in a reduction in ROS production and infarct size after I/R in mice[138]. In addition, calcium-dependent mitochondrial swelling was also decreased in systemic Nox2 KO and cardiac-specific Nox4 KO mice[138].

Downregulation of Nox4 by siRNA attenuated infarct size in mice after I/R[135]. Several studies suggested that both Nox2 and Nox4 contributed to myocardial oxidative stress and damage in response to I/R.

ROS form when the Nox enzymes transfer an electron from NADPH to molecular oxygen. Nox1, Nox2, Nox3 and Nox5 produce superoxide, whereas Duox1, Duox2, and Nox4 mainly generate hydrogen peroxide[139] . Redox homeostasis is regulated by several systems such as Nicotinamide adenine dinucleotide (NAD^+)/reduced NAD^+ (NADH), phosphorylated NAD+(NADP+)/reduced NADP+ (NADPH), and reduced glutathione (GSH)/GSH disulfide (GSSG). NADH is an important electron donor during mitochondrial oxidative phosphorylation (OXPHOS) and in cardiomyocytes most of NADH is produced via the TCA cycle, whereas NAD+ is an electron acceptor during glycolysis. The NADH and NADPH pools are regulated through many enzymes. NADPH is important for the correct functioning of antioxidant mechanisms such as glutathione reductase and thioredoxin reductase[140]. However, NADH and NADPH are also participants of ROS generation since they can be electron donors for ROS formation, especially in response to physiological stimuli, including growth factors, cytokines and hormones [141].

4.5. Nitric Oxide (NO)

Apart from the NOX-dependent ROS production, the nitric oxide synthase also contributes to the generation of ROS. Endothelial nitric oxide synthase (eNOs) become uncoupled and utilizes its oxygenase domain to produce superoxide in a Ca^{2+}/calmodulin dependent reaction in the absence of tetrahydrobiopterin (BH_4)[142], which subsequently triggers the oxidation of the remaining BH_4[143]. Superoxide may react with NO, forming peroxynitrite, whereas the heightened activity NADPH oxidases triggers a chain reaction of radical generation by producing superoxide as a primer radical followed by bursts of peroxynitrite ($ONOO^-$) that oxidizes BH_4 to BH_3 and intensifies eNOS uncoupling, starting a bonfire of radical production by eNOS. In addition, $ONOO^-$ can induce the irreversible nitration of tyrosine residues on various other proteins, leading to impaired phosphorylation and enzymatic malfunction. Rapid generation of $ONOO^-$ during reperfusion of the ischemic heart have been detected[144] and administration of low concentrations of the NOS inhibitor N^G-monomethyl-L-arginine (L-NMMA), protected the hearts from ischemia-reperfusion injury, comparable to a cell permeable SOD mimetic, MnTBAP[145].

5. Nrf2: Master Regulation of Antioxidant Defense

5.1. The NRF2 Transcription Factor

NRF2, also known as the Nuclear Factor-Erythroid Related Factor 2, has been widely recognized as the “master regulator of oxidative stress”. Nrf2 gene was discovered in 1994 as a member of the human CNC-bZIP transcription family for the transcriptional stimulation of beta-globin gene[146]. Activation of the NRF2 transcription factor has been linked to cytoprotection against a variety of stresses, most significantly the oxidative stress[147]. The genes best known under the control of NRF2 include antioxidant and detoxification genes. Additionally, NRF2 has been found to regulate genes participating in cell signaling, transcription, autophagy, anabolic metabolism, cell proliferation and organ development[148].

Like most of proteins inside a cell, NRF2 protein is constantly transcribed, translated, and degraded under normal physiological conditions to maintain a balance. This lends the merit of the NRF2 mediated antioxidant pathway because cells invest a large amount of energy to transcribe and translate a protein that will succumb to degradation in a matter of minutes. Indeed, when cells are under oxidative stress, the prompt activation of NRF2 becomes crucial for cell survival, and thus the persistent presence of this transcription factor becomes necessary to coordinate a defense system against further damage. There are several ways to regulate the level of NRF2 protein under the circumstance of oxidative stress (see Figure 1.5)[149].

The redox-regulated transcription factor NRF2 has been well established as the key regulator of the antioxidant response among all cell types. In an unstressed state,

NRF2 protein is kept at a low basal level through degradation via the 26S proteasome following Kelch-like ECH-associated protein 1 (KEAP1) dependent ubiquitination. KEAP1, the negative regulator of NRF2, recruits E3 ligase to promote the polyubiquitylation, allowing NRF2 protein degradation by the proteasome[150]. Binding to KEAP1 also prevents NRF2 from translocating to the nuclei.

ROS exposure leads to oxidation of critical cysteine residues in KEAP1 protein[151], altering the confirmation of KEAP1 protein and resulting in dissociation of NRF2 from KEAP1. This allows NRF2 protein to accumulate[152] and translocate from the cytosol into nuclei, where it binds with sMaf to form a heterodimer for binding to the Antioxidant Response Element (ARE) sequence, located in the promoter of many cytoprotective genes (Figure 1.5).

5.2. Regulation of the KEAP1-NRF2 Pathway by P62/SQATM1

P62/SQSTM1, a cellular protein that is recruited by autophagy to ubiquitinated outer mitochondrial membrane proteins in response to stress, plays a key role in the autophagy-lysosome pathway by acting as a cargo receptor that targets proteins for degradation. Dysregulation of autophagy can lead to accumulation of autophagosomes, which allows P62 to capture KEAP1 and prevents KEAP1 from sequestering NRF2, therefore resulting in NRF2 protein stabilization[153]. This P62/SQSTM1-mediated NRF2

activation is regulated by phosphorylation events in response to Oxidative stress signaling. Phosphorylation of P62/SQSTM1 by the mammalian target of rapamycin C1 (mTORC1) allows for enhanced binding affinity of P62/SQSTM1 to KEAP1[154], indicating that phosphorylation of P62/SQSTM1 is sufficient for potentiating NRF2 protein elevation due to disruption of KEAP1-mediated NRF2 ubiquitination (Figure 1.5).

5.3. NRF2 Activation via Regulating De Novo NRF2 Protein Translation

NRF2 can be activated via de novo protein translation under oxidative stress condition [155]. A marked decrease in global protein expression occurs upon exposure to stress including oxidative stress, viral infection, heart shock, nutrient deprivation and DNA damaging agents by inhibiting 5'-cap-mediated translation. NRF2 mRNA, containing an internal ribosomal entry site (IRES), can bypass the cap-dependent translation and undergo IRES dependent translation of NRF2 protein[156]. NRF2 is rapidly translated from mRNA via an IRES-dependent mechanism when cells are exposed to oxidants[157]. Cells are capable of sensing a range of oxidative stress, with moderate levels triggering IRES-mediated translation reprogramming, while high levels lead to mRNA association with ribosomes for stress granule formation, sheltering from both mRNA species and translation apparatus from damages[158].

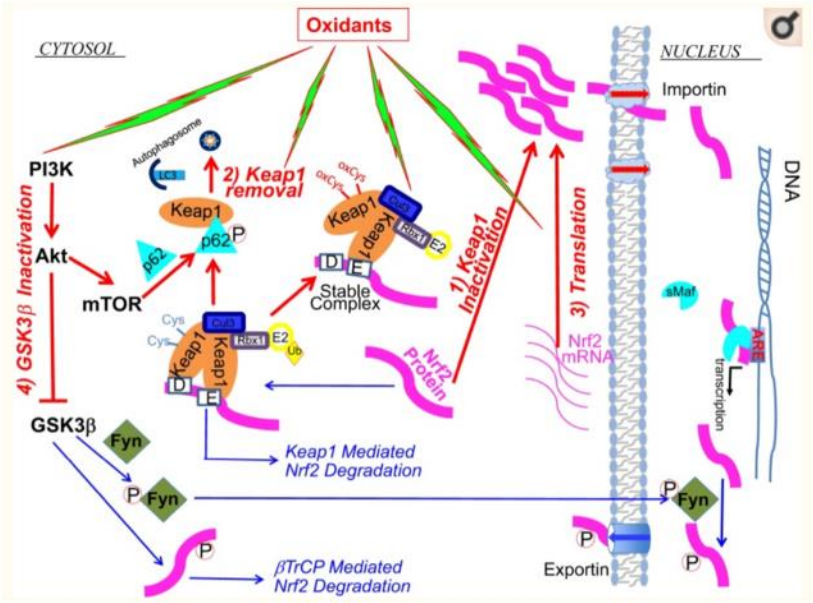

Figure 1. 5. Mechanisms of Oxidant - Induced NRF2 Activation.

6. Nrf2 and CPB

While there is clear evidence for enhanced ROS production and reduced antioxidant enzyme expression, the role of Nrf2 has not been studied in the setting of cardiac surgery. However, there is some evidence pointing to Nrf2 mediating cardiac protection during cardiopulmonary bypass. Although Nrf2 has received considerable attention with regards to cytoprotection in a variety of organ systems, a few studies have investigated the protective effects of Nrf2 in the heart. The overwhelming evidence supporting a role of oxidative stress in the pathology of heart disease, along with the observed benefits of Nrf2 downstream targets in protecting against cardiac injury, justify

the need to understand the role of Nrf2 in the heart. The work presented in this dissertation investigates the importance of Nrf2 induction in heart surgery (Chapter II), cardioplegia effects on metabolic change by oxidative stress (Chapter III), and Involvement of YTHDF2 in Nrf2 *de novo* protein translation during oxidative stress (Chapter IV).

CHAPTER II: Del NIDO CARDIOPLEGIA OR POTASSIUM IUDUCES NRF2 AND PRPTECTS CARDIOMYOCYTES AGANIST OXIDAITVE STRESS

Abstract

Open heart surgery is often an unavoidable procedure for treatment of coronary artery disease. The procedure associated reperfusion injury affects postoperative cardiac performance and long-term outcomes. We addressed here whether cardioplegia essential for cardiopulmonary bypass surgery activates Nrf2, a transcription factor regulating the expression of antioxidant and detoxification genes. With commonly used cardioplegic solutions, High K^+, Low K^+, Del Nido (DN), histidine-tryptophan-ketoglutarate (HTK) and Celsior (CS), we found that DN caused an increase of Nrf2 protein in AC16 human cardiomyocytes. Tracing the ingredients in DN led to the discovery of KCl at the concentration above 5 mM capable of Nrf2 protein induction. The Antioxidant Response Element (ARE) luciferase reporter assay confirmed Nrf2 activation by DN or KCl. Transcriptomic profiling using RNA-seq revealed that oxidation-reduction as a main gene ontology group affected by KCl. KCl indeed elevated the expression of classical Nrf2 downstream targets, including TXNRD1, AKR1C, AKR1B1, SRXN1 and G6PD. DN or KCl induced Nrf2 elevation is Ca^{2+} concentration dependent. We found that KCl decreased Nrf2 protein ubiquitination and extended the half-life of Nrf2 from 17.8 to 25.1

mins. Knocking out Keap1 blocked Nrf2 induction by K^+. Nrf2 induction by DN or KCl correlates with protection against ROS generation or loss of viability by H_2O_2 treatment. Our data support that high K^+ concentration in DN cardioplegic solution can induce Nrf2 protein and protect cardiomyocytes against oxidative damage.

Introduction

Cardiopulmonary bypass (CPB) surgery has undergone significant evolution since its inception in 1953 to its current state of being safe and effective[159-161]. Technical refinements over the past 6 decades have contributed to life saving of millions who suffer coronary artery disease or other disease requiring open heart surgery. As a result, cardiothoracic surgery has become a viable option even for older and sicker patients. For all CPB patients, especially the high-risk population, current myocardial protection strategies can be further improved to protect against procedure associated reperfusion injury[159, 162].

An essential adjunct to CPB is the ability to temporarily arrest the heart in order to provide a motionless operative site for surgical precision. This is achieved through perfusion of a cardioplegic solution with strict monitoring of the blood flow, blood pressure, blood volumes, body temperature, and biochemical parameters while maintaining the blood circulation via an extracorporeal device. The cardioplegic solutions have been

modified and revised prior to 1990s, for achieving controlled cardiac arrest with the ability of full restoring the contractile function post-operatively[163].

Cardioplegia induces cardiac arrest by modulating the membrane potential of cardiomyocytes. Diastolic arrest is induced by establishing a negative resting membrane potential, -65 to -35 mV, to cause a depolarized arrest[11], or greater than the negative resting membrane potential, around -90 mV, to provoke a polarized arrest. The depolarized arrest locks the transmembrane gradient at a voltage that exceeds the sodium channel threshold of -70 mV, therefore preventing sodium-induced action potential. In contrast, a polarized arrest maintains the membrane potential at or close to the resting membrane potential of myocardial cells[11, 164, 165]. An “extracellular” cardioplegic solution, such as Del Nido (DN), contains a relatively high concentration of K^+ to provide a depolarized diastolic arrest, whereas an “intracellular” cardioplegia, for example HTKCustodiol® has low Na^+ and Ca^{2+} content to induce a polarized diastolic arrest. Despite decades of history of using cardioplegia in cardiothoracic surgery, little has changed in the formulations since the last cardioplegic solution, DN, was developed in 1995.

Excluding the heart from blood circulation followed by restoration of blood flow during CPB causes procedure-associated myocardial reperfusion Injury. Ischemia occurs due to cessation of or suboptimal blood supply to the myocardium, resulting in uncoupling of the mitochondrial electron transport[166]. Transferring single instead of double

electrons to oxygen molecule in the mitochondrial Complex I or III causes formation of superoxide[167-169]. Biochemical deviations during the ischemic phase, such as intracellular acidosis, Ca^{2+} overload, electron transport chain uncoupling, and ROS generation, alter the integrity of mitochondria, leading to continuous production of ROS during reperfusion. Reperfusion produces an array of events, such as activation of xanthine oxidase or NADPH oxidases (NOXs) to further elevate ROS[170]. In addition, repeated passage of the patients' blood through the non-endothelialised extracorporeal circuit system triggers activation of polymorphonuclear leukocytes, which are a major source of ROS. Moreover, blood transfusion during surgery is associated with an increased ROS from abnormal erythrocytes due to blood storage. Therefore, multiple sources contribute to oxidative stress as a side effect of CPB.

The redox-sensitive transcription factor Nrf2 has been well established as the key regulator of the antioxidant and detoxification responses. Nrf2 protects against oxidative stress via upregulating the expression of genes containing the Antioxidant Response Element (ARE) in their promoters[147, 170]. The downstream targets of Nrf2 include antioxidant and detoxification genes[155, 170, 171]. Additionally, Nrf2 has been found to regulate genes participating in cell signaling, transcription, autophagy, anabolic metabolism, cell proliferation and organ development[170, 171]. Here we address whether or not cardioplegic solutions exhibit cardiac protection by examining their effect on Nrf2 induction.

Materials and Methods

Reagents

Cardioplegic solutions of Del Nido (DN), hyperkalemic (High K+, HK), hypokalemic (Low K+, LK), Histidine-Tryptophane-ketoglutarate (HTK, HTK Custodiol®, Bretschneider, Cardiolink Group, Barcelona, Spain) and Celsior (CS, Sanofi, Bridgewater, NJ) were collected as the leftovers from cardiothoracic surgery at the Banner-University Medical Center Tucson or Phoenix Children's Hospital. DN, HK and LK were made at Banner University of Arizona Hospital Pharmacy from Plasma-Lyte A (Baxter Healthcare Corporation, Deerfield, Illinois, USA). KCl and most reagents were obtained from Sigma Aldrich unless specified. MG132 was obtained from Calbiochem™.

Cell lines, Culture Conditions and Treatments

Human cardiomyocyte AC16 cells were purchased from the Millipore Sigma-Aldrich and cultured in Dulbecco's modified Eagle's medium mixed with F12 medium (DMEM/F12, GIBCO, ThermoFisher) supplemented with 12.5% fetal bovine serum (FBS, R&D Systems, Minneapolis, MN) and antibiotics (1% of 100 U penicillin/50g/mL streptomycin solution, GIBCO) for culture in a 5% CO_2 incubator at 37°C. The cells were seeded at the density of $0.3x10^6$ cells per well in 6-well plates and grown to 90% confluence before experimental use. To mimic their clinical use, 1.6 ml DN was mixed

with 0.4 ml DMEM/F12, 0.4 ml HK or LK was mixed with1.6 ml DMEM/F12. For HTK and Celsior, 2 ml pure crystalloid solution without mixing with DMEM/F12 was added into AC16 cells. For controls, the volume of cardioplegic solutions were replaced with PBS for the same ratio of mixing with DMEM/F12. Varying the ratio of PBS/DMEM/F12 did not induce Nrf2 or affect the induction of Nrf2 (data not shown).

Myocardial Tissue

Male C57BL/6 mice, age 6–8 weeks, were obtained from Charles River (Wilmington, MA), and were cared for according to the National Institutes of Health Guidelines for the Use of Laboratory Animals. The protocol for animal use was reviewed and approved by the University of Arizona Institutional Animal Care and Use Committee. After 1 week of acclimation from arrival, mice were divided randomly into 6 experimental groups (n = 4/group) for treatment of DMEM, HK, LK, DN, HTK, or CS cardioplegic solution.

Heparin (300 U/kg) was injected intraperitoneally over 5 mins before euthanasia by carbon dioxide (CO_2) asphyxiation. Immediately after, the thoracic cavity was exposed, and an incision was made in the right atrium using an iris scissor to create an outlet. A cardioplegic solution (5 ml) was introduced by intraventricular injection after clamping of the aorta, to produce deep myocardial tissue perfusion via the coronary vasculature. The heart was excised, minced into small pieces and immediately immersed in an ice-

cold cardioplegic solution on a shaking platform. Four hours later, the cardioplegic solution was removed and myocardial tissues were stored at -80°C.

Frozen myocardial tissues were grinded by mortar and pestle in a liquid nitrogen bath and fine powders (60 mg) were resuspended in 600 µl of RIPA buffer (Tris–HCl pH 8.0, 50 mM sodium chloride, 1% NP-40, 0.5% sodium deoxycholate, 0.1% SDS) containing freshly added 1x protease inhibitors (EDTA-free), 1 mM DTT and 20 µM MG132. The tissues were homogenized and transferred to a new tube for shearing by a bead mill homogenizer (Fisherbrand, Fischer Scientific). Following centrifugation at 13,000 rcf at 4 °C for 10 mins, the supernatants were collected for protein concentration measurements by Pierce BCA Protein Assay Kit (ThermoFisher). The tissues extracts were diluted 1:1 in 2X sample buffer [2% SDS, 10% glycerol, 50 mM Tris-Cl, pH 6.8, 0.002% bromphenol blue, 5% 2-mercaptoethanol), and then were boiled for 10 min. An equal amount of protein (60 µg) was loaded and separated by SDS-PAGE gel for Western Blot analysis.

Western Blotting

Cells were harvested in 1 x Laemmli Lysis buffer (2% SDS, 10% Glycerol, 62.5 mM Tris-HCl, pH 6.8, 0.002% Bromophenol blue, 5% 2-Mercaptoethanol) before boiling and sonicating. The Western blot was performed by loading the samples in a 7.5% SDS-polyacrylamide gel for electrophoresis. Separated proteins on the gel were transferred onto an Immobilon-P polyvinylidene difluoride (PVDF) membrane (Millipore, Bedford, MA)

using a rapid transfer system (BioRad, Hercules, CA). The membranes were blocked with 5% non-fat milk in Tris-buffered saline (TBS) with 0.1% Tween® 20 (TBST) for 1 hour (hr) at room temperature, followed by incubation overnight at 4°C on a shaker with primary antibodies (1:1000 dilution) in TBST containing 5% bovine serum albumin (BSA). The primary antibodies were against Nrf2 (sc-13032), Keap1 (sc-365626), GAPDH (sc-32233), TXNRD1 (sc-28321), AKR1C (sc-166297), AKR1B1 (sc-166918), SRXN1 (sc-514940), or G6PD (sc-373886, Santa Cruz Biotechnology). The primary antibody against FLAG or HA epitope was purchased from Sigma (catalog no. F7425) or Biolegend (catalog no. 901502). Following the removal of the primary antibodies and washes, the membrane was incubated 1 hr at room temperature with horse radish peroxidase conjugated secondary antibodies (anti-rabbit IgG-HRP, A9169-2ML; anti-mouse IgG-HRP, A9044-2ML, or anti-goat IgG-HRP, sc-2354, Sigma Aldrich) diluted 1:5000. Bound antibodies were detected with a SuperSignal Western Blot Enhancer, and the intensities of the bands were recorded with a BioRad ChemiDoc XRS system (Hercules, CA).

ARE Activity Assay

The pGL4.37 [luc2P/ARE/Hygro] vector was purchased from Promega. This construct contains 4 copies of ARE sequence derived from mouse glutathione S-transferase Ya gene. To generate a second reporter under the control of ARE from human NQO1 gene, pGL4.37 was modified by replacing the mGST-ARE sequence with 41 bp human NQO1 ARE sequence

(AATCCGCAGTCACAGTGACTCAGCAGAATCTGAGCCTAGGG). Either pGL4.37-mGST-ARE or pGL4.37-hNQO1-ARE vector was transfected into AC16 cells using Lipofectamine™ 3000 Transfection Reagent (Invitrogen). Stably transfected cells were selected by 200 μg/ml hygromycin B (Santa Cruz Biotechnology) in culture medium. For measurement of ARE activation, the stably transfected AC16 cells were seeded in 24-well plates and treated with DN, KCl or D, L-sulforaphane (Santa Cruz Biotechnology) for 16 hrs before harvesting in 100 μL/well 1× Passive Lysis Buffer (Promega). Cell lysates were used for detecting the firefly luciferase activity using Luciferase Reporter Assay System (Promega).

RNA-Seq

Total RNAs were extracted from control or 26 mM KCl treated AC16 cells at 16 hrs by RNeasy Kits (Qiagen). Sample quality control, transcriptome library preparation, library quality control, sequencing, raw data output, data quality control and bioinformatics analysis were performed by BGI Americas Corporation (San Jose, CA) and validated by R-programming. Raw reads were filtered to remove the reads containing the adaptor sequence, unknown nucleotides greater than 5%, or a quality score less than 15 by SOAPnuke software[172]. The clean reads were aligned to a reference genome GRCh38.p12 using HISAT[173] or to a reference transcriptome using Bowtie 2[174]. RSEM was used to calculate the gene expression level of each sample[175]. For detecting differential genes, the DESeq2 method was employed with Qvalue (Adjusted

Pvalue) ≤ 0.05[175]. The raw RNA-seq data has been deposited in GEO-Gene Expression Omnibus with a series entry number GSE221058, with a release date of January 1st, 2023.

RT-qPCR Analysis

Total RNA was isolated using Trizol reagent (Invitrogen). Each sample containing 1 µg RNA was converted to cDNA using a qScript cDNA SuperMix (95048, QuantaBio) for subsequent quantitative PCR (qPCR). The qPCR primer pairs were: Nrf2 forward, 5'-TTCCCGGTCACATCGAGAG-3'; Nrf2 reverse, 5'-TCCTGTTGCATACCGTCTAAATC-3'; GAPDH forward, 5'- GGAGCGAGATCCCTCCAAAAT-3'; GAPDH reverse, 5'-GGCTGTTGTCATACTTCTCATGG-3'. 18s rRNA forward 5′-TCAACTTTCGATGGTAGTCGCCGT-3′ and 18s rRNA reverse 5′-TCCTTGGATGTGGTAGCCGTTTCT-3′. The qPCR was performed using PowerUp SYBR Green (A25777, Applied Biosystems) on a BioRad CFX96 thermal cycler, with Nrf2 mRNA abundance calculated with the BioRad CFX Manager Software.

Isolation of Ribosomes

AC16 cells were treated with 10 µg/ml cycloheximide (CHX) for 10 minutes at 37°C before harvesting. After removal of the culture medium, cells were washed twice and scrapped off in ice cold PBS containing 100 µg/ml CHX. Cell pellets were collected by

spinning down at 500 ×g for 5 minutes and resuspended in 800 µl polysome lysis buffer containing freshly added 1x protease inhibitor (EDTA-free), 100 µg/ml CHX, 1 mM DTT, 20 µM MG132 and 100U/mL RNase Inhibitor. The cells were lysed by 5 seconds of vortex followed by sitting on ice for 10 minutes before centrifugation to collect cytosolic fractions. Cell debris, nuclei and mitochondria were removed by centrifugation at 16,000 ×g for 10 minutes. The supernatant was transferred onto the top of 10%+35% sucrose cushion and centrifuged at 32,000 rpm (Beckman Coulter Optima L-90K Ultracentrifuge) with a Beckman SW41 rotor for 2 hrs at 4°C. Ribosomal pellets at the bottom of centrifuge tubes were collected and resuspended in Trizol for RNA collection and RT-qPCR.

Immunoprecipitation to Measure Nrf2 Ubiquitination

Hela cells were transiently transfected with HA tagged ubiquitin and Flag tagged Nrf2 expression vector (pcDNA3). At 48 hrs after transfection when the culture reached 90% confluency, the cells were treated with 5 µM SFN or 26 mM KCl for 4 hrs in the presence of 10 µM MG132. After washing with ice-cold PBS, the cells in 35 mm dishes were lysed in 100 µL of SDS/TBS buffer (2% SDS, 0.5% deoxycholate, 10 mM Tris, pH 8.0, 150 mM NaCl, 1 mM DTT). The cell lysate was boiled for 10 mins to denature proteins, followed by sonication for 20 seconds. An aliquot (10 µL) of cell lysates was mixed with 360 µL of 1% Triton-X-100 in TBS containing 1 mM DTT for immunoprecipitation, with pre-clearing by 30 min incubation at 4°C with Protein A beads, followed by 30 mins centrifugation (14000 rpm at 4°C) to remove non-specific binding.

The cell lysates were incubated with an anti-HA antibody at 4°C for 2 hrs followed by overnight incubation with Protein A beads. The beads were washed with 0.5 M LiCl in TBS containing 1 mM DTT followed by two additional washed with 1% Triton-X-100/TBS with 1 mM DTT. Detached proteins from the Protein A beads were loaded onto 7.5% SDS-PAGE for Western blot to detect ubiquitin.

KEAP1 Knockout Using CRISPR-Cas9.

A CRISPR/Cas9 kit (sc-400190-KO-2, Santa Cruz Biotechnology) containing 3 different sequences of guide RNA (gRNAs) and an expression vector for GFP-Cas9 fusion protein was used for transfection of AC16 cells. GFP positive cells were sorted by flow cytometry (BD FACSAria™ III) to select for Cas9 positive expression. The cells were seeded at single cell density in 96-well plate for colony growth. Clonal cells were validated for Keap1 knockout by Western blot analysis.

ROS Detection

Intracellular ROS were detected using a hydroxy radical-sensitive fluorescent probe 2′, 7′-dichlorodihydrofluorescein diacetate (DCFH-DA). Following pretreatment of KCl or DN for 16 or 4 hrs, respectively, DCFH-DA was added to a final concentration of 10 μM for 30-mins incubation at 37°C in a 5% CO_2 incubator. The positive control 200 μM H_2O_2 was added to cells for recording ROS level by a fluorescence plate reader at an

Excitation wave length of 485 nm and Emission wavelength of 535 nm (CLARIOstar Plus, BMG Labtech, Ortenberg, Germany).

Cell Viability Assay

AC16 cells seeded in 6-well plates were pretreated with DN or KCl for 3 hrs and overnight, respectively, before treatment with 300 μM H_2O_2 for 1 hr in PBS. The cells in 6-well plates were fixed with 2% paraformaldehyde and stained with 0.1% Coomassie blue for recording cell morphology under an inverted microscope with 20x lens (Rebel, Echo, San Diego).

For metabolic activity, Cell Counting Kit-8 (CCK-8, APExBIO, Boston) was added to cells in 96- well plate for 2-hrs incubation under cell culture condition at 37°C in a 5% CO_2 incubator. The conversion of a water-soluble tetrazolium salt WST-8 to an orange-colored formazan by cellular dehydrogenase was quantified by measuring the absorbance at 450 nm using a microplate reader (CLARIOStarPlus, BMG Labtech, Offenburg, Germany).

Statistics

One way ANOVA was used followed by Dunnett's multiple comparisons test to identify statistical significance from the control group. When two samples were compared,

the student's t-test was used. Statistical analyses were performed by GraphPad 9. In all cases, $P < 0.05$ was considered statistically significant.

Results

Del Nido Cardioplegic Solution or KCl Induces Nrf2 Protein

A number of cardioplegic solutions have been developed for CPB surgery. Table 1 lists the contents of five commonly used cardioplegic solutions in the US and internationally. To evaluate whether these cardioplegic solutions induce Nrf2 protein, we treated AC16 human cardiomyocytes with these solutions at the ratio corresponding to their clinical applications. We found that DN induced elevation of Nrf2 protein significantly (Fig 2.1A). To demonstrate induction of Nrf2 occurring *in vivo*, mouse heart tissues were exposed to each of these five types of cardioplegic solutions. We found that DN was indeed capable of inducing Nrf2 protein elevation in the mouse heart tissues (Fig. 2.1B).

Con(mM)	HK	LK	DN	HTK	CS
Ratio (blood : crystalloid)	4:1	4:1	1:4	–	–
K^+	80 (19.6; 19.3)	30 (9.6; 9.3)	31 (25.7; 25.6)	10	15
Ca^{2+}	2.4 (2.5; 1.3)	0 (2.0; 0.8)	0 (0.5; 0.2)	0.02	0.25
Na^+	130 (138; 146.9)	160 (144; 152.9)	153 (152.4, 152.6)	15	100
Mg^{2+}	32 (7.2; 7.0)	3 (1.4; 1.2)	19.6 (15.9; 15.8)	4	13
Mannitol	–	–	18.15 (3.6; 3.6)	30	60
Lidocaine	0.427 (0.085; 0.085)	0.427(0.085; 0.085)	0.555(0.44; 0.44)	–	–
Histidine	–	–	–	198	30
Tryptophan	–	–	–	2	–
Ketoglutarate	–	–	–	1	–
Glutamate	–	–	–	–	20
Glutathione	–	–	–	–	3

Table 2. 1. Components of Common Cardioplegic Solutions.

The number represents the concentration of the stock with the final concentration in the blood or in DMEM/F12 listed in the parentheses. The final concentration in the blood was calculated based on the baseline blood concentration of K^+, Ca^{2+}, Na^+, or Mg^{2+} being 4.5 mM, 2.5 mM, 140 mM or 1 mM respectively. DMEM/F-12 contains 4.16 mM K^+, 1.05 mM Ca^{2+}, 151.08 mM Na^+ and 0.7 mM Mg^{2+}.

Activation of Nrf2 transcription factor by cardioplegic solutions was confirmed using an ARE reporter assay. We have obtained a luciferase reporter construct with 4 copies of ARE from a promoter sequence of mouse GST Ya gene. Since ARE sequence can be

polymorphic, we generated an additional reporter construct with 1 copy of ARE from 41 nucleotides long sequence of human NQO1 gene. Stably transfected cells were treated with cardioplegic solutions. With either form of ARE reporter constructs, elevated ARE activity was observed with DN (Fig 2.1C&D).

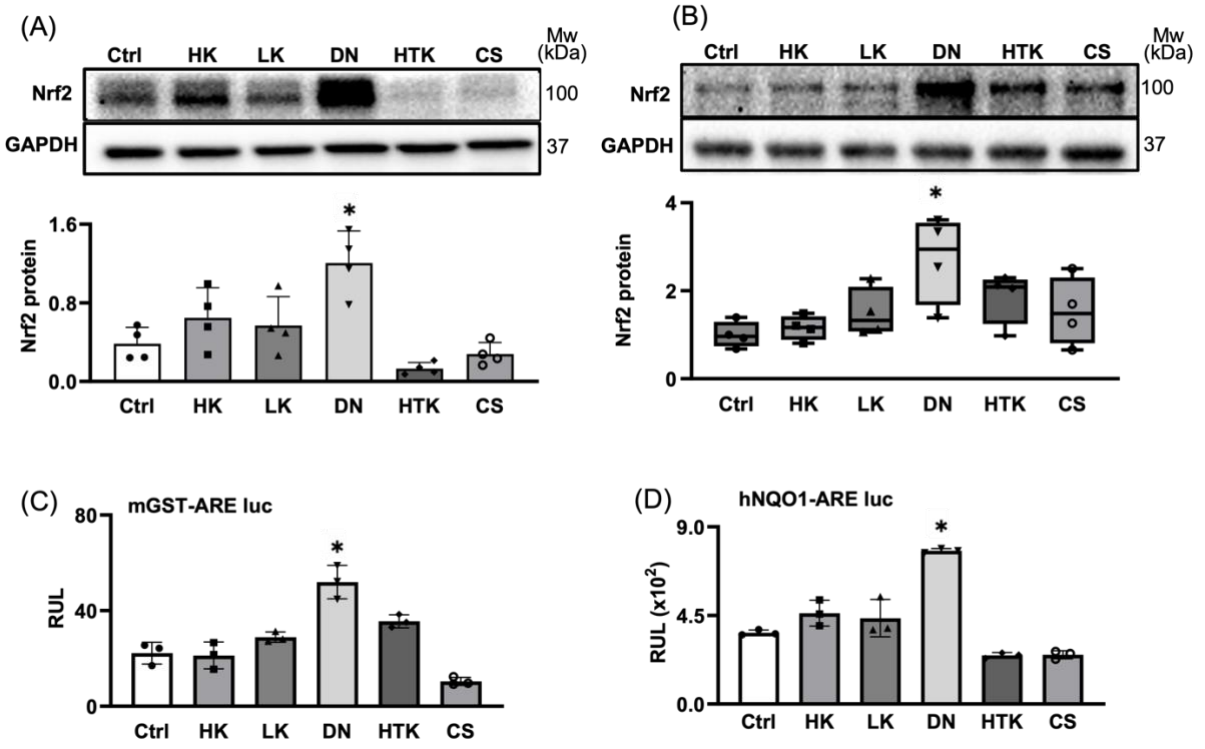

Figure 2. 1. Del Nido Cardioplegic Solution Induces Nrf2 Protein and Activates Nrf2 Transcription factor.

AC16 human cardiac myocytes were seeded in 6-well plates and cultured in DMEM/F12 containing 12.5% FBS for 3 days before treatment with a cardioplegic solution as described in the Methods. Following 3-hrs incubation under tissue culture condition, cells were harvested for immunoblotting using GAPDH as a loading control (A). Mouse hearts were perfused with a cardioplegic solution followed by 4-hrs incubation as described in the Methods for Western blot to detect Nrf2 protein using GAPDH as a loading control (B). AC16 cells stably transfected with pGL4.37-mGST-ARE luc vector (C) or pGL4.37- hNQO1-ARE luc vector (D) were exposed to cardioplegic solutions for 16 hrs before harvesting for Luciferase activity assay. The images of Western blot were from one representative experiment, with quantification of band intensities by NIH Image J from 3 independent experiments or 4 animals presented as means ± SD (A, B). The activity of Firefly luciferase was expressed as

means + SD from triplicate samples of one experiment representative of three. * indicates $P<0.05$ compared to control by students' t test.

DN cardioplegia contains KCl (K^+), $MgSO_4$ (Mg^{2+}), $NaHCO_3$ (Na^+), lidocaine (Lido), and mannitol (Mann)[44, 46]. The solution is made by diluting in Plasma-Lyte A (PL, containing 140 mM Na^+ from sodium chloride, sodium gluconate and sodium acetate trihydrate) for clinical use. Each of the components in DN was added to cells for identifying the one responsible for Nrf2 induction. We found that KCl alone is sufficient for inducing Nrf2 protein (Fig 2.2A).

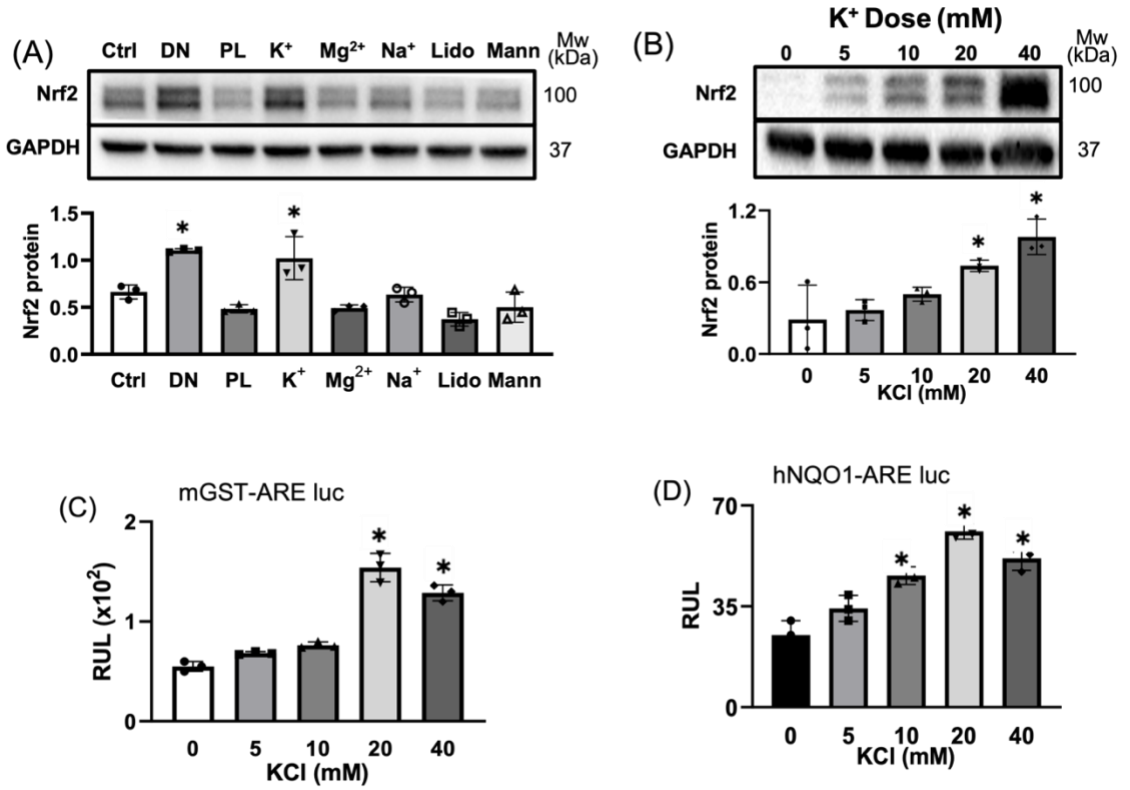

Figure 2. 2. KCl Induces Nrf2.

AC16 human cardiomyocytes were seeded in 6-well plates and cultured in DMEM/F12 containing 12.5% FBS for 3 days before treatment. Cells were treated 4 hrs with DN, PlasmaLyte-type A (PL, containing 140 mM sodium from NaCl, sodium gluconate, sodium acetate trihydrate), 26 mM KCl (K+), 9.63 mM Mg2+ MgCl2 (Mg2+), 153 mM NaOH (Na+), 130 mM Lidocaine (Lido), or 18.1 mM Mannitol (Mann, A), or with KCl at indicated dose for 4 hrs (B). Cells were harvested at the end of the treatment for Western blot using GAPDH as a loading control (A, B). The image from one Western blot experiment representative of three is shown, whereas the bar graphs represent means ± SD of band intensities quantified by NIH Image J from three independent experiments (A, B). AC16 cells with stably transfected mouse GST-ARE-luc or human NQO1-ARE-luc were seeded in 24-well plates for KCl treatment at the indicated dose

for 16 hrs before harvesting for luciferase assays (C, D). The activity of Firefly luciferase was expressed as means + SD from triplicate samples of one experiment representative of three (C, D). * indicates $P<0.05$ compared to control by student's t test.

A dose dependent increase in Nrf2 protein level was observed with KCl from 5 to 40 mM (Fig 2.2B). Activation of Nrf2 transcription factor by KCl was confirmed using two different versions of ARE reporters. KCl induces a dose dependent activation of either mGST-ARE or hNQO1-ARE in stably transfected AC16 cell line (Fig 2.2C&D). When treated with 40 or 26 mM KCl, with 26 mMKCl concentration equivalent to that in DN cardioplegia, AC16 cells showed elevation of Nrf2 starting at 30 mins, reached to the peak at 6 hrs, and returned to the baseline by 24 hrs with 26 mM KCl treatment (Fig 2.3A&B, whereas AC16 cells showed elevation of Nrf2 starting at 60 mins, reached to the peak at 4 hrs with 40 mM KCl. (Fig 2.3C&D). ARE activity time course shows an expected delay in activation of Nrf2 transcription factor from induction of Nrf2 protein (Fig 2.4A&B).

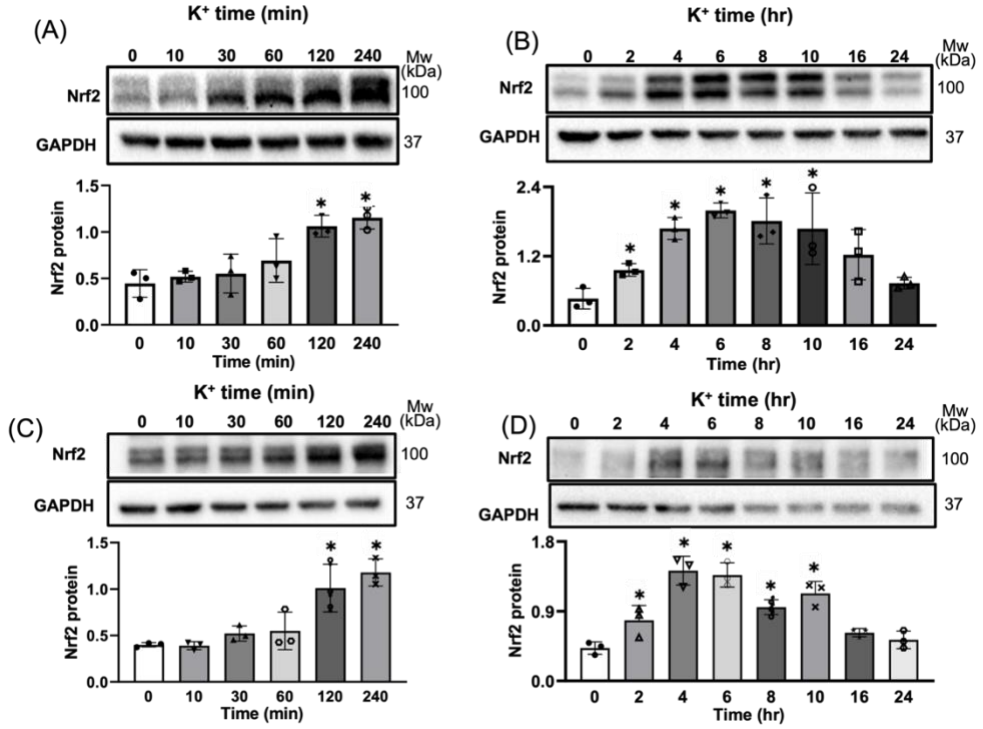

Figure 2. 3. Time Course of Nrf2 Induction by KCl.

AC16 human cardiac myocytes were seeded in 35 mm tissue culture dishes with DMEM/F12 containing 12.5% FBS for 3 days before treatment with 40 (A, B) or 26 Mm (C, D) KCl for the indicated time point. Cells were harvested for Western blot to measure Nrf2 protein level using GAPDH as a loading control. The results from one experiment representative of three are shown, whereas the bar graphs represent means ± SD of band intensities quantified by NIH Image J from three independent experiments. * indicates $P<0.05$ compared to control (0) group by one-way ANOVA.

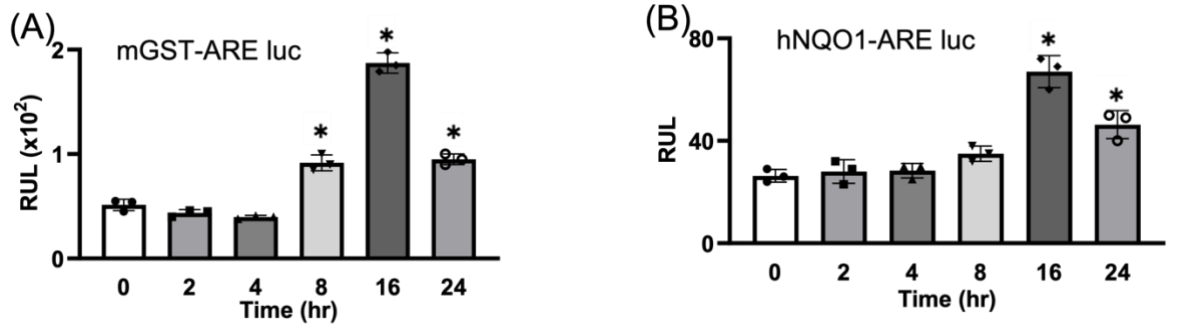

Figure 2. 4. Nrf2 Induction by KCl.

Stably transfected GST-ARE-luc (A) or human NQO1-ARE-luc (B) AC16 cells were seeded in 24-well plates for 26 mM KCl treatment for indicated time before harvesting for luciferase assay.The activity of Firefly luciferase was expressed as means ± SD from triplicate samples of one experiment representative of three. * indicates $P<0.05$ compared to control by one-way ANOVA.

RNA-sequencing technology was employed to determine the transcriptomic landscape due to KCl treatment. Gene ontology (GO) biological process enrichment analysis indicated that the Oxidation-Reduction process was among the GO terms having the highest number of genes altered by KCl treatment (Fig 2.5A). The heatmap revealed that many genes in this category are Nrf2 targets (Fig 2.5B), supporting that activation of Nrf2 serves as a main molecular event of KCl treatment. The Volcano mapping of differentially expressed genes indicated that Nrf2 downstream targets, including TXNRD1, AKR1C3, AKR1B1, NQO1, and AKR1C1, were among those having the highest fold changes (Fig 2.5C). Activation of Nrf2 transcription factor by KCl treatment was further validated by measuring Nrf2 downstream genes using Western blot. Fig 2.5D shows that

KCl indeed induced elevation of TXNRD1, AKR1C, AKR1B1, SRXN1 and G6PD at the protein level. Therefore, ARE reporter assay, RNA-seq or Nrf2 downstream gene measurements have demonstrated that KCl indeed activates Nrf2 transcription factor.

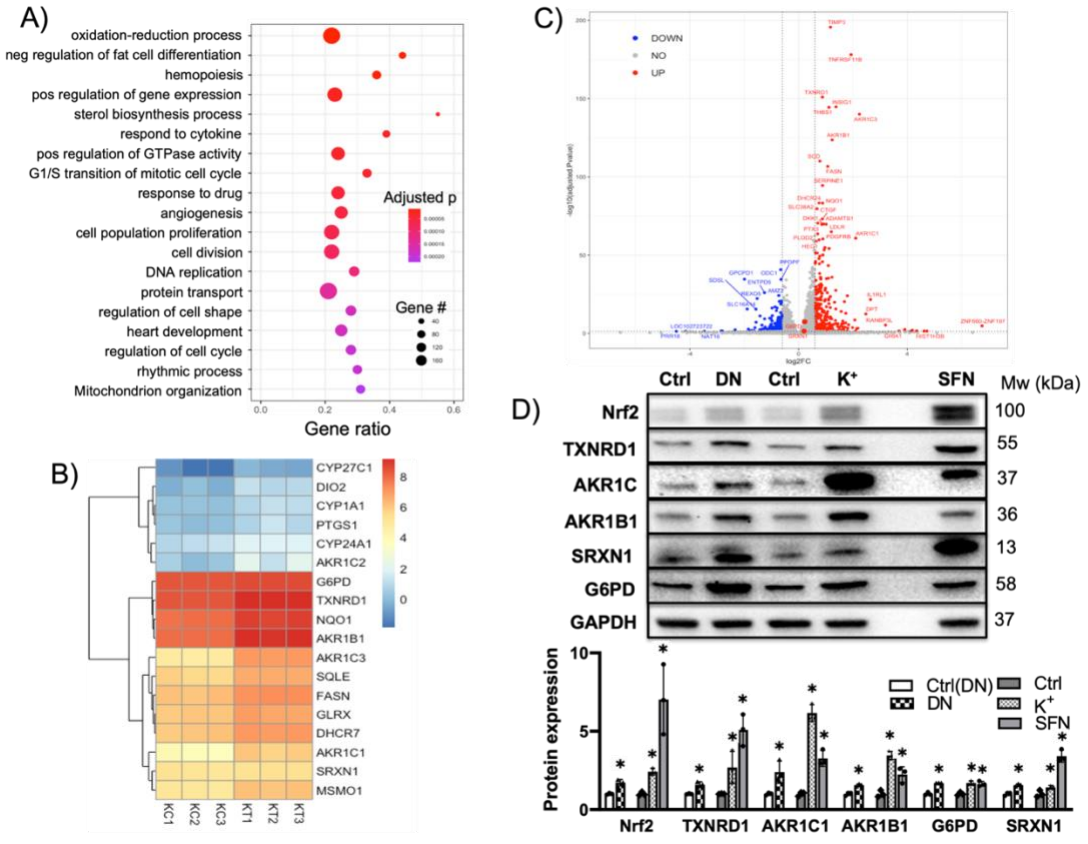

Figure 2. 5. Differentially Expressed Genes Due to KCl Treatment.

AC16 human cardiomyocytes were seeded in 6-well plates and cultured in DMEM/F12 containing 12.5% FBS for 3 days before treatment with 26 mM KCl for 16 hrs. Cells were harvested for total RNA isolation from three independent experiments for RNA-Seq. Gene Oncology (GO) for Biological Process Enriched terms are shown in a dot plot (A). The heatmap representing the expression of 18 up-regulated genes annotated to oxidation-reduction process (B). Overall changes of gene expression are shown in a volcano plot (C). Red dots, except SRXN1 or G6PD, indicate significantly up-regulated genes, whereas blue dots show down regulated genes, with $-\log_{10}$ (Q value) > 1.3 and $\log_2$ (fold change) > 0.6, which correspond to adjusted P value > 0.05 and fold change > 1.5. The expression of Nrf2 downstream genes at the protein level was measured by Western blot at 16 hrs after 4 hrs treatment with DN or 26 mM KCl

(D). Sulforaphane (5 mM) treatment for 16 hrs was included as a positive control (D). The intensities of the bands were quantified by NIH Image J and normalized to that of GAPDH, and presented as means ± SD from three independent experiments. * indicates significant difference ($P<0.05$) from corresponding controls for each gene as determined by student's t test.

Ca^{2+} Dependent Induction of Nrf2 by K^+

High K^+ concentration from cardioplegic solutions activates L-type Ca^{2+} channel, causing Ca^{2+} influx from extracellular sources such as the blood or cardioplegia. In our cell culture experiments, the culture medium contains 1.05 mM Ca^{2+}. To address whether Nrf2 induction by KCl requires Ca^{2+} influx, we treated cells with DN or KCl in the absence of Ca^{2+}. We found that in Ca^{2+} free medium, DN or KCl could not induce Nrf2 protein (Fig 2.6A&B). When Ca^{2+} was added back in a dose dependent manner to the Ca^{2+} free medium, induction of Nrf2 protein by KCl was restored with increasing concentration of Ca^{2+} from 0.125 to 0.5 mM (Fig 2.6B). At the highest concentration, 8 mM, an inhibition of Nrf2 induction was observed (Fig 2.6B). Adding Ca^{2+} alone to Ca^{2+} free medium without KCl, did not cause an induction of Nrf2 (data not shown). Ca^{2+} chelator EDTA and cell permeable EGTA-AM were added to the complete medium to confirm Ca^{2+} dependency for Nrf2 induction (Fig 2.6C).

We next addressed whether L-type Ca^{2+} channel blockers, Verapamil and Nicardipine, blocked Nrf2 induction by KCl. The data show that either Verapamil or

Nicardipine was able to block Nrf2 induction by KCl (Fig 2.6D). These results suggest that Nrf2 induction by KCl is Ca^{2+} dependent, mediated by Ca^{2+} influx via L-type Ca^{2+} channel in cardiomyocytes.

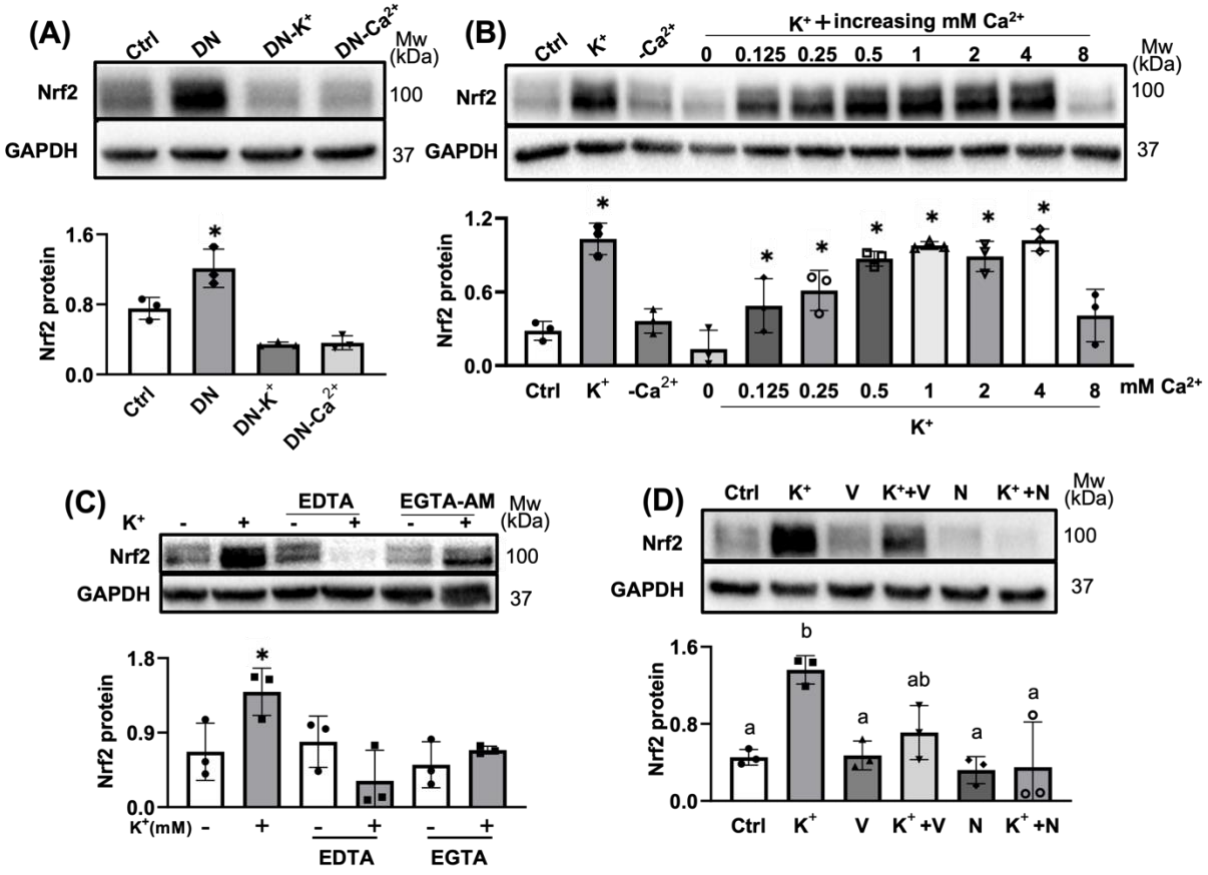

Figure 2. 6. Ca^{2+} Dependent Induction of Nrf2 by DN or KCl.

AC16 human cardiac myocytes were plated in 6-well plates and cultured in DMEM/F12 containing 12.5% FBS for 3 days before treatment of DN with or without K^+ or Ca^{2+} (A), or for co-treatment of 26 mM KCl with various doses of Ca^{2+} as indicated in Ca^{2+} free medium (B). Cells were pre-treated with 4 μM EDTA or 0.6 μM EGTA-AM for 30 mins before 4 hrs treatment with 26 mM KCl (C). Alternatively, cells were pre-treated with 2 mM Verapamil (V) and 80 mM Nicardipine (N) for 10 mins followed by 4-hrs treatment with 26 mM KCl (D). Cells were harvested for Western blot analysis using GAPDH as a loading control, with the image of one experiment representative of three shown. The bar graph represents band intensities as quantified by NIH Image J with means ± SD

from three independent experiments. * indicates significant difference (P<0.05) from the control as determined by student's t test Letters indicate statistical significance (P<0.05) as determined by One-way ANOVA. The means labeled with a is significant different from that labeled b, whereas ab indicates no significant difference between the means labeled with a or b.

KCl Prolongs the Half-life of Nrf2 Protein by Inhibition of Ubiquitination

An elevation of Nrf2 protein can result from an increase of Nrf2 gene transcription, translation, or a decrease of Nrf2 protein degradation. We first measured total Nrf2 mRNA levels and Nrf2 mRNA association with polysomes, in order to determine whether K^+ induced an increased transcription or *de novo* Nrf2 protein translation. Lack of Nrf2 mRNA increase in total RNA pool (Fig2.7A) and no increase of Nrf2 mRNA association with ribosomes (Fig 2.7B) pointed our attention to Nrf2 protein stability. To measure Nrf2 protein half-life, new protein synthesis was inhibited with cycloheximide (CHX) at 4 hrs after KCl treatment. The cells were collected from 0 to 120 mins to determine the time point when Nrf2 protein disappeared. We found that the half-life of Nrf2 was extended from 17.8 min in untreated cells to 25.1 min in the cells exposed to KCl (Fig 2.8A&B). This suggests that KCl treatment increased Nrf2 protein stability.

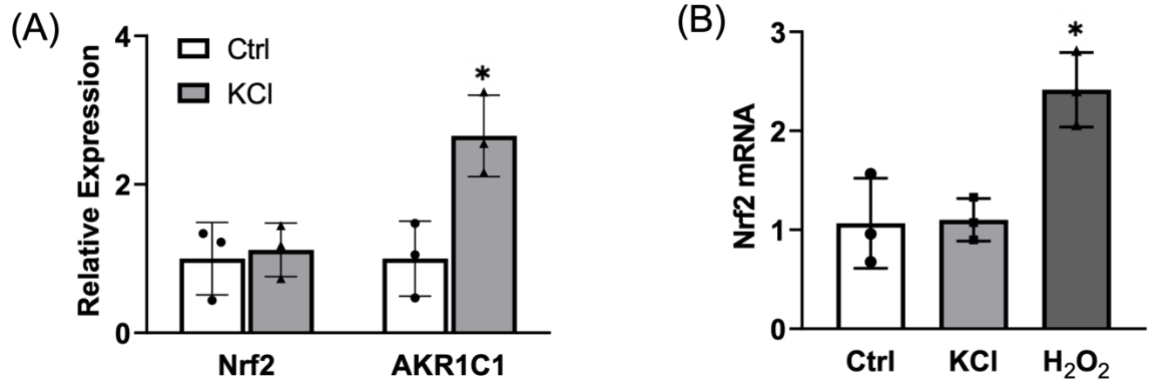

Figure 2. 7. Lack of Nrf2 Transcript Increase or Nrf2 mRNA Association with Ribosomes by KCl.

AC16 human cardiomyocytes were seeded in 6-well plates (A) or 100 mm dishes (B) with DMEM/F12 containing 12.5% FBS for 3-days culture before treatment with 26 mM KCl for 4 hrs. Total RNA was extracted from cell lysates. Nrf2 mRNA level was determined by real-time PCR and corrected by GAPDH mRNA level in the corresponding group, with AKR1C1 mRNA level serving as a positive control (A). After isolation of ribosomes from cell lysates by ultracentrifugation, RNA was extracted for real-time PCR, with 18S rRNA as a loading control (B). In the same experiment, a sample from 100 μM H_2O_2 treatment for 10 mins and harvested at 1 hr was included as a positive control (B). * indicates significant difference (P<0,05) from control group

To measure Nrf2 ubiquitination status due to the treatment of KCl, we performed immunoprecipitation experiments to pull down Nrf2 protein from the cell lysates, and then detected ubiquitin by immunoblotting using SFN as a positive control. The levels of ubiquitinated Nrf2 decreased when AC16 cells were treated with KCl compared to the control (Fig2.8C). The degree of decrease by KCl treatment was similar to that of SFN (Fig 2.8C).

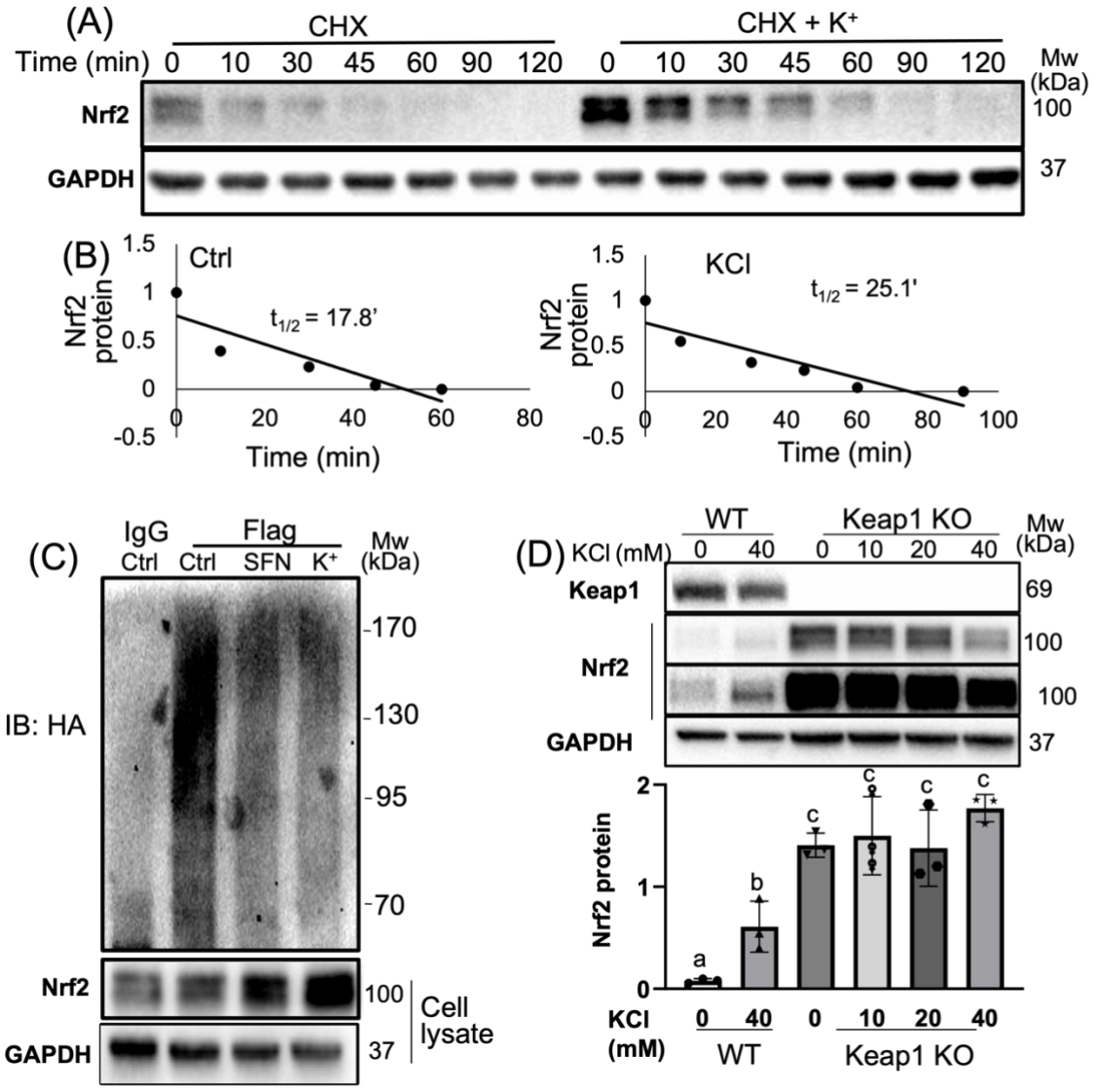

Figure 2. 8. KCl Increases Nrf2 Protein Stability and Decreases Nrf2 Ubiquitination.

AC16 human cardiac myocytes were seeded in 35 mm tissue cultured dishes with DMEM/F12 containing 12.5% FBS for 3-days culture before treatment with 26 mM KCl for 4 hrs, followed by 100 μg/mL cycloheximide (CHX) treatment for indicated time before harvesting for Western blot to measure Nrf2 with GADPH serving as a loading control (A). The relative Nrf2 expression was plotted over the time after adding CHX

for calculation of the half-life by a linear regression (B). AC16 cells were cotransfected with expression vectors for HA-Ubiquitin (HA-UB) and Flag-Nrf2. The transfected cells were treated with 26 mM KCl for 4 hrs using 5 μM SFN as a positive control, along with 10 μM MG132 (C). Immunoprecipitation was carried out using cell lysates containing 200 mg protein and anti-Flag antibodies. Ubiquitin was detected by anti-UB antibodies via Western blot (C). The level of endogenous Nrf2 protein is shown with GAPDH as a loading control (C). Keap1 knockout (KO) AC16 cells were established by CRISPR Cas9 technique (D). Three clones of Keap1 KO cells were treated with KCl at indicated doses for 4 hrs. Cell lysates were analyzed by Western blot to determine the level of Keap1 and Nrf2 proteins with GAPDH as a loading control. The band intensities from three clones were quantified by NIH Image J and presented as means $\pm$ SD, with letters indicate statistical significance ($P<0.05$) as determined by One-way ANOVA (D). The means labeled with a is significant different from that labeled b or c, whereas b indicates significant difference from the means labeled with c.

Keap1 is known as the main modulator of Nrf2 protein stability due to its binding to Nrf2 and recruitment of culin3 complex of ubiquitin E3 ligase for Nrf2 ubiquitination. It is commonly known that Keap1 oxidation disables Nrf2 ubiquitination and therefore inhibits Nrf2 protein degradation. Using CRISPR-cas9 to knock out Keap1 gene, we tested whether this abolished Nrf2 induction by KCl. With 3 clones of Keap1 knockout, KCl could no longer induce Nrf2 in any clone (Fig 2.8D). This suggests that Nrf2 induction by KCl is Keap1 dependent.

Del Nido or KCl Protects Against ROS Generation and Cell Death

It is well known that ROS causes Nrf2 induction. Ca^{2+} dependency of K^+ induced Nrf2 suggests the possibility of ROS generation by KCl, since high concentrations of intracellular Ca^{2+} can cause mitochondrial depolarization, permeability transition and therefore increasing ROS production. We measured $^{\bullet}OH$ generation by KCl treatment using DCFH-DA, but did not find elevation of DCF fluorescence, whereas the positive control 200 μM H_2O_2 showed a time dependent increase of $^{\bullet}OH$ (Fig 2.9A). Because KCl or DN induces Nrf2, we asked whether K^+ alone or DN is able to prevent H_2O_2 from generating $^{\bullet}OH$. When pretreating cells with 5, 10, 20 and 40 mM of KCl or DN, respectively, we found a dose dependent reduction of H_2O_2 induced $^{\bullet}OH$ generation (Fig 2.9B) by KCl and an inhibition of H_2O_2 induced $^{\bullet}OH$ generation by DN (Fig 2.9C)

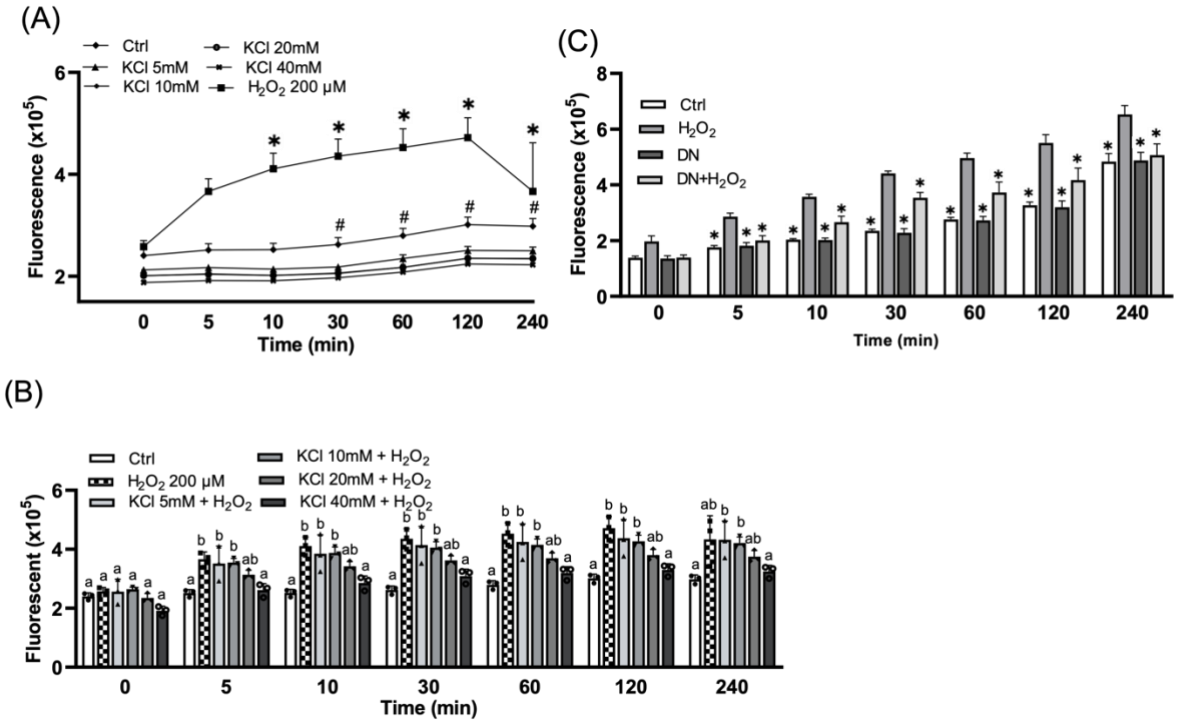

Figure 2. 9. DN or KCl Protects Against ROS Generation.

AC16 human cardiac myocytes were seeded in 96-well plates and cultured in DMEM/F12 containing 12.5% FBS for 3 days. DCFH-DA (10 mM) was added to cells for 30 mins before treatment of 26 mM KCl or DN for recording of ROS generation over 4 hrs with 200 mM H_2O_2 treatment as a positive control (A,B). Following overnight incubation with KCl at an indicated dose or 4 hrs incubation with DN, cells with KCl treatment alone (A) or with addition of 200 mM H_2O_2 (B) or with DN (C)were loaded with DCFH-DA for recording ROS generation by a fluorescence microplate reader. * indicates significant difference ($P<0,05$) from control or K^+ treated cells (A), whereas # indicates significant difference ($P<0.05$) between control and KCl treated cells (), and letters indicate statistical significance ($P<0.05$, B),the means labeled with a is significant different from that labeled b, whereas ab indicates no significant difference from the means labeled with a or b. * indicates significant difference ($P<0,05$) from H_2O_2 treated group (C) as determined by One-way ANOVA.

To demonstrate the functional significance of Nrf2 induction by DN cardioplegia or K^+, we tested cytoprotective capacity of DN and KCl. Neither DN nor KCl (5 to 40 mM) produced cytotoxicity as determined by cell morphology or CCK8 cell metabolism assay (Fig 2.10A-C). AC16 cells lost about 40% viability as measured by CCK8 assay following 3- hrs exposure to 300 μM H_2O_2 in PBS and 24 hrs of recovery (Fig 2.10A). DN or KCl pretreatment resulted in protection against the loss of cell viability (Fig 2.10B&C). AC16 cells maintain viability as measured by CCK8 assay following overnight exposure to various concentrations of KCl up to 60 mM (Fig 10D). Therefore, induction of Nrf2 by DN or KCl correlates with a cytoprotective effect.

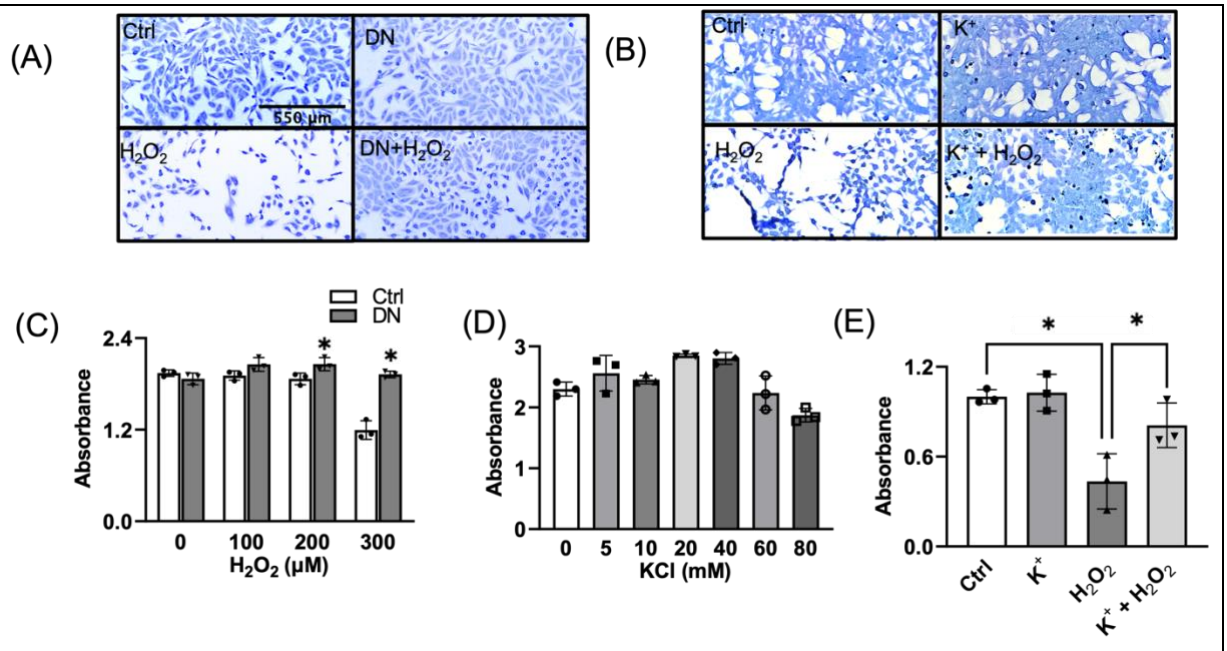

Figure 2. 10. KCl Protects Against Cytotoxicity.

To measure the protective effect, the cells were exposed to 300 µM or indicated dose of H_2O_2 for 3 hrs following 3- hrs pretreatment with DN cardioplegia or with 26 mM KCl. Cell morphology was recorded under a light microscope after fixing cells in 4% formalin buffered phosphate and stained with 0.1% Coomassie blue for 10 mins (A, B). Metabolic activity was examined by Cell Counting Kit-8 (CCK-8) after 24 hrs recovery in fresh DMEM (C-E). The bar graphs represent the means ± SD from three independent experiments. * indicates statistically significant difference between the H_2O_2 verse corresponding KCl+H_2O_2 treated groups ($P< 0.05$) as determined by One-way ANOVA (D, E).

Discussion

In this study, we have found that DN cardioplegic solution induced Nrf2 protein and activation of Nrf2 transcription factor in AC16 human cardiomyocytes. Tracing the ingredients in DN lead to the discovery of K+ at the concentration above 5 mM capable of Nrf2 protein induction. ARE luciferase reporter assays revealed Nrf2 activation by DN and KCl. KCl mediated Nrf2 activation has been validated by RNA-seq, which revealed multiple Nrf2 downstream genes induced by KCl exposure. Nrf2 downstream genes, including TXNRD1, AKRs, G6PD and SRXN1, have been validated for induction by KCl at the protein levels. Nrf2 induction is Ca2+ dependent, since depleting Ca^{2+} blocked Nrf2 elevation by KCl or DN treatment. Knocking out Keap1 prevented KCl from elevating Nrf2 protein. We have detected an extended half-life of Nrf2 protein and decreased Nrf2 protein ubiquitination by KCl treatment in wild type cells. Nrf2 induction by DN cardioplegia or KCl protected cells against ROS production or loss of viability by H2O2 treatment. Our data support the hypothesis that high KCl concentration in DN cardioplegic solution activates Nrf2, serving to protect cardiomyocytes from oxidant toxicity.

How cardioplegia exhibits cardiac protective effect has not been addressed at the cellular level prior to this study. The ability to induce Nrf2 serves as a measure of cardiac protection, since Nrf2 encodes a transcription factor controlling the expression of antioxidant and detoxification genes. Our results showed that DN cardioplegia is most effective for Nrf2 induction. There is evidence supporting that DN cardioplegia offers

better myocardial preservation compared to other conventional cardioplegia in adult cardiac surgery[50, 176-180]. Clinical complications of open-heart surgery include arrhythmias, vasospasm, bleeding, thrombosis, and a generalized inflammatory response[181, 182]. A prospective randomized trial comparing DN with St. Thomas cardioplegia concluded that DN cohorts had reduced incidence of postoperative ventricular arrhythmia, shorter ICU stay and less complications from CPB surgery[183]. A retrospective comparative study revealed a shortened cross clamp or CPB time with DN compared to multi-dose blood cardioplegia[184]. Six systematic reviews with meta-analysis have found that DN is a safer choice compared to other blood cardioplegia for routine adult and pediatric cardiac surgery[178, 179, 185-188]. The DN groups showed reduced aortic cross-clamp or CPB time, required less volume of cardioplegia, and had decreased incidence of intraoperative defibrillation[178, 179, 185-188]. Additionally, postoperative cardiac troponin release was lower in patients with DN[178, 187], supporting the cytoprotective effect of DN.

Our data revealed that $Ca2^{+}$ plays an indispensable role in K+ induced Nrf2 protein elevation. It appears that K^{+} induces Nrf2 only in the presence of an optimal range of extracellular Ca^{2+}. Higher concentration (8 mM) of Ca^{2+} inhibits Nrf2 induction by K^{+}, providing a possible explanation for the weak Nrf2 induction by HK cardioplegic solution, as HK delivers high concentrations of K^{+} as well as high concentration of Ca^{2+}. It is perhaps not a coincidence that Ca^{2+} dependence matches with the optimal Ca^{2+} concentration for cardioplegic solutions as reported earlier[189-191].

High K^+ concentration in cardioplegic solutions effectively arrest the heart during open heart surgery by depolarizing the sarcolemma and maintaining the membrane potential between -65 to -35 mV. A consequence of such hyperkalemic depolarized arrest is an increase of intracellular Ca^{2+}[164]. Intracellular Ca^{2+} overload due to membrane depolarization contributes to the development of ventricular dysfunction [192]. Cytosolic Ca^{2+} elevation also triggers opening of the mitochondrial membrane permeability transition pore (mPTP), leading to mitochondrial depolarization, loss of coordinated electron transport, and increases in superoxide production[170].

Myocardial Ca^{2+} accumulation plays an important role in the pathogenesis of myocardial injury, partially, due to the onset of ischemic contracture[193-195]. Administration of Ca^{2+} free cardioplegia during ischemic phase, and subsequent reperfusion by resuming the blood flow leads to a Ca^{2+} paradox[196]. This "Ca^{2+} paradox" has been linked to ventricular dysfunction and massive cellular destruction due to necrosis[196]. The damage associated with Ca^{2+} overload or Ca^{2+} paradox during ischemic reperfusion are the main issues for post-operative complications. To minimize Ca^{2+} overload, extracellular Ca^{2+} concentrations need to be controlled at a safe range.

It is commonly accepted that Keap1 plays a main role in the regulation of Nrf2 protein stability and the activity of Nrf2 as a transcription factor [197-199]. Under physiological conditions, Nrf2 protein is kept at a low basal level through degradation mediated by Keap1 dependent ubiquitination. This contributes to a short half-life of Nrf2 protein, 10-15 mins. When Keap1 becomes covalently modified by oxidation or alkylation, or removed by autophagy, Nrf2 is relieved from ubiquitination, resulting in an increase in Nrf2 half-life to 40-60 mins. Here, we found that KCl extends the half-life of Nrf2 protein from 18 mins to 25 mins. Although Keap1 knockout experiment revealed the dependency of Keap1 for Nrf2 induction by KCl, how KCl regulates Keap1 and Nrf2 interaction remains to be determined.

Keap1 recruits Cul3/Rbx1 ubiquitin ligase complex for transferring ubiquitin from a E2 ubiquitin ligase to Nrf2[200]. Keap1 can be removed by phosphorylated p62 via autophagy involving ATG13. There is evidence that phosphorylated ATG13 is a substrate of calcineurin, a calcium and calmodulin dependent serine/threonine protein phosphatase[201]. Since non-phosphorylated form of ATG13 participates in autophagosome formation, activation of calcineurin due to K^+ coupled Ca^{2+} influx may lead to an increase in autophagy to remove Keap1. Elevated cytosolic Ca^{2+} activates Ca^{2+} calmodulin-dependent kinase, which in turn activates AMP-activated protein kinase (AMPK) and induces autophagy[202]. As a result, Keap1 removal by autophagy disables Nrf2 ubiquitination and prolongs the half-life of Nrf2 protein.

A standard Nrf2 inducer, such as SFN, extends the half-life of Nrf2 protein from 10-15 mins to 40-60 mins. The fact that KCl only increased the half-life of Nrf2 to 25 mins indicates therapeutic possibilities for further Nrf2 induction by a pharmacological agent. Most Keap1 modifiers are oxidants or electrophilic agents, which may exhibit toxic or off target effects. A non-cytotoxic agent for effective Nrf2 induction, such as a peptide or peptidomimetics that fully disrupts the interaction of Keap1 with Nrf2, may serve well for expanding the potential of Nrf2 mediated cardiac protection. Strategies for cardiac protection are important to reduce CPB surgery complications.

Limitation

One limitation of this study is that it was conducted in vitro using AC16 human cardiomyocytes. while these cells provide a useful model for studying the effects of KCL and DN cardioplegic solution on Nrf2 induction and downstream gene expression, which could not fully possess the characters of cardiomyocytes. It is better to validate the regulation of NRf2 by K+ or DN in primary isolated or iPS cardiomyocytes. Additionally, the study focused on the effects of KCl and DN cardioplegic solution on Nrf2 activation and downstream genes but did not examine the potential effects of other components in the solution or potential interactions with other signaling pathways. Future research could explore these factors to further elucidate the mechanisms underlying Nrf2 activation and cardioprotective effects.

Chapter III: HYPERKALEMIC OR LOW POTASSIUM CARDIOPLEGIA PROTECTS AGANIST RRDUCTION OF ENERGY METABOLISM BY OXIDATIVE STRESS

Abstract

Open-heart surgery is often an unavoidable option for the treatment of cardiovascular disease and prevention of cardiomyopathy. Cardiopulmonary bypass surgery requires manipulating cardiac contractile function via the perfusion of a cardioplegic solution. Procedure-associated ischemia and reperfusion (I/R) injury, a major source of oxidative stress, affects postoperative cardiac performance and long-term outcomes. Using large-scale liquid chromatography–tandem mass spectrometry (LC-MS/MS)-based metabolomics, we addressed whether cardioplegic solutions affect the baseline cellular metabolism and prevent metabolic reprogramming by oxidative stress. AC16 cardiomyocytes in culture were treated with commonly used cardioplegic solutions, High K^+ (HK), Low K^+ (LK), Del Nido (DN), histidine–tryptophan–ketoglutarate (HTK), or Celsior (CS). The overall metabolic profile shown by the principal component analysis (PCA) and heatmap revealed that HK or LK had a minimal impact on the baseline 78 metabolites, whereas HTK or CS significantly repressed the levels of multiple amino acids and sugars. H2O2-induced sublethal mild oxidative stress causes decreases in NAD, nicotinamide, or acetylcarnitine, but increases in glucose derivatives, including glucose 6-P, glucose 1-P, fructose, mannose, and mannose 6-P. Additional increases include metabolites of the pentose phosphate pathway, D-ribose-5-P, L-arabitol, adonitol, and xylitol. Pretreatment

with HK or LK cardioplegic solution prevented most metabolic changes and increases of reactive oxygen species (ROS) elicited by H2O2. Our data indicates that HK and LK cardioplegic solutions preserve baseline metabolism and protect against metabolic reprogramming by oxidative stress.

Introduction

Cardiovascular disease is the principal cause of mortality worldwide. Most cardiac patients suffering from coronary artery disease have plaque buildup in the wall of the coronary arteries. With advancements in medical technology, an occluded coronary artery can be re-opened by the percutaneous coronary intervention technique. Open-heart surgery remains an option of treatment, especially for multivessel disease, diffuse or complex coronary disease, with or without valvular disease[5]. The development of cardiopulmonary bypass (CPB) using a heart–lung machine to sustain systematic circulation during the operation has revolutionized cardiac surgery and reduced the mortality of patients with coronary artery disease. However, approximately 67% of CPB patients have post-operative complications, including atrial fibrillation, pulmonary dysfunction, or renal failure[203]. One contributing factor to these types of organ injury is procedure-associated ischemia and reperfusion (I/R), which produce oxidative stress.

In order to achieve surgical precision, cardiac contraction is minimized by the perfusion of a cardiac solution. This procedure causes controlled cessation of blood flow

to the myocardium, i.e., myocardial ischemia. Upon completion of the surgical procedure, cardiac contraction and blood flow are resumed. Either ischemia or reperfusion results in an increased production of reactive oxygen species (ROS)[169, 170]. Ischemia results in incomplete electron transport, impairment of mitochondrial respiration, and mitochondrial ROS production[199]. Reperfusion activates xanthine oxidase and NADPH oxidase in cardiac cells, which already inherit impaired mitochondria from ischemia, causing further increases of ROS[170]. Elevated levels of lipid peroxidation products such as malon-dialdehyde, have been detected in the myocardium of patients following I/R from the coronary artery bypass graft surgery (CABG)[204]. Preventing oxidative stress is expected to reduce surgical-procedure-associated complications.

Cardioplegic solutions along with induced hypothermia during open heart surgery are designed to prevent many detrimental effects of ischemia and reperfusion[205-207].The most commonly used cardioplegic solutions include modified St. Thomas, i.e., highpotassium (high K, HK) and low potassium (low K, LK), Del Nido (DN), and Histidine-Tryptophane-Ketoglutarate Custodiol® (HTK). Celsior (CS) was developed as acardioplegia as well as a solution for donor organ preservation for heart transplant[208]. The HK, DN, and CS cardioplegic solutions, also known as extracellular cardioplegia, are hyperkalemic, delivering K+ via the coronary vasculature to reach the localized concentration of 15 to 25 mM[9]. Such high concentrations of K+ cause the resting membrane potential of the myocardium to change from −80 mV to −50 mV[11]. When the

membrane potential reaches −50 mV, the voltage-dependent Na+ channels are inactivated, preventing the Na+ induced spike and rapid propagation of the action potential, thereby causing depolarized diastolic cardiac arrest. LK is used following the administration of HK to maintain the diastolic arrest. HTK, also called intracellular cardioplegia, is low in Na+. Depletion of Na+ in the extracellular spaces produces a hyperpolarization of the plasma membrane of cardiomyocytes, causing cardiac arrest in diastole[23]. Although these cardioplegic solutions have been widely used for open-heart surgery worldwide, little is known about the impact of these agents on the metabolism of cardiomyocytes.

Metabolomics provides an effective method for measuring overall chemical intermediates or metabolic state[209]. The application of metabolomics will not only help to identify new biomarkers for metabolic complications associated with cardioplegia, but also allow us to provide scientific evidence for the choice of an ideal cardioplegic solution. In this study, using large-scale liquid chromatography tandem mass spectrometry (LC-MS/MS) based metabolomics and AC16 human cardiomyocytes, we evaluated the metabolic impact of 5 commonly used cardioplegic solutions and addressed whether any of these solutions prevent metabolic changes by oxidative stress.

Material and Methods

Reagents

Cardioplegic solutions of HK, LK, DN, HTK (HTK Custodiol®, Bretschneider, Cardiolink Group, Barcelona, Spain) and CS (Sanofi, Bridgewater, NJ) were collected as the leftovers from cardiothoracic surgeries at the Banner-University Medical Center Tucson or Phoenix Children's Hospital. HK, LK and DN were made at Banner University of Arizona Hospital Pharmacy from Plasma-Lyte A (Baxter Healthcare Corporation, Deerfield, Illinois, USA).

Cell lines, Culture Conditions and Treatments

AC16 human cardiomyocytes were purchased from the Millipore Sigma-Aldrich and cultured in Dulbecco's modified Eagle's medium mixed with Ham's F12 (DMEM/F12, GIBCO, ThermoFisher) supplemented with 12.5% fetal bovine serum (FBS, R&D Systems, Minneapolis, MN) and antibiotics (1% of 100 U penicillin/50g/mL streptomycin, GIBCO) for culture in 5% CO_2 incubator at 37°C with weekly subculture. The cells were seeded at a density of 0.3x10 6 cells per well in 6-well plates and grown to 90% confluence before experiments.

Cells were treated with cardioplegic solutions according to the ratios used clinically. HK or LK (0.4 ml) was mixed with 1.6 ml DMEM, whereas DN (1.6 ml) was mixed with 0.4 ml DMEM. For HTK or CS, 2 ml pure crystalloid solution was added to AC16 cells. Cells

in 6-well plates were serum starved overnight in 0.5%FBS/DMEM/F12, treated with a cardioplegic solution for 3 hours (hrs), followed by exposure to 200 μM H_2O_2 for 1 hr.

Metabolomics

The samples were collected for LC-MS/MS metabolomics as described[210, 211]. Following a quick rinse with phosphate buffered saline (PBS), cells were placed in1 mL/well of 8:2 (v:v) methanol: H_2O for 30-mins incubation on dry ice. This serves to quench metabolism and extract the metabolites. The cells were scrapped from the culture plates and transferred to centrifuge tubes. Another 0.7 mL/well of 8:2 (v:v) methanol: H_2O was added to the plates on the dry ice to scrape and combined with the corresponding centrifuge tubes. Cell free extracts were collected after 10-mins centrifugation at 13,000 rpm under 4 C. The soluble fraction of the extracts was dried at 4 C using a speed vacuum. The samples were processed for LC-MS/MS as described.

LC-MS/MS analyses were performed using an Agilent 1290 UPLC-6490 QQQ-MS system (Santa Clara, CA). Each sample was injected twice by an auto-sampler set at 4℃, 10 μL for analysis using a negative ionization mode or 4 μL for analysis using a positive ionization mode. Both chromatographic separations were performed in the hydrophilic interaction chromatography mode on a Waters XBridge BEH Amide column (150×2.1 mm, 2.5 μm particle size, Waters Corporation, Milford, MA), with a flow rate of 0.3 mL/min and

the column compartment temperature of 40℃. The mobile phase contains Solvent A (10 mM ammonium acetate, 10 mM ammonium hydroxide in 95% H_2O/5% ACN) and Solvent B (10 mM ammonium acetate, 10 mM ammonium hydroxide in 5% H_2O/95% ACN). After an initial 1 min isocratic elution of 90% Solvent B, the percentage of Solvent B decreased to 40% by t = 11 min. Solvent B was maintained at 40% for 4 min (t = 15 min) before gradually returning to 90%, in preparation for next injection. The mass spectrometer was equipped with an electrospray ionization source, and targeted data acquisition was performed in the multiple-reaction-monitoring (MRM) mode. An Agilent Masshunter Workstation software (Santa Clara, CA) was used to control the operation of the LC-MS/MS system, whereas the extracted MRM peaks were integrated using the Agilent MassHunter Quantitative Data Analysis (Santa Clara, CA).

Statistical Analysis

Changes in metabolites or pathways between control versus treatment were analyzed using the web-based software MetaboAnalyst 5.0 (https://www.metaboanalyst.ca/MetaboAnalyst/ModuleView.xhtml). PCA, heatmap clustering, and pathway analysis overview of altered metabolic profiles were analyzed using MetaboAnalyst 5.0. Bar graphs were presented as means ± standard deviations (SD) of relative abundance of metabolites and analyzed via one way ANOVA for multiple comparisons with GraphPad Prism 9 software. When two samples were compared, the student’s t-test was used. In all cases, p < 0.05 was considered statistically significant.

Results

Effects of Cardioplegic Solutions on Metabolome

Table 3.1 lists the components of 5 cardioplegic solutions commonly used in the US and internationally for CPB surgeries (HK, LK, DN, and HTK) or cardiac transplant (CS). To evaluate the impact of these solutions on cellular metabolism, we treated AC16 cardiomyocytes according to their clinical applications, with final concentration of each component listed in Table 1. The length of treatment is 4 hrs, mimicking the average CPB surgical time. A total of 94 metabolites were detected among the control

	Ratio (Blood: Crystalloid)	Type \ Con (mM)	K^+	Ca^{2+}	Na^+	Mg^{2+}	Mannitol	Lidocaine	Histidine
Blood cardioplegia	4:1	HK	19.3	1.32	146	6.8	–	0.085	–
	4:1	LK	9.32	0.84	152	1.0	–	0.085	–
	1:4	DN	21.63	0.21	152.4	15.78	3.63	0.444	–
Crystalloid cardioplegia	–	* HTK	10	0.02	15	4	–	–	198
	–	** CS	15	0.25	100	13	60	–	30

Table 3. 1. Key Components of Common Cardioplegic Solutions.

* HTK contains 2 mM tryptophan and 1 mM ketoglutarate; ** CS contains 20 mM glutamate and 3 mM glutathione. The concentrations were calculated on the basis of the dilution of HK, LK, and DN in DMEM/F12.

(Ctrl) and cells treated with a cardioplegic solution, as shown in the heatmap (Fig 3.1A). When compared to Ctrl, a similar pattern of metabolites was found in HK and LK

treated groups, but HTK and CS treated cells exhibited a clear difference, showing decreases of 12 amino acids and 4 sugars (Fig 3.1A). The metabolic profile of DN treated cells is closer to that of Ctrl, HK or LK (Fig 3.1A, B). The overall metabolic profiles as summed by the principal component analysis (PCA) revealed that HK or LK cardioplegia treated cells showed no significant difference from the Ctrl (Fig 3.1B).

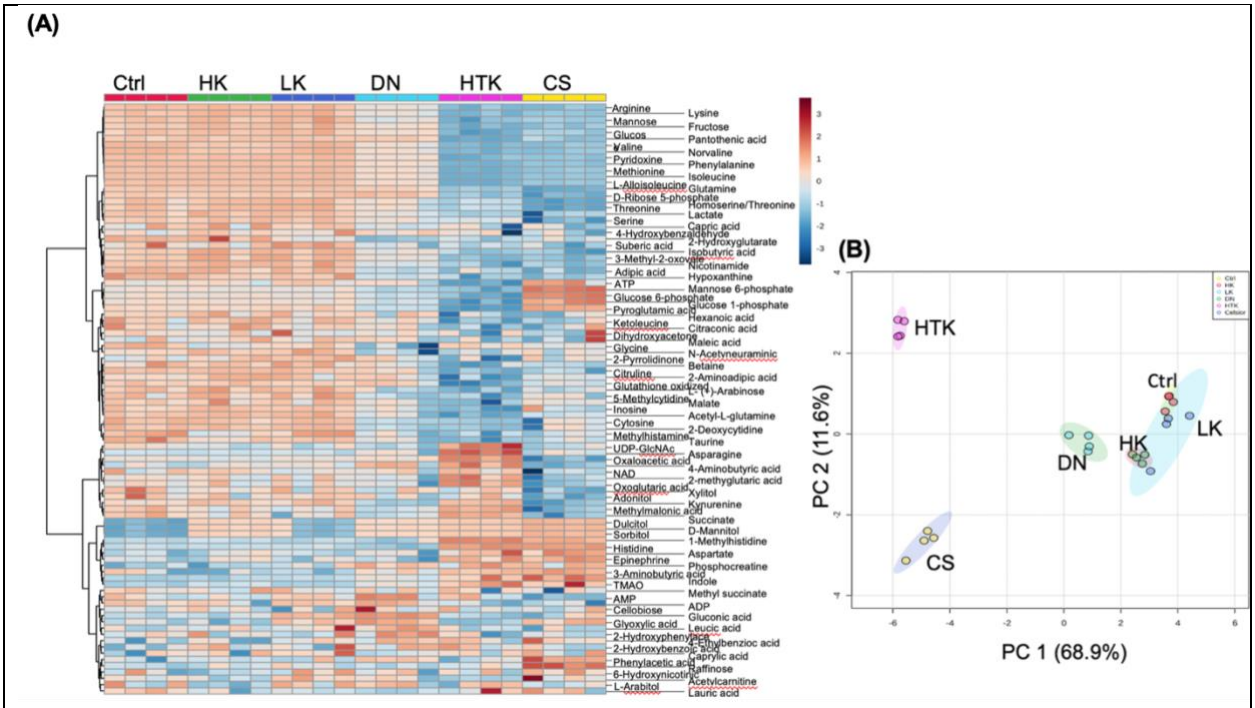

Figure 3. 1. Effects of 5 Cardioplegic Solutions on Cellular Metabolism.

AC16 human AC16 human cardiac myocytes were seeded in 6-well plates and cultured in DMEM containing 12.5% FBS. When reaching 90% confluency, cells were placed in 0.5% FBS/DMEM/F12 for overnight serum starvation. The cells were treated with HK, LK, DN, HTK, and CS for 4 h before extraction of aqueous metabolites from cell lysates for LC-MS/MS-based metabolomics. The overall metabolic profile differences between control (Ctrl) and cells treated with a cardioplegia solution (n = 4) are shown in the heatmap (A) and by a principal component analysis (PCA) score plot (B).

PCA indicates significant deviations in the profile of HTK or CS treated cells (Fig3.1B). The differences in the metabolites are displayed in a volcano plot (Fig 3.2A, B). The pathway analyses showed that HTK and CS caused significant perturbations of the pathway of: 1) Alanine, aspartate & glutamate metabolism; 2) Histidine metabolism;

3) Arginine biosynthesis; 4) tricarboxylic acid (TCA) cycle; 5) Aminoacyl-tRNA biosynthesis; 6) Valine, leucine & isoleucine biosynthesis (Fig 3.2C, D). CS also affected glyoxylate and dicarboxylate metabolism pathway (Fig 3.2D). Those results indicate that unlike HTK or CS, HK or LK cardioplegic solution preserves the basal metabolic profile.

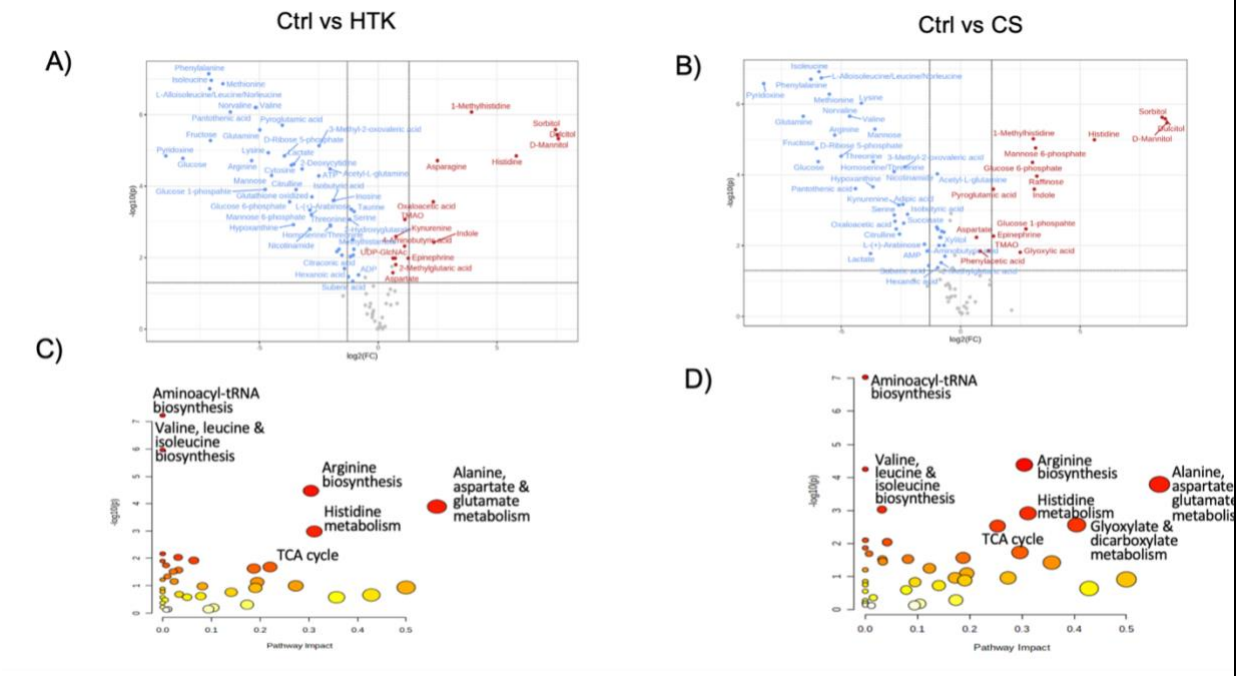

Figure 3. 2. Metabolites and Metabolic Pathways Altered by HTK and CS.

AC16 cells seeded in 6-well plates were used for the collection of aqueous metabolites as described in Figure 1 for LC-MS/MS-based metabolomics. A total of 67 or 65 metabolites showed statistically significant differences as determined by Student's t-test ($n = 4$, $p < 0.05$) between control versus HTK or CS and are displayed in the volcano plots (A,B) generated by the MetaboAnalyst 5.0 software. The altered metabolic pathways are displayed with the x-axis representing the pathway impact score computed from pathway topological analysis and the y-axis being the -log10 of the p-value obtained from pathway enrichment analysis (C,D). The metabolic pathways perturbed by the HTK and CS treatment are displayed in the gradient from yellow to red, reflecting the p-value from statistical analysis, as shown in the y-axis, from non-significant (≤1 for −log10, $p \geq 0.1$, light yellow) to significant (≥1 but ≤2 for −log10, $p \leq 0.01$ to $p \geq 0.001$, orange) to highly significant (≥2 for −log10, $p \leq 0.0001$, red). The sizeof the circles reflects the number of metabolites altered in the metabolic pathway (C,D).

Metabolic Profiles of Oxidative Stress and Impact of Cardioplegic Solutions

The dose of 200 μM H_2O_2 was chosen here for metabolomics experiments, since it does not cause detectable cytotoxicity, as measured by cell morphology, cell number, or general metabolic activity via CCK-8 assay[212, 213]. This dose mimics the level of oxidants in the myocardium during I/R, 10 – 30 mM, based on the common belief that intracellular oxidants are 10-100 fold lower than extracellular H_2O_2 concentration[214].

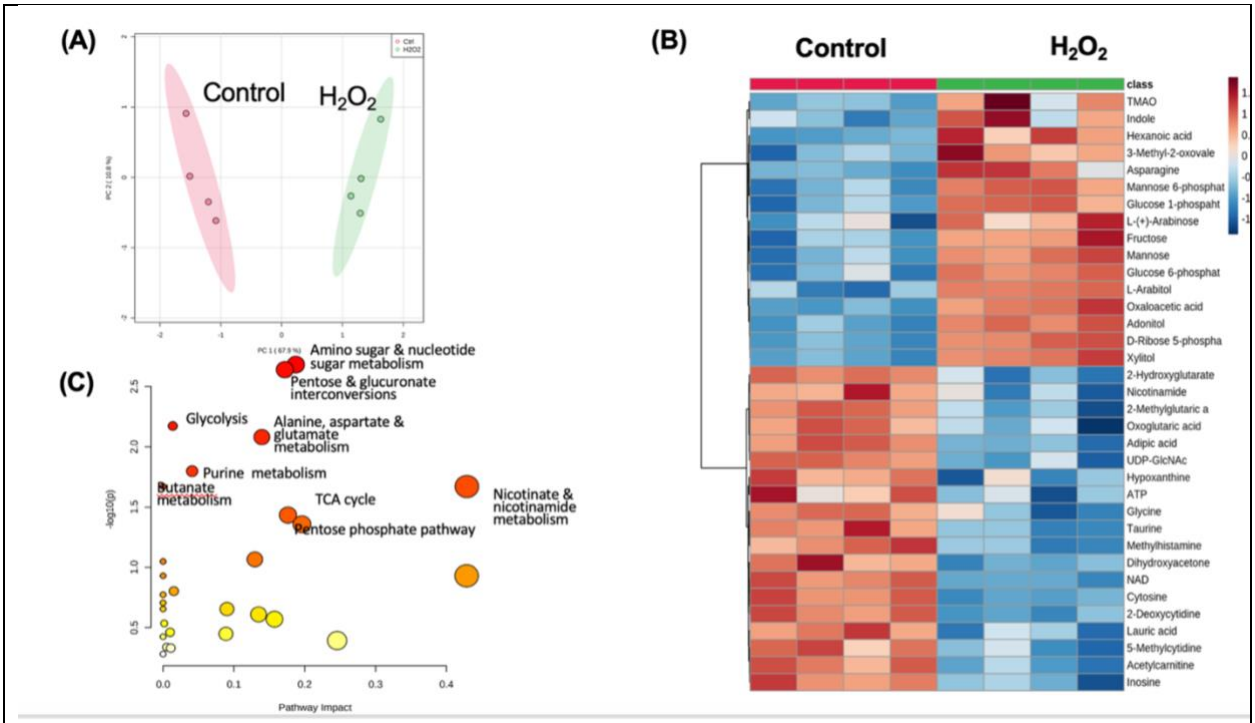

Figure 3. 3. Metabolites and Metabolic Pathways Altered by H2O2 treatment.

AC16 human cardiac myocytes were seeded in 6-well plates and cultured in DMEM containing 12.5% FBS. When reaching 90% confluency, cells were serum-starved in 0.5% FBS DMEM/F12 overnight. The cells were treated with 200 μM of H2O2 for 1 h before extraction of aqueous metabolites by 80% methanol from cell lysates for LC-MS/MS-based metabolomics. The overall metabolic profile differences between ctrl and H2O2-treated cells are shown by the PCA score plot (A). The heatmap shows significant differences ($n = 4$, $p < 0.05$) in 35 metabolites between Ctrl and H2O2-treated cells (B). The altered metabolic pathways by H2O2 treatment are displayed with the x-axis representing the pathway impact score computed from pathway topological analysis and the y-axis being -log10 of the p-value obtained from the pathway enrichment analysis (C). Metabolic pathway analyses by MetaboAnalyst 5.0 software depict the impact of H2O2 treatment, with the x-axis, y-axis, color, or size of the circle reflecting the information as described in Figure 2C.

A significant separation of metabolic profiles was discovered between Ctrl and H_2O_2 treated group by PCA (Fig 3.3A). The heatmap shows 35 metabolites that were significantly up- (16) or down (19) -regulated as determined by the student's t-test with FDR correction (Fig 3B). Among the significantly decreased metabolites are NAD and acetylcarnitine (Fig 3.3B). Increased metabolites include glucose derivatives, glucose 6-P, glucose 1-P, fructose, mannose and mannose 6-P. Several sugar alcohols in the pentose phosphate pathway, also increased, including L-arabitol, adonitol, ribosoe 5-P and xylitol (Fig 3.3B). Pathway analyses revealed that significant alteration of 9 metabolic pathways by H_2O_2 treatment ($P<0.05$): 1) nicotinate and nicotinamide metabolism; 2) pentose phosphate pathway; 3) TCA cycle; 4) amino sugar and nucleotide sugar metabolism; 5) pentose and glucuronate interconversions; 6) alanine, aspartate and glutamate metabolism; 7) purine metabolism; 8) glycolysis; and 9) Butanate metabolism(Fig 3.3C).

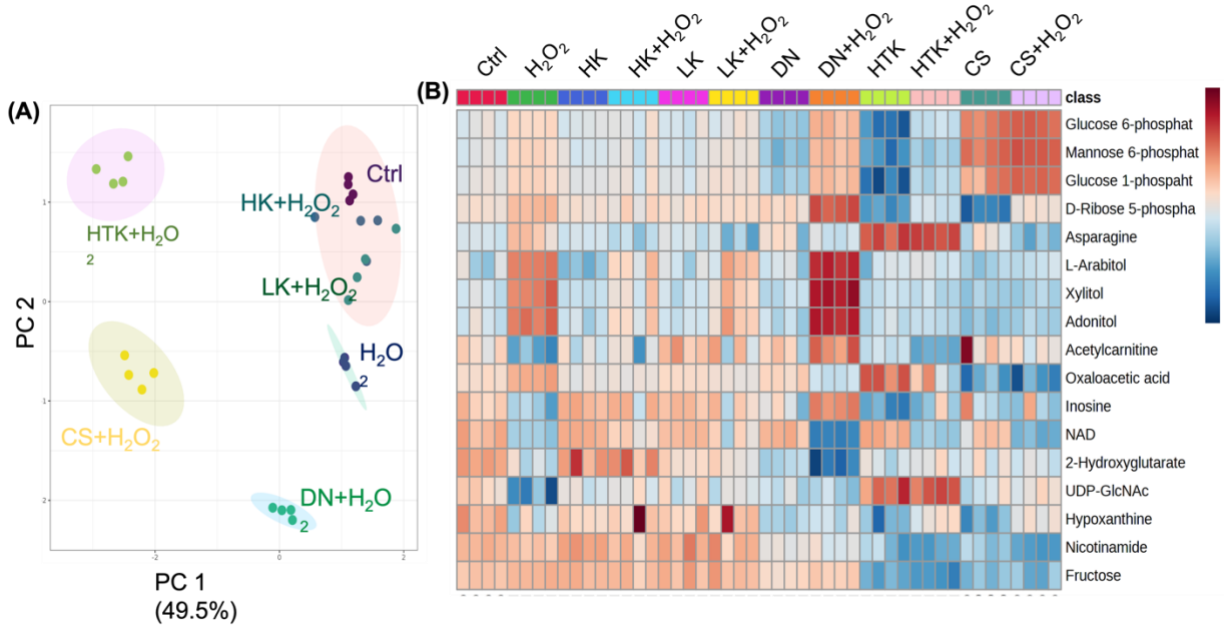

Figure 3. 4. Effect of Cardioplegic Solutions on Metabolites Changed by H_2O_2 Treatment.

AC 16 cells at 90% confluency were serum-starved in 0.5% FBS DMEM/F12 overnight. The cells were treated with HK, LK, DN, HTK, or CS for 3 h as described in the Methods section, followed by exposure to 200 μM of H_2O_2 for 1 h before extraction of aqueous metabolites by 80% methanol for LC-MS/MS-based metabolomics. K-means clustering shows the overall metabolic profile altered by H_2O_2 and pretreatment with each cardioplegia solution ((A), n = 4). The heatmap displays the metabolites in the 9 metabolic pathways significantly altered by H_2O_2 treatment for all groups of comparisons ((B), n = 4).

Compared to Ctrl or H_2O_2 treated cells, pretreatment with HK or LK was able to shift the metabolic profile of H_2O_2 treated cells towards that of Ctrl (Fig 3.4A). Among the 17 metabolites of 9 significantly changed pathways due to H_2O_2 treatment, HK or LK pretreatment was able to block H_2O_2 from inducing increases or decreases of the majority

of these metabolites (Fig 3.4B). Specifically, the decrease of NAD or acetylcarnitine was attenuated by HK or LK treatment (Fig 3.5A, B). H_2O_2 induced increases of glucose 6-P, glucose 1-P and mannose 6-P, and oxaloacetic acid were inhibited by HK or LK (Fig 3.5B, C). The increases of the metabolites in the pentose phosphate pathway, i.e., Xylitol, L-Arabitol, Adonitol, and D-Ribose 5-P due to H_2O_2 treatment were prevented by HK or LK (Fig 3.5D). This data indicate the capacity of HK or LK for protection against metabolic shift by oxidative stress.

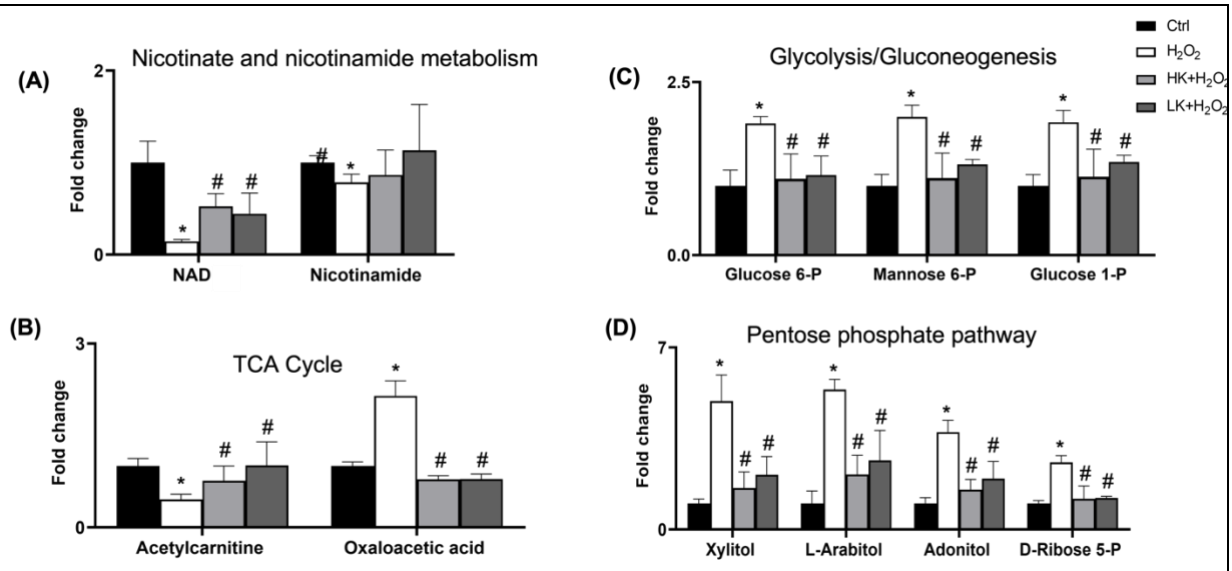

Figure 3. 5. HK or LK Protects against H_2O_2 from Inducing Changes in the Metabolites.

The metabolites altered by H_2O_2 treatment belonging to nicotinate and nicotinamide metabolism, TCA cycle, glycolysis/gluconeogenesis, and pentose phosphate pathway were analyzed for the protective effect of HK or LK cardioplegia solution. * indicates significant difference (n = 4, $p < 0.05$) between control and H_2O_2-treated cells, whereas # indicates significant difference (n = 4, $p < 0.05$) between HK or LK with H_2O_2 treatment in comparison with H_2O_2 treatment alone. These data were analyzed for the significant differences by one-way ANOVA using GraphPad Prism 9 software.

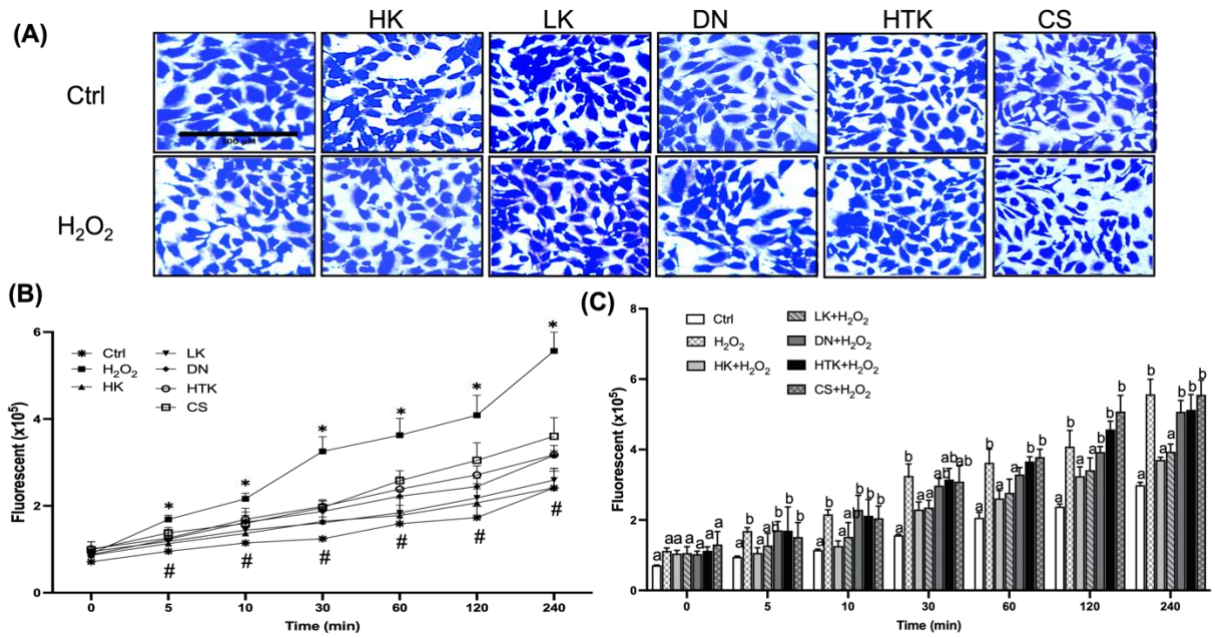

Figure 3. 6. Effects of Cardioplegic Solutions on Cell Morphology and ROS Generation.

AC16 cells were seeded in 6-well (**A**) or 96-well plates (**B**,**C**) for pretreatment with cardioplegic solutions for 3 h. After 1 h exposure to 200 μM H_2O_2, cell morphology was recorded under an inverted light microscope after fixing and staining in 0.1% Coomassie blue (**A**). Following pretreatment with a cardioplegic solution, the cells were incubated with 100 μM DCFH-DA for 30 min before recording ROS generation with 200 μM H_2O_2 treatment by a fluorescence microplate reader (**B**,**C**). The bar graphs represent the means ± SD from 4 replicates of one representative experiment (**C**). * indicates a significant difference (p < 0.05) of H_2O_2-treated cells from Ctrl or a cardioplegic-solution-treated cells, whereas # indicates a significant difference (p < 0.05) of Ctrl from DN-, HTK-, or CS-treated cells (**B**). indicates significant difference from H_2O_2-treated cells (**C**). These data were analyzed for the significant differences by one-way ANOVA using GraphPad Prism 9 software.

Discussion

Using LC-MS/MS-based metabolomics, we have evaluated the impact of 5 cardioplegic solutions on cellular metabolism and the metabolic alteration by oxidative stress. Our data indicate that HK and LK cardioplegia solutions did not cause significant changes in the baseline metabolic profile, whereas HTK and CS induced significant metabolic shift. Induction of oxidative stress by H_2O_2 treatment resulted in decreases of NAD and acetylcarnitine but increases of glucose 6-P, glucose 1-P, mannose 6-P, oxaloacetic acid and 4 sugar alcohols from the pentose phosphate pathway. Our data suggest that HK and LK cardioplegic solutions can provide protection against alterations in energy metabolism due to oxidative stress at the cellular level.

The cardioplegic solutions are capable of supporting an extended period of myocardial ischemia with organ preservation during cardiac surgery. The choice of which cardioplegic solution is based on the preference and experience of each surgeon. HK, LK and DN, the so-called blood cardioplegia, require isogenic mixing of patient's blood for their clinical application, whereas HTK or CS is perfused into the myocardium as a pure crystalloid. Experimental or clinical evidence suggests that blood cardioplegia is superior over the crystalloids for cardiac protection[44, 179, 215-219] . Among many advantages of blood cardioplegia are oxygen carrying, continuous supply of metabolic substrates, physiologic buffering, and consistent osmotic pressure[220, 221]. We have mimicked the

clinical application by mixing HK, LK and DN with the culture medium. This approach has maintained the supply of nutrients, including glucose, amino acids, vitamins and minerals, which were absent in the crystalloid solution HTK or CS. Therefore, the large deviation in the basal metabolic profile by HTK or CS could result from nutrient deprivation in the cell culture experiments. Nevertheless, our finding of HK or LK having a minimal impact on the baseline metabolic profile yet protecting against metabolic switch by oxidants supports the clinical observation of the superiority of blood cardioplegia.

The metabolic shift detected here by oxidative stress has resemblance with that by surgery induced ischemia. A decrease of NAD level has been reported in the myocardial tissue due to CABG surgery[222, 223]. Metabolic reprogramming indeed occurs with CPB, since nuclear magnetic resonance study of the left atrial tissue showed increases of glucose, pyruvate, citrate and lactate, indicating a reduction of glycolytic energy metabolism[224]. On the other hand, increases in sugar alcohols have been linked to apoptosis of cardiomyocytes during ischemia[225-227]. Although xylitol, adonitol, arabitol, and ribose-5-P may not be inducers of apoptosis, the correlation of their elevations with cell death suggests the functionality as a biomarker of cell injury. Inhibiting H_2O_2 induced NAD decrease, sugar alcohol increases or changes in the metabolites in glycolysis or TCA cycle by HK and LK indicatting their cytoprotective capacity against ischemia injury or oxidative stress.

Ischemia causes a shift from aerobic to anaerobic metabolism, where ATP production is decreased due to O_2 deprivation for the respiratory chain. Glycolysis, the main ATP source in the ischemic myocardium, is progressively limited by the restraint of glyceraldehyde 3-phosphate dehydrogenase flux due to NADH accumulation [228]. High levels of NADH and $FADH_2$ inhibit β-oxidation, leading to an accumulation of long-chain acyl CoA, acylcarnitine esters and free fatty acids [229, 230]. These lipophilic compounds can act as “detergents”, altering membrane functions such as Na^+ /K^+ ATPase, and sarcoplasmic reticular Ca^{2+} -stimulated ATPase [231]. Upon reperfusion, these changes contribute to elevation of cytosolic Ca^{2+}[232]. Oxidative stress can cause Ca^{2+} influx and elevation of cytosolic Ca^{2+}. Elevation of cytosolic Ca^{2+} either by ischemic reperfusion or oxidative stress causes mitochondrial membrane permeability transition and further increase in oxidant production[169, 170].

HK and LK deliver 20 mg/L or 0.085 mM lidocaine, whereas DN introduces 104 mg/L or 0.444 mM lidocaine to the cells in culture. In contrast, lidocaine is absent in HTK and CS. Lidocaine is a sodium channel blocker that inhibits the entry of Na^+ into cells through fast voltage-gated Na+ channel (Nav). A number of publications have reported cytotoxicity of lidocaine in a variety of cell types in mM concentration range[233] Cytotoxicity may result from high doses that allow lidocaine to act as a surfactant and disrupt the plasma membrane[234]. This may explain the lack of full protection of DN against metabolic change of oxidative stress.

In cardiomyocytes, lidocaine appears to serve as a cytoprotective agent. Lidocaine protects H9C2 cardiomyocytes against loss of viability by hypoxia[235]. Protection against myocardial infarction has been reported in mice with lidocaine injection[236]. A similar discovery was reported with regional ischemia in rats[237]. CPB in a canine model showed that lidocaine protected against mortality due to global myocardial ischemia and reperfusion[238]. An early study using a canine model of regional ischemic reperfusion showed a reduction of infarct size by lidocaine in association with decreased lipid peroxidation[239]. The protective effect of lidocaine against myocardial infarction was also observed in a porcine experimental model[240]. These protective effects may result from the inhibition of Nav and the prevention of intracellular Na^+ increase. Na^+ efflux is coupled to Ca2+ influx via the sodium–calcium exchanger (NCX). Inhibition of intracellular Ca2+ elevation by lidocaine has been demonstrated by pacing isolated rat hearts[241]. In cardiomyocytes, late openings of the sodium channel by H_2O_2 treatment may contribute to an increase in cytosolic Ca^{2+}[242]. Lidocaine may block H2O2 from inducing elevation of cytosolic Ca^{2+} and, therefore, production of ROS from the mitochondria. A preliminary experiment indeed showed protection against ROS generation by lidocaine (Figure 3.7). Early evidence indicates that lidocaine preserved mitochondrial oxidative phosphorylation during ischemic reperfusion[243]. Consistent with the protective role of lidocaine, an inhibitor of NCX was capable of preventing intracellular Ca^{2+} overload or mitochondrial Ca^{2+} increase and enhancing cardiac recovery following ischemia[244,

245]. Therefore, the observed protective effect of HK or LK may be related to the presence of lidocaine and the inhibition of ROS generation.

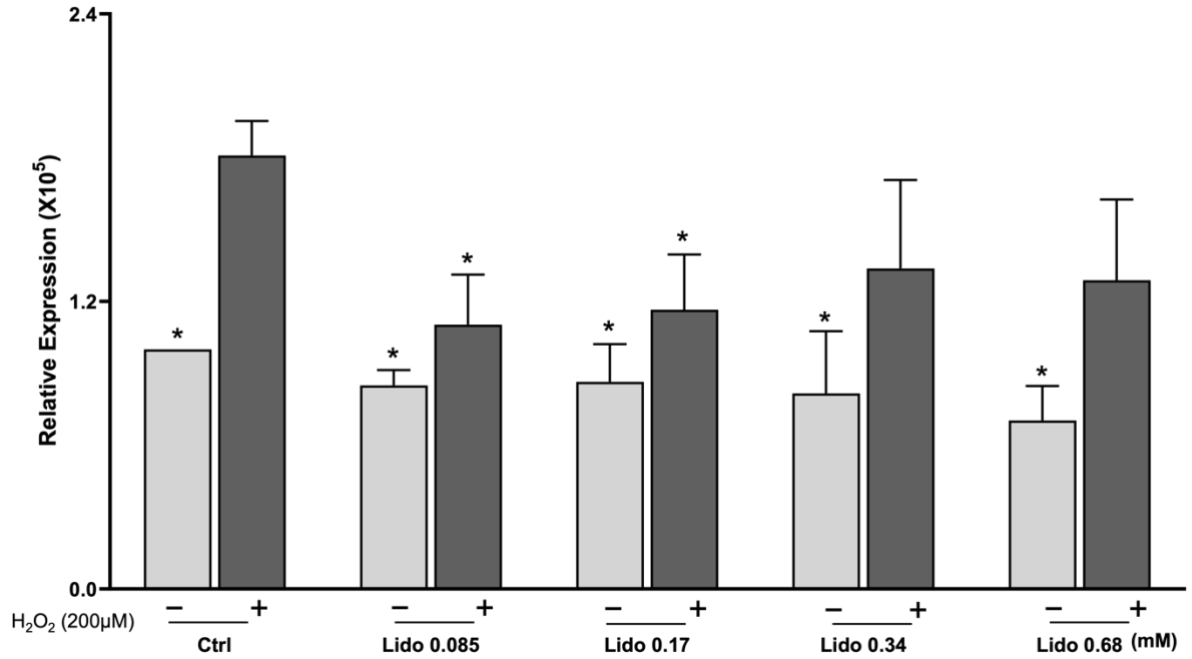

Figure 3. 7. Lidocaine Prevents ROS Generation by H_2O_2.

AC16 human cardiac myocytes were seeded in 96-well plates and were pretreated with indicated concentrations of lidocaine for 3 h before 30 min incubation with 100 μM DCFH-DA. H_2O_2 was added to the final 200 μM for recording the fluorescence of hydroxy radical formation. The bar graphs represent the means ± SD from 3 replicates of one representative experiment. A letter indicates statistical significance ($p < 0.05$) from the means that is labeled with a different letter as determined by one-way ANOVA. * indicates significantly different from H_2O_2 alone treated group.

Limitation

One limitation of this study is that the cellular model used in this study may not fully represent the complex and dynamic metabolic changes that occur during ischemia-reperfusion injury in vivo. Although the use of LC-MS/MS-based metabolic provides a comprehensive and sensitive approach to evaluate metabolic changes, the results obtained from this model may not fully translate to the in vivo situation. Additionally, the study was conducted in vitro using a single cell line, and further research is needed to validate these findings in vivo and primary isolated cardiomyocytes to determine the potential clinical relevance of these findings. Moreover, while lidocaine was found to prevent ROS production and preserve metabolism under oxidative stress, additional studies are needed to further investigate its mechanism of action and potential interactions with other cardioprotective agents.

CHAPTER IV: YTH N6-METHYLADENOSINEl RNA BINDING PROTEIN 2 (YTHDF2) PARTICIPATES IN DE NOVO NRF2 PROTEIN TRANSLATION UNDER OXIDATIVE STRESS

Abstract

The process of protein translation typically begins with the recruitment of the 43S ribosomal complex to the 5′ cap of mRNAs by a cap-binding complex. Some transcripts are translated in a cap-independent manner through poorly understood mechanisms under stress conditions. Work from our laboratory indicates that oxidative stress causes rapid de novo synthesis of Nrf2 protein. Nrf2 encodes a transcription factor controlling a myriad of genes important for antioxidation, detoxification, wound repair and tissue remodeling. We report here that Nrf2 mRNA increases N6-methyladenosine (m6A) in their 5' Untranslated Region (5'UTR). YTHD2, a YTH domain containing N(6) methyladenosine (m6A) binding protein, increased the association with Nrf2 mRNA and ribosomes by oxidative stress. Inhibiting the expression of YTHD2 or adenosine methylation "writer" METTL3 using siRNAs prevented oxidants from inducing Nrf2 protein. In vitro RNA binding and in vivo ribonucleoprotein immunoprecipitation showed H2O2 dose and time dependent increases of YTHDF2 and METTL3 binding to Nrf2 5'UTR. While no nuclear to cytoplasmic translocation was detected, cytosolic redistribution to the ribosomal fractions was observed due to oxidant treatment. An increased presence of

YTHDF2 in 40/43/48S ribosomal fractions validates its involvement in translation initiation of Nrf2 protein. YTHDF2 interacts with eIF3h in an RNA dependent manner. Our data supports a role of YTHDF2 binding to m6A in Nrf2 mRNA promotes the attachment of 43S pre-initiation complex to Nrf2 mRNA for translation initiation of Nrf2 protein under oxidative stress.

Introduction

Nrf2 (nuclear factor erythroid 2-related factor 2) gene encodes a transcription factor best known as the master controller for the antioxidant and detoxification response[246]. Nrf2 binds to the Antioxidant Response Element (ARE) in the promoter of downstream genes to initiate transcription of these genes[247]. Typical examples of Nrf2 downstream target genes including: aldoketo reductases (AKRs), heme oxygenase-1 (HO-1), carbonyl reductases (CBRs), quinone oxidoreductase 1 (NQO1), glutamate-cysteine ligase catalytic subunit (Gclc) and regulatory subunit (Gclm), glutathione S-transferases (GSTs), and UDP-glucuronosyltransferase[149]. Beyond the genes in antioxidant and detoxification response, Nrf2 also targets genes involved in cell proliferation, energy metabolism, extracellular matrix response or autophagy regulation[148, 248, 249].These illustrate the importance of Nrf2 transcription factor in cellular defense as well as damage removal and tissue repair. We have reported that Nrf2 protein undergoes stress induced protein translation during oxidative stress[155, 213, 250, 251].

Protein synthesis is a highly regulated process for maintaining cellular homeostasis. The rate of protein translation determines the equilibrium of specific proteins and therefore functional outcome of genes[252]. Since translating a strand of mRNA into a protein is an energy-expensive process, the regulatory elements for such processes are complex but critical to reveal. In response to a diverse array of stress

conditions, eukaryotic cells inhibit protein synthesis in general. Selective protein translation under stress conditions set one example of the beauty of evolution for maintaining cellular homeostasis.

The process of protein translation is divided into three steps, namely initiation, elongation and termination, with initiation being a rate-limiting step. Under physiological conditions, the vast majority of mRNA species are translated in a cap-dependent manner for translation initiation. This involves recognition of the m7G cap at 5’ end of an mRNA strand by eIF4E, circulating the mRNA strand due to Poly (A) Binding Protein (PABP) association with the 3’ poly(A) RNA tail, and participation of at least 12 eukaryotic Initiation Factors (eIFs)[253, 254]. During stress, this 5’ m7G cap - dependent translation is inhibited. One mechanism for bypassing the general protein synthesis inhibition is Internal Ribosomal Entry Site (IRES)-driven translation. IRES are discrete elements present in the 5’ Untranslated Region (5’UTR) of the mRNA species and recognized by its trans-acting factor (ITAFs)[255]. ITAFs are RNA binding proteins that act to facilitate ribosome recruitment to the IRES, thus initiating translation of these mRNA [256]. Work from our laboratory have demonstrated increased Nrf2 protein translation involving the interaction of RNA binding proteins with the 5′UTR of Nrf2 mRNA. Using proteomic techniques in combination with traditional laboratory techniques, we have reported an increase binding of several RNA binding proteins, La, EF1a, Far Upstream

Element Binding Protein 1 (FUBP1), and DHX9 to 5'UTR of Nrf2 mRNA for oxidative stress induced Nrf2 protein translation.

N^6-methyladenosine (m^{6}A) is the most abundant modification in the transcripts of eukaryotic RNAs and can be detected in 25% of the transcriptome[257-259]. Such modification has been detected in 5'UTR, coding sequence (CDS) and 3′UTR, and is usually embedded within the consensus sequence of 5′-RRACU-3′ (R = A or G). Reported functions of m^{6}A include assisting nuclear export of RNAs, and regulating mRNA splicing, stability, folding, translation or RNA-protein interaction[260-262].The m^{6}A modification is catalyzed by "writers", i.e. methylase, with its function interpreted by "readers", i.e. m6A binding protein. The modification can be removed by "erasers", i.e. demethylase[263].

The m6A methytransferase complex consists of catalytic subunit methytransferase-like 3 (METTL3), the regulatory subunit methytransferase-like 14 (METT14), and adaptor proteins, such as Wilms Tumor 1-Associating protein (WTAP), Vir Like m6A Methytransferase associate protein (VIRMA), RNA-binding motif protein 15/15B (RBM15/15B), Cbl Proto-Oncogene Like 1 (CBLL1) and Zinc Finger CCCH-Type Containing 13 (ZC3H13)[264-267]. The functional significance of m6A is executed by its readers, with YTH domain containing family proteins being well characterized readers of m6A. This family contains 5 members including YTHDC1/2, YTHDF1/2/3 [268]. YTHD1-3 share extensive sequence homologies, and are cytosolic proteins that bind to m6A site upon the nuclear export of the mRNA species. The m6A modification can be dynamically

reversed by the erasers of m6A demethylases, including Fat Mass and Obesity-Associated Protein (FTO) and alpha-ketoglutarate dependent hydroxylase homolog 5 (ALKBH5). Both enzymes are dioxygenases, and carry out oxidative demethylation of m6A under a specific condition. Here we examine m6A in Nrf2 5'UTR and test the role in oxidant induced Nrf2 protein translation.

Materials and Methods

Cell Culture and Reagents

HeLa cells (CCL-2) were originally obtained from ATCC and maintained in DMEM (10013CV, Corning) containing 10% FBS (S11150H, R&D Systems), 100 U/ml penicillin and 100 µg/ml streptomycin (15140122, Gibco). Cells were seeded in 6-well, 24-well or 86-well plates or 100 mm dishes. When grew to 80% confluency, cells were cultured in DMEM containing 0.5% FBS overnight for serum starvation. The cells were treated with H_2O_2 for 10 mins to induce oxidative stress followed by removal of oxidized medium for culture in fresh DMEM with 0.5% FBS for 1 hour. The stock 30% hydrogen peroxide was purchased from Sigma-Aldrich (2167630), with the rest of reagents obtained from Sigma-Aldrich unless specified. Antibodies used in these experiments are listed below: anti-YTHDF2(1:1000 WB, 1:400 ICC); anti-METTL3 (1;1000 WB); ant-m6A (1:1000 m6A immunoblotting).

Isolation of Ribosomes

HeLa cells were treated with 100 µg/ml cycloheximide (CHX) 10 minutes before harvesting. After washes in ice cold PBS twice, cells grown in 100 mm dishes were scrapped off in ice cold PBS containing 100 µg/ml CHX. Cell pellets were collected by spinning down at 500 ×g for 5 minutes and resuspended in 1 ml polysome lysis buffer [20 mM Tris-HCl (pH 7.5), 5 mM MgCl2 and 100 mM KCl, 0.5% NP-40] containing freshly

added 1x protease inhibitor (EDTA-free), 100 µg/ml CHX, 1 mM DTT, 100 µM MG132 and 100U/mL RNase Inhibitor. The cell lysates were vortexed for 5 seconds then placed on ice for 5 minutes before collection of cytoplasmic fractions. Cell debris and nuclei were removed by centrifuging at 1000g x 3 mins. Supernatant was centrifuging at 16,000 ×g for 10 minutes to remove postmitochondria fraction. The supernatant was loaded on the top of 10%+35% sucrose cushion and centrifuged at at 32,000 rpm (Beckman Coulter Optima L-90K Ultracentrifuge) with a Beckman SW41 rotor for 2 hours at 4°C. Ribosomal pellets were collected at the bottom of the centrifugation tubes and resuspended in Trizol or 1×Laemmli sample buffer (2% SDS, 10% glycerol, 62.5 mM Tris-Cl, pH 6.8, 0.002% bromphenol blue, 5% 2-mercaptoethanol) for RT-qPCR or Western Blot analysis.

For fractionation of ribosomes, the postmitochondrial supernatant was loaded onto a linear sucrose gradient (10-50% w/v) cushion and centrifuged at 33,000 rpm with a SW41 rotor for 2 hours at 4°C. The gradient was displaced upright with 60% sucrose and the distribution of ribosome was recorded at absorbance of OD 254nm with a BioLogic Liquid Chromatography System (BioRad). With a flow rate of 0.5 mL/min, the fractions were collected and subjected to 2x volume 100% ethanol for overnight protein precipitation in -20 ℃. The precipitated proteins were dissolved in 1x Laemmli sample buffer (2% SDS, 10% glycerol, 50 mM Tris-Cl, pH 6.8, 0.002% bromphenol blue, 5% 2-mercaptoethanol) for Western blot analysis.

Immunocytochemistry

HeLa cells were seeded onto 0.13-0.17 mm thick circle cover glasses in 6-well plates and grown to 50% confluency. After treatment with H_2O_2 , the cells were washed twice with phosphate-buffered saline (PBS) before fixation in 4% paraformaldehyde for 10 minutes at 4 ℃, cells were permeabilized with 0.2% Triton X-100 for 10 minutes at room tempereatur. Following the blockage with 10% rabbit serum in PBS-T (3.2mM Na_2HPO_4, 1.3mM KCl, 137mM NaCl, 0.5mM KH_2PO_4, 0.05% Tween 20, pH 7.4) for 1 hour, cells were stained with YTHDF2 primary antibody (1: 50 dilution, 24722-1-AP; ThermoFisher) or Phospho-S6 antibody (1: 200 dilution, Cell Signaling Technology) overnight at 4°C, followed by incubation with Alexa Fluor 488 conjugated Donkey anti-Rabbit IgG (Invitrogen, A10042) secondary antibody or Alexa Fluor 568 anti-mouse secondary antibody (1:2000 dilution) for 1 h at room temperature. after PBS washes, the coverslips were mounted onto a microscope slide withGProLong™ Gold Antifade Mountant Medium containing DAPI (Invitrogen, P36931). Images were captured under 63× objective with a Marianas system (3i Biotechnology, Denver, CO).

In Vitro Transcription. Nrf2 5'UTR was cloned into pJet hsa plasmid as described previously[250]g. To generate the full length or fragments of Nrf2 5'UTR, 10 ng of the plasmid DNA was used as a template for PCR with forward primer containing T7 polymerase binding site: 5'-TAATACGACTCACTATAGGGAAATCAGGGAGGCGCAGCTC-3'. The reverse primer

for was 5’-GATGAGCTGTGGACCGTGTG-3’ for -555 to 0 fragment; 5’-GGCAAGAGTCCGGGCCCTTC-3’ -555 to -225 fragment; 5’-AAGGGACTGCCAGCTGGGGT-3’ for -555 to -333 fragment; 5’-CGAGATAAAGAGTTGTTTGC-3’ for -555 to -450 fragment. The PCR products were validated and purified by agarose gel electrophoresis, before serving as a template (1 μg) for in vitro transcription with a TranscriptAid T7 High Yield Transcription Kit (K0441, Thermo Scientific) in the presence of Biotin-16-UTP (11388908910, Roche) following the manufacturer’s instruction for 2 hours incubation at 37°C. The synthesized RNA was purified by RNeasy Mini Kit (74104, Qiagen).

Far Western Blot. HeLa cells grown in 100 mm dishes were treated with H2O2 and lysed in 400 μL polysome lysis buffer containing 1 mM DTT and 1x protease inhibitors from a cocktail (P8340, Sigma Aldrich). The cytosolic fraction (300 μL) was mixed with 100 μL 10× Protein-RNA Binding Buffer [0.2M Tris (pH 7.5), 0.5M NaCl, 20mM MgCl2, 1% Tween-20], 300 μL 50% glycerol, 300 μL nuclease-free water, 100U RNase inhibitor and 50 pmol of biotinylated RNA. The mixture was incubated overnight at 4°C, followed by addition of 30 μL streptavidin agarose beads (20349, Thermo Scientific) for another 4 hours incubation with rotation at 4°C. The beads were washed 4 times with 1× wash buffer (20mM Tris, pH 7.5, 10 mM NaCl, 0.1% Tween-20) before 50 μL 1× Laemmli buffer was added to the beads for boiling. The released proteins were then analyzed by Western blot.

Western Blot and Subcellular Fractionation

For total cell lysates, HeLa cells in culture dishes were dissolved in 1×Laemmli sample buffer. Samples were heat-denatured for 10 min at 100º and then subjected to SDS-PAGE. For collection of cytosolic versus nuclear enriched fractions, HeLa cells were scrapped off the dishes in ice-cold PBS and span down by centrifugation at 1000 xg for 5 mins. The cell pellets were dissolved in the polysome lysis buffer containing protease inhibitors. Upon centrifugation at 13000xg for 10 mins at 4ºC, the supernatant was collected as the cytosolic fraction and the pellet was treated as the nuclear enriched fraction. After denaturing the cytosolic or nuclear fractions in the sample buffer, boiling and sonicating, samples originated from equal cell number were loaded onto the SDS-gel for electrophoresis. After separation, proteins were transferred to a PVDF membrane using a Bio-Rad Trans-Blot Turbo Transfer System. Membranes were blocked for 1 h in 1xTBST containing 5% non-fat milk, followed by incubation with primary antibodies overnight at 4ºC: Nrf2 antibody (sc-13032), GAPDH antibody (sc-32233), Lamin B1 antibody (sc-377000), S6 antibody (sc-74459), L36a antibody (sc-100831), eIF4E antibody (sc-9976), eIF4B antibody (sc-82587), eIF3η antibody (sc-16377), eIF2α antibody (sc-133132), or eIF1 antibody (sc-390122). The bound antibodies were recognized by secondary antibodies: anti-mouse IgG-HRP (A9044), anti-rabbit IgG-HRP (A9169), or anti-goat IgG-HRP (sc-2354, Santa Cruz). All antibodies were obtained from Santa Cruz Biotechnology, except anti-mouse or anti-rabbit secondary antibodies, which were purchased from Mlillipore Sigma-Aldrich. Immunoblots were visualized using SuperSignal™ West Femto (ThermoFisher)

RNA- Protein Complex Immunoprecipitation

HeLa cells were lysed on ice with polysome lysis buffer with freshly added 1x protease inhibitors (EDTA-free), 100 µg/ml CHX, 1 mM DTT, 100 µM MG132 and 100U/mL RNase Inhibitor. The cell lysate was centrifuged at 18,000 xg at 4ºC for 10 minutes to remove cell debris, nuclei and mitochondria. The supernatant was collected and pre-cleared with 30 µl of Protein A/G Magnetic Agarose Beads (78609, Thermo Scientific) for 1 hour to remove non-specific binding. The pre-cleaned cell lysate wree incubated with 1 µg anti-YTHDF2 antibody (24722-1-AP; ThermoFisher) or control mouse IgG (sc-2025, Santa Cruz) with rotation at 4ºC overnight and additional 4 hours in the presence of pretein A/G Magnetic Beads at 4ºC. Unbound proteins were removed by 4 times washes with polysome lysis buffer. Bound RNA was extracted with Trizol (15596018, Invitrogen) from the beads and was converted to cDNA for detection of Nrf2 mRNA by RT-qPCR.

RT-qPCR Analysis

Total RNAs were extracted from cell lysates by Trizol and ethonal precipitation followed by converted to cDNA with a qScript cDNA SuperMix (95048, QuantaBio) for subsequent quantitative PCR (qPCR). The primers used for qPCR were: Nrf2 forward, 5’-TTCCCGGTCACATCGAGAG-3’; Nrf2 reverse, 5’-

TCCTGTTGCATACCGTCTAAATC-3'; GAPDH forward, 5'-GGAGCGAGATCCCTCCAAAAT-3'; GAPDH reverse, 5'-GGCTGTTGTCATACTTCTCATGG-3'. The qPCR was performed with PowerUp SYBR Green (A25777, Applied Biosystems) on a BioRad CFX96 thermal cycler, with Nrf2 mRNA abundance calculated with BioRad CFX Manager Software.

siRNA Transfection

Control siRNA (sc-37007) or YTHDF2 siRNA (sc-45706) were purchased from Santa Cruz Biotechnology. HeLa cells grown in 12-well plates at 80% confluency were transfected with siRNA, cells were exposed to 40 pmol siRNA and 4 µL Lipofectamine 3000 in Opti-MEM (51985034, Gibco) under culture conditions overnight. After 48 hours of recovery, cells were serum starved for 16 hours before H_2O_2 treatment.

Immunoprecipitation

HeLa cells were seeded and treated in 100mm dishes. When harvesting, cell were lysed in radioimmunoprecipitation (RIPA) buffer (1% Triton X-100, 140 mM NaCl, 0.1% SDS, 0.1% sodium deoxycholate, 10 mM Tris, pH 8.0) containing 1 mM DTT, 100 µM MG132 and 1x protease inhibitors. For treatment of RNase, 0 U/mL RNase A/T1 mix (EN0551, Thermo Scientific) or RNase inhibitors (EO0384, Thermo Scientific) was added to the buffer. After removal of precipitates by centrifugation at 18,000×g for 15 minutes

at 4 ℃, the supernatant was pre-cleared with 20 µl of Protein A/G Agarose beads for 1 hour before overnight incubation at 4 °C with 1 µg YTHDF2 antibody (24722-1-AP; Thermo Fisher) or mouse IgG (sc-2025; Santa Cruz Biotechnology). After mixing with 30 µl of Protein A/G Agarose beads for 4-hours incubation with rotation at 4°C, the antibody-protein complex was captured by centrifugation. After three washes with RIPA buffer, proteins were released from the beads by boiling in 1x Laemmli sample buffer for Western blot analysis.

Statistics

Data are presented as means ± SD. Means were compared by 2-tailed Student's *t* test or 1-way ANOVA when comparing multiple groups. $p \leq 0.05$ was considered significant.

Results

An Increased YTHDF2 Association with Ribosomes by Oxidative Stress.

In studying the changes in ribosomal associated proteins in cellular response to oxidative stress, we have discovered YTHDF2. To characterize such an association, we performed H2O2 treatment dose response and time course experiments. A dose dependent increase of YTHDF2 association with ribosomes was observed with 50-200 mM H2O2 treatment (Fig 4.1A). With the most potent dose of 200 mM, the time course study showed an increase at 10 mins, reached the highest level at 120 mins and returned towards the baseline at 240 mins (Fig 4.1B).

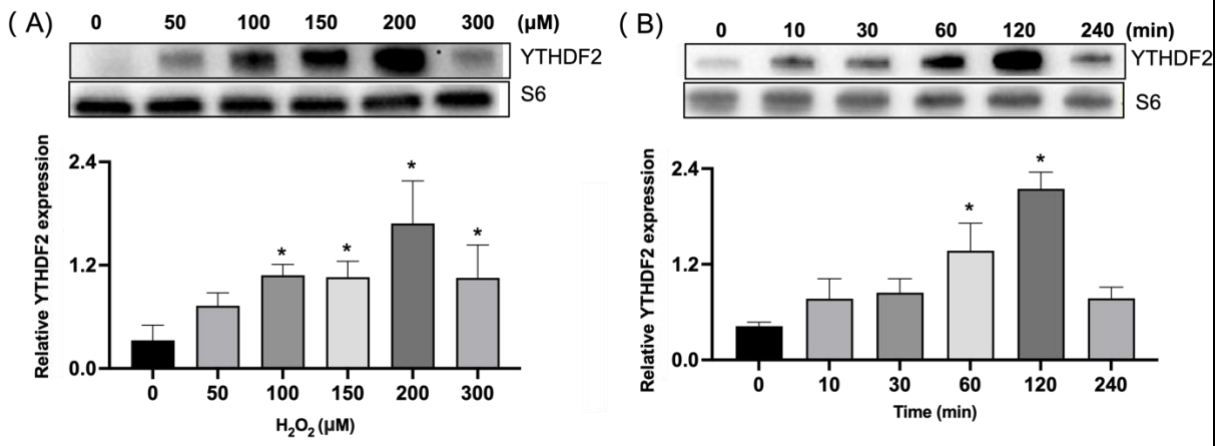

Figure 4. 1. H_2O_2 Causes an Increase of YTHD2 in Total Ribosomes.

HeLa cells were treated with 100 mM H_2O_2 (A) or various concentrations (B) or for 10 mins and harvested at indicated time point (A) or 1 hr (B) for isolation of total ribosomes. Cells were lysed and ribosomes were spun down by ultracentrifugation at 32,000 rpm for 2 hours with SW41Ti rotor in 10%+35% sucrose cushion. The isolated ribosome was denatured by 1× Laemmli buffer and YTHD2 protein was detected by Western blot using S6 and L36 as a loading. Quantification of band intensities was shown as mean±SD, n=3. * $p<0.05$ compared to the control group.

Total ribosomes contain 40S small subunit, 60S large subunit, 80S monosomes and polysomes. In the phase of translation initiation, 40S small subunit is assembled into 43S pre-initiation complex (PIC) by joining of eIF1A, eIF3 and the ternary complex of eIF-GTP-Met-$tRNA_i^{Met}$. When 43S PIC lands on a targeted mRNA species recognized by eIF4F, eIF4B, and eIF4H, a 40S initiation complex (48S IC) is formed (Marintchev, 2009 #746). Joining of a 60S large subunit of ribosome produce 80S ribosomal intiation complex. During translation elongation, the target strand of mRNA is occupied by multiple ribosomes, forming polysomes. We were able to separate these ribosomal units and address which fractions of ribosomes having an increase of YTHDF2 association. We observed that although YTHDF2 distributes in 40/43/48S, 60S/80S and lighter polysomes, an increased abundancy of YTHDF2 protein was detected in 40/43/48S ribosomal fractions (Fig 4.2). Ribosomal protein S6 is phosphorylated when the ribosomes are actively participating in the process of translation. With immunocytochemistry, we observed co-localization of YTHDF2 with phosphor S6 (Fig 4.3), suggesting a role of YTHDF2 in protein translation.

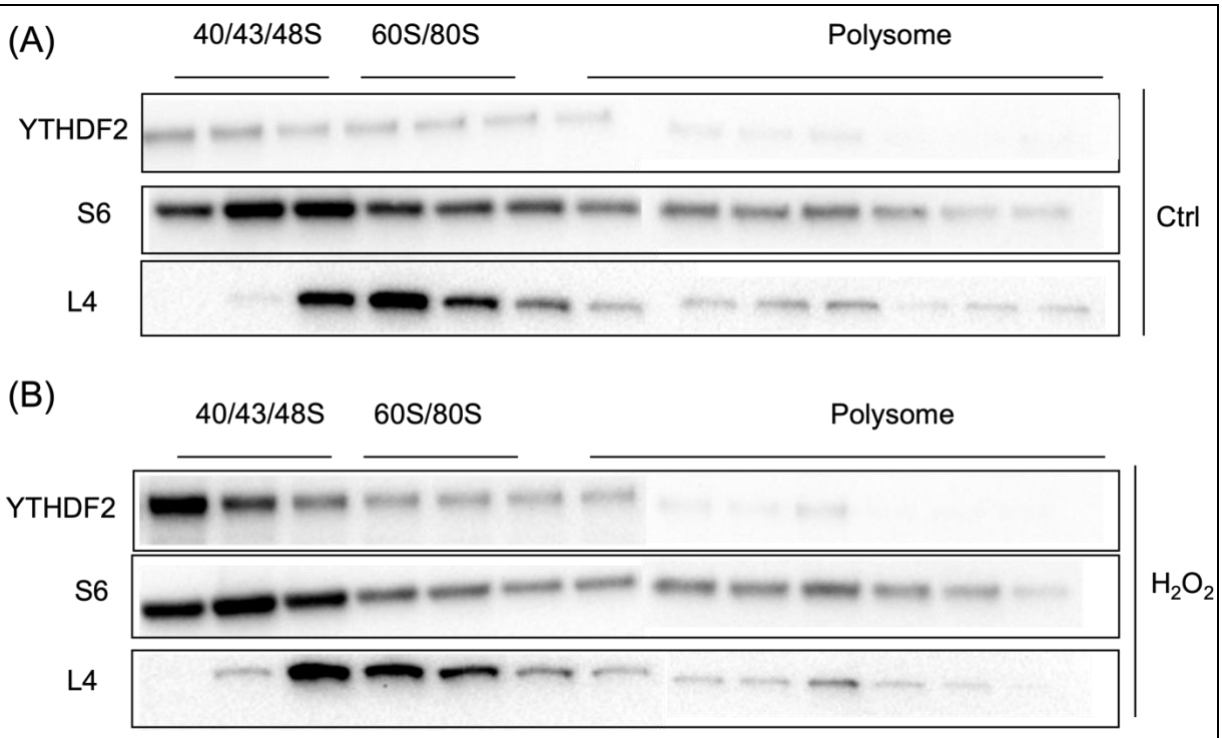

Figure 4. 2. YTHDF2 Distribution in 40/60/80s Ribosome and Polysome Was Enhanced by H_2O_2 Treatment.

Hela cells were either untreated or treated with 100 μM H_2O_2 for 1 hour and 100 μg cycloheximide was added for another 10 minutes. Cells were harvested in polysome lysis buffer containing inhibitors and cell nucleus, cell debris and mitochondria were removed by centrifugations. Then cell lysate was layered on top of 10% to 50% linear sucrose gradient and centrifuged at 32,000 rpm for 2 hours with SW41Ti rotor. The ribosomal fractions were collected and the proteins associated with were analyzed by Western blot.

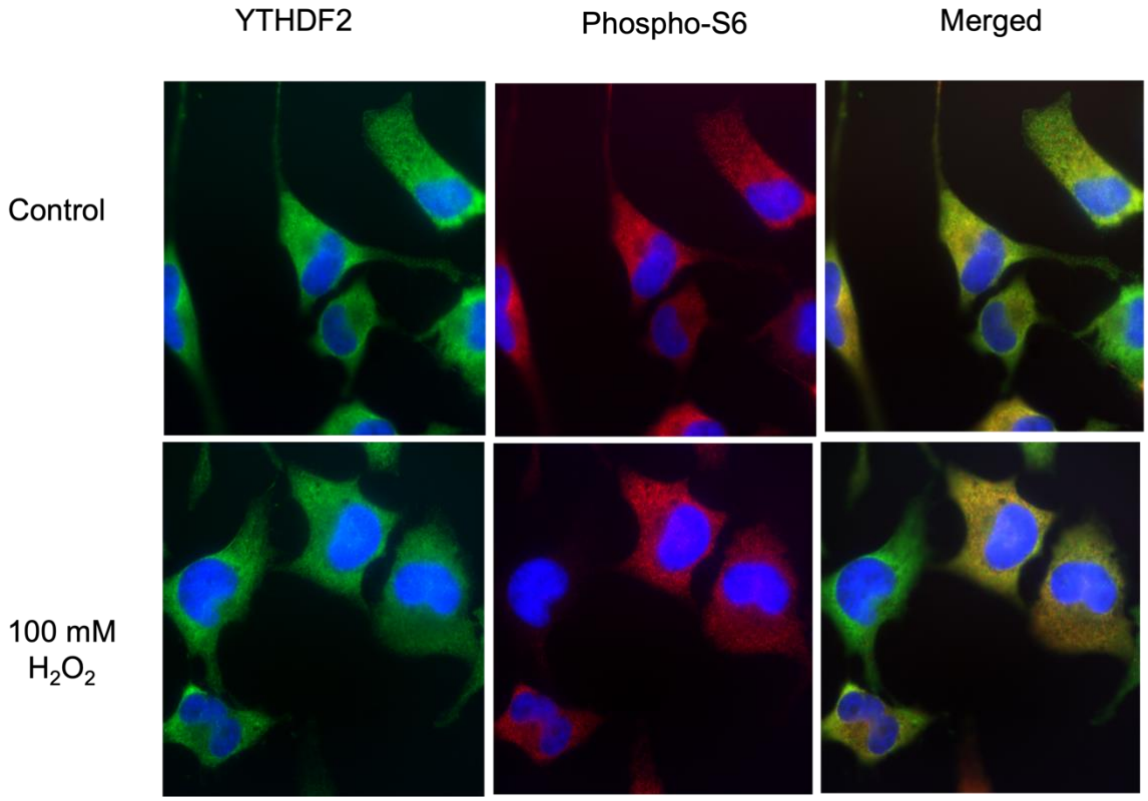

Figure 4. 3. H_2O_2 Treatment Enhances YTHDF2 Co-localization with Phospho-S6.

HeLa cells at a confluency of 50% were treated with 0 and 00 μM H2O2 for 1 hr. After fixing with 4%paraformaldehyde, cells were permeabilized by either 0.2% Triton X-100 (A) or 0.5% saponin. YTHDF2 was detected by immunocytochemistry with secondary antibody conjugated with Alexa Fluor 488 (green) and nuclei counter stained with DAPI (blue). Phospho S6 was recognized by pecific primary antibody and Alexa Fluor 568 conjugated secondary antibody (red).

YTHDF2 Mediates De Novo Nrf2 Protein Translation under Oxidative Stress.

We have found that oxidants induce de novo Nrf2 protein translation and Nrf2 5'UTR plays a role [157, 213, 250, 251, 269] o test whether YTHDF2 plays a role in de novo Nrf2 protein translation under oxidative stress, we determined the interaction between YTHDF2 and Nrf2 mRNA.

To measure YTHDF2 binding to Nrf2 5'UTR, we used biotinylated Nrf2 5'UTR as a bait to isolate binding proteins. The dose response studies showed that H_2O_2 caused a dose dependent increase of YTHDF2 binding to Nrf2 5'UTR, with 100 or 150 μM being the optimal dose (Fig 4.4A). The time course revealed the increased YTHDF2 interaction with Nrf2 5'UTR started at 10 mins and reached the highest at 120 mins after H_2O_2 treatment (Fig 4.4B). The dose response and time course studies also revealed H2O2 induced increases of Nrf2 mRNA in YTHDF2 IP complex (Fig 4.4C, D).

We performed Ribonucleoprotein Immunoprecipitation (RNP-IP). In this assay, the cytosolic YTHDF2 was isolated by immunoprecipitation (IP) for detection of Nrf2 mRNA by RT-qPCR. The dose response and time course showed H2O2 indeed induced increases of Nrf2 mRNA association with YTHDF2 (Fig 4.4C, D).

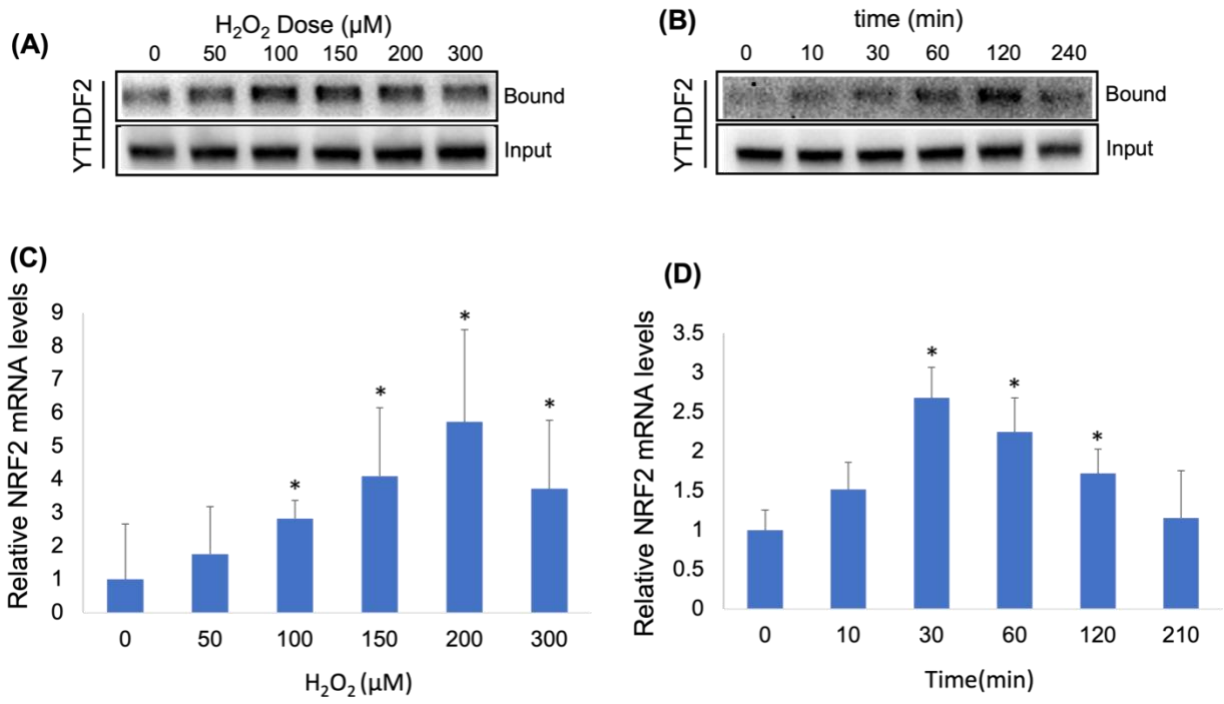

Figure 4. 4. The Binding Between YTHDF2 and NRF2 5'UTR mRNA Was Increased with H_2O_2 Treatment in A Dose and Time Dependent Manner.

The cDNA containing Nrf2 5'UTR sequence was derived from HeLa cells, and cloned into pJet1.2/blunt vector. A forward primer containing T7 promoter sequence was used to generate cDNA, which was purified and used as the template to synthesize biotinylated RNA by *in vitro* transcription. The RNA fragment (50 pmol/ea) was incubated overnight with HeLa cell lysates collected at 1 hr after various doses of H_2O_2 treatment (A) or at various time after 100 mM H_2O_2 treatment (B). Streptavidin agarose beads were added to the reaction mixture for isolating the RNA-protein complex. Bound proteins were eluted by sample buffer for SDS-PAGE and Western blot to detect YTHD2. HeLa cells were treated with 100 μM H_2O_2 (C) or various concentrations (D) for 10 mins and harvested at indicated time point (C) or 1 hr(D). HeLa cell lysates were incubated overnight with YTHDF2 specific antibodies. The immunoprecipitates were used for RT-PCR to detect Nrf2 mRNA.

To determine whether or not YTHDF2 mediates de novo Nrf2 protein translation, we used siRNA to knock down YTHDF2 gene. With decreased levels of YTHDF2 protein, the basal level of Nrf2 was reduced and H_2O_2 induced induction of Nrf2 were blocked (Fig 4.5). These lines of data suggest that YTHDF2 plays a role in oxidants induced de novo Nrf2 protein translation.

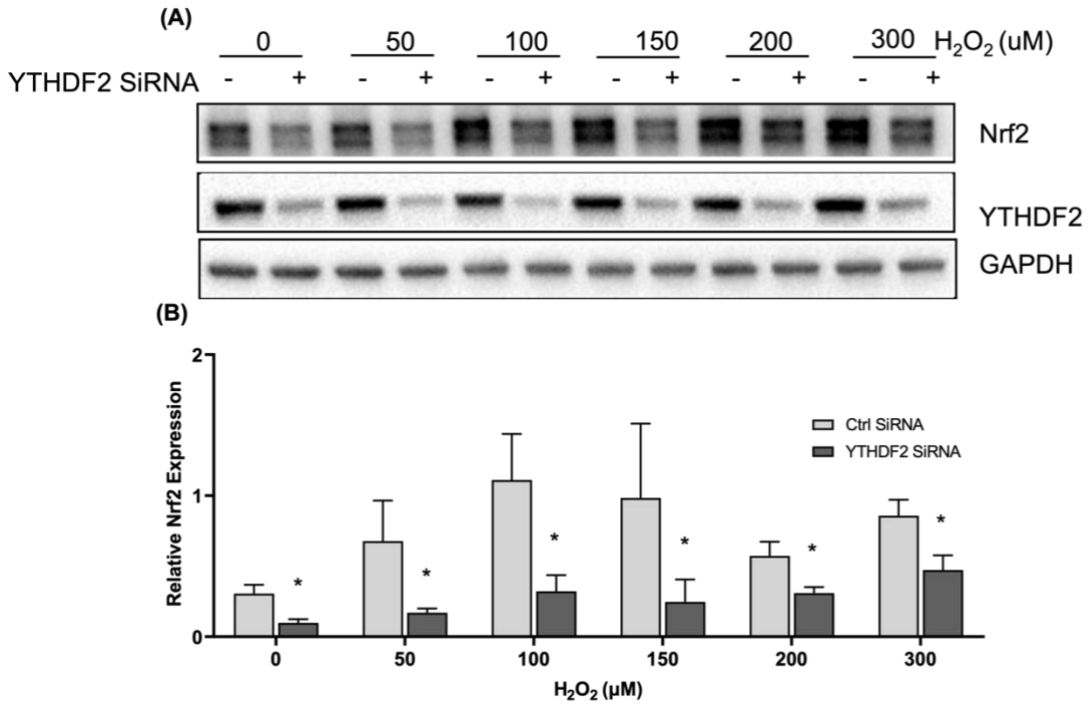

Figure 4. 5. YTHD2 Is Required for Nrf2 Protein Induction by H_2O_2.

Hela cells were transfected with control or YTHDF2 siRNA for 48 hours and then treated with 100 μM H_2O_2 for 1 hour as described. The protein level of Nrf2 and YTHDF2 were assessed by Western blot , with GAPDH as a loading control. (B) Quantification of band intensities was shown as mean±SD, n=3. * $p<0.05$ compared to control siRNA + 0 μM H_2O_2 group, # $p<0.05$ compared to control siRNA + 100 μM H_2O_2 groupThen cells were treated with indicated doses of H_2O_2 for 1 hour.

RNA dependent YTHDF2 association with ribosomes.

Many RNA binding proteins translocate from the nuclei to the cytosol to participate in the process of protein translation. We addressed whether or not H_2O_2 treatment caused an increase of YTHDF2 protein in the cytosol. H_2O_2 dose response studies did not reveal an increase of cytosolic YTHDF2 increase despite of an elevation of Nrf2 protein (Fig 4.6). No significant changes of YTHDF2 level were observed in total cell lysates or the nuclear fraction (Fig 4.6). The majority of YTHDF2 protein is present in the cytosol, consistent with immunocytochemistry results of the cytosolic localization of YTHDF2 (Fig 4.6).

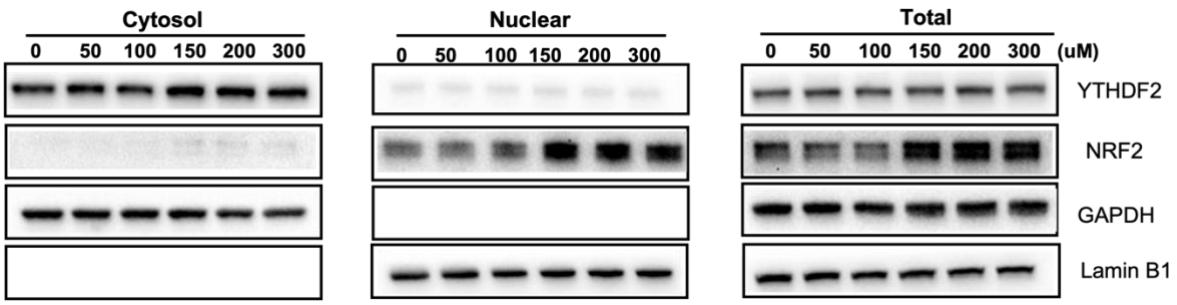

Figure 4. 6. Lack of YTHDF2 Protein Increase in the Cytosol with H_2O_2 Treatment.

Hela cells treated with 100 μM H_2O_2 for indicated time and subcellular fractions were isolated. The level of Nrf2 and YTHDF2 in cytosol, nuclear and total cell lysate were detected by western blot. Lamin B1 was used as loading control for nuclear fraction and GAPDH were used as loading control for cytosol fractions and total.

To confirm the YTHDF2 association with ribosomes is RNA dependent, we performed RNase digestion experiments. With RNase digestion, the association of YTHDF2 and ribosome complex is diminished while the ribosomal preparation from cell lysate showed an increased YTHDF2 association with the ribosomes following RNase treatment (Fig 4.7). Therefore, RNA is essential for the presence of YTHDF2 in ribosome (Fig 4.7)

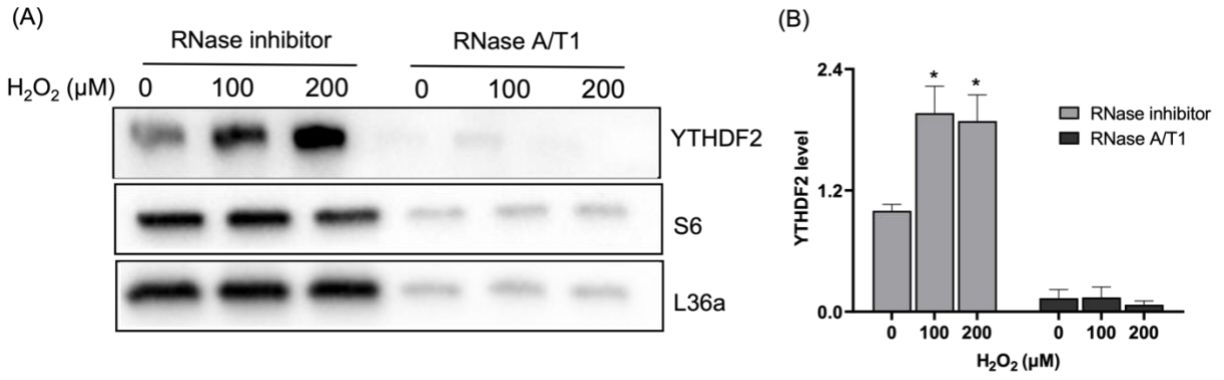

Figure 4. 7. YTHDF2 Associates with Ribosomes Dependent of RNA Binding.

HeLa cells treated with indicated doses of H_2O_2 for 1 hr before lysis in the presence of RNase inhibitor or RNase A/T1. Ribosomes were isolated by ultracentrifugation from cell lysates for measuring associated proteins by Western blot (A). YTHDF2 bands were quantified by ImageJ and presented as means ±SD from three independent experiments. * indicates $p<0.05$ compared to the 0 μM H2O2 group with RNase inhibitor by one-way ANOVA.

Translation initiation requires recognition of the target mRNA strand by binding of eIF4F complex containing eIF4E, eIF4G and eIF4A[270]. This mRNA-eIF4F complex becomes available for landing of 43S PIC to form 48S IC, containing eIF1, eIF1A, eIF3,

eIF2/GTP/tRNAi Met ternary complex, and the 40S small subunit of the ribosome. We performed co-IP experiments to investigate the translation initiation factors that bind to YTHDF2. Despite the co-localization of YTHDF2 with phospho S6, there was no physical binding of YTHDF2 with phospho S6 or total S6 (Fig 4.8).

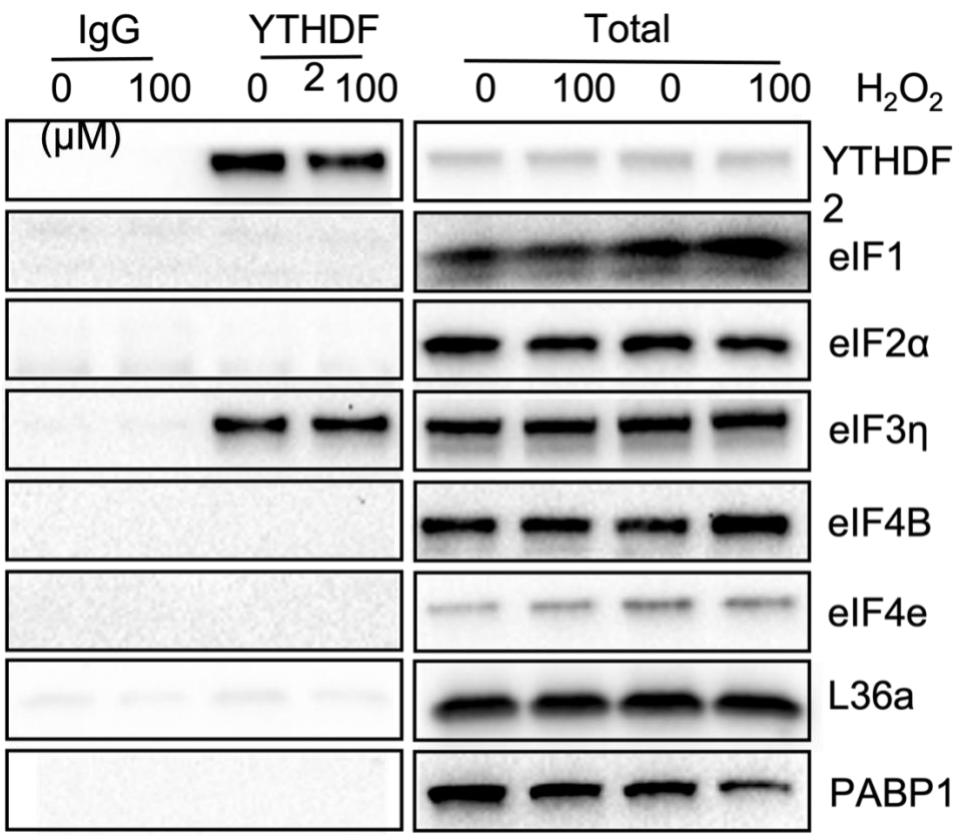

Figure 4. 8. Immunoprecipitation of YTHDF2 for Detection of eIFs.

Hela cells were treated with 100 μM H_2O_2 for 10 minutes and lysed in RIPA buffer 1 hour after for immunoprecipitation. YTHDF2 was captured and pulled down from cell lysate by anti-YTHDF2 antibody and agarose-protein A/G beads. Mouse IgG was used as a control for immunoprecipitation. Protein aliquots from total cell lysates were used as input or loading control. Immunoprecipitated proteins and input were resolved by SDS-PAGE gel for detection of binding proteins as indicated.

We discovered that YTHDF2 increases its interaction with eIF3h due to H_2O_2 treatment (Fig 4.8). Such interaction is consistent with YTHDF2 increasing its distribution in the 43/48S fraction of ribosomes as observed (Fig 4.2). Nevertheless, our RNase digestion experiments suggest that the interaction of YTHDF2 with eIF3h was dependent of RNA binding, since removal of RNases treatment removed an enhanced YTHDF2 association with eIF3h (Fig 4.8). Since eIF3h is a component of 43S PIC, such interaction is consistent with a role of YTHDF2/Nrf2 mRNA interaction for recruitment of 43S PIC in the steps of translation initiation.

m6A in Nrf2 5'UTR for YTHDF2 Binding and Protein Translation

YTHDF2 is a reader of m6A, a modification in RNA catalyzed by METTL3. To show m6A indeed increased in Nrf2 5'UTR due to H2O2 treatment, we used m6A specific antibody to detect m6A in Nrf2 mRNA.We performed Ribonucleoprotein Immunoprecipitation (RNP-IP). In this assay, the m6A was isolated by immunoprecipitation (IP) for detection of Nrf2 mRNA by RT-qPCR. The dose response and time course showed H_2O_2 indeed induced increases of Nrf2 mRNA association with m6A (Fig 4.9A, B)

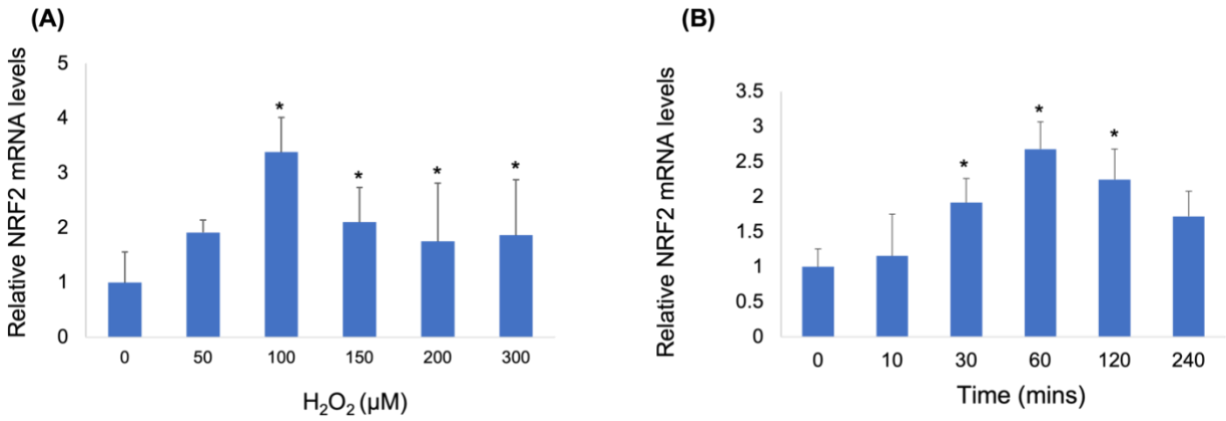

Figure 4. 9. H_2O_2 Induces Increase of m^6A in Nrf2 mRNA.

HeLa cells were treated with 100 μM H_2O_2 (A) or various concentrations (B) for 10 mins and harvested at indicated time point (A) or 1 hr(B). HeLa cell lysates were incubated overnight with m^6A specific antibodies. The immunoprecipitates were used for RT-PCR to detect Nrf2 mRNA. * indicates statistically significant different from time 0.

To address whether such RNA modification plays a role in Nrf2 protein translation, we used siRNA to knock down METTL3 protein. With decreased METTL3, the basal level of Nrf2 was reduced and H_2O_2 induced induction of Nrf2 were blocked (Fig 4.10).

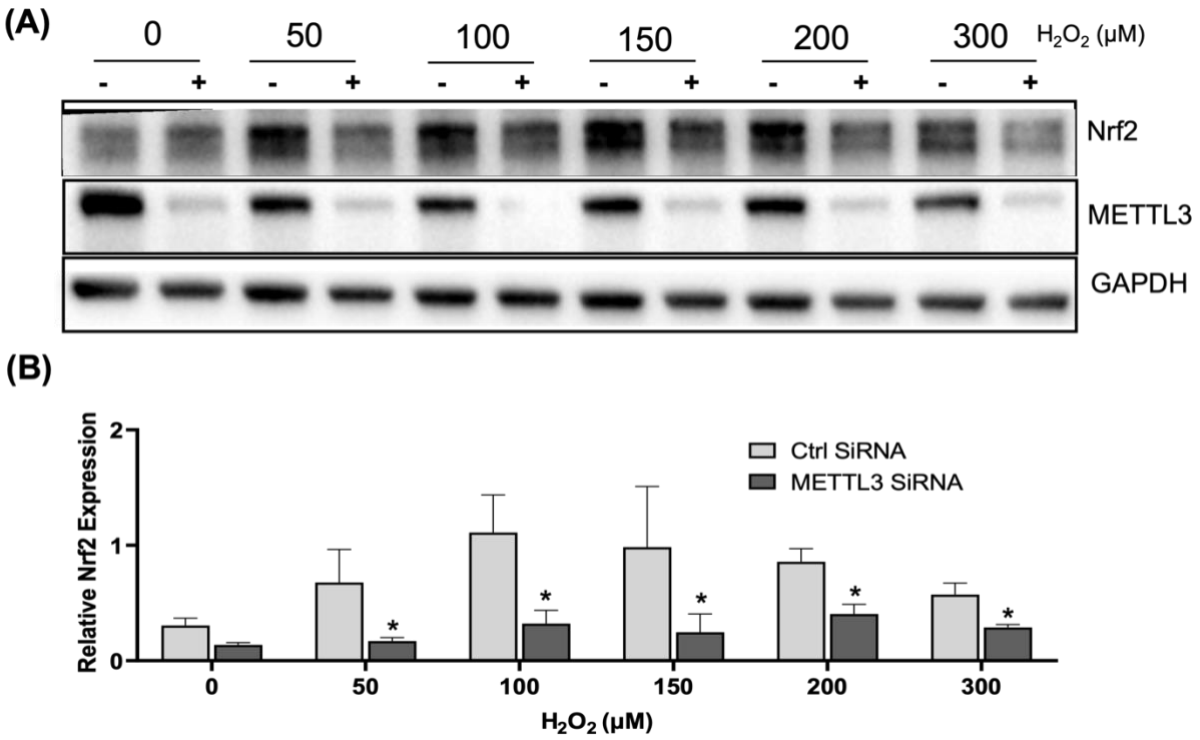

Figure 4. 10. METTL3 Is Required for Nrf2 Protein Induction by H_2O_2.

Hela cells were transfected with control or METTL3 siRNA for 48 hours and then treated with 100 μM H_2O_2 for 1 hour as described. The protein level of Nrf2 and YTHDF2 were assessed by Western blot , with GAPDH as a loading control. (B) Quantification of band intensities was shown as mean±SD, n=3. * $p<0.05$ compared to control siRNA + 0 μM H_2O_2 group, # $p<0.05$ compared to control siRNA + 100 μM H_2O_2 groupThen cells were treated with indicated doses of H_2O_2 for 1 hour.

In an attempt to elucidate the biological function of METTL3 involved in protein translation, we validated METTL3 increasing binding to Nrf2 5'UTR by Far Western blot using biotinylated Nrf2 5'UTR as a bait. The dose response studies showed that H_2O_2 caused a dose dependent increase of METTL3binding to Nrf2 5'UTR, with 100 or 150 mM being the optimal dose (Fig 4.11A). The time course revealed the increased YTHDF2 interaction with Nrf2 5'UTR started at 10 mins after H_2O_2 treatment (Fig 4.11B). The time course studies also revealed H_2O_2 induced increases of Nrf2 mRNA in METTL3 IP complex (Fig 4.11C).

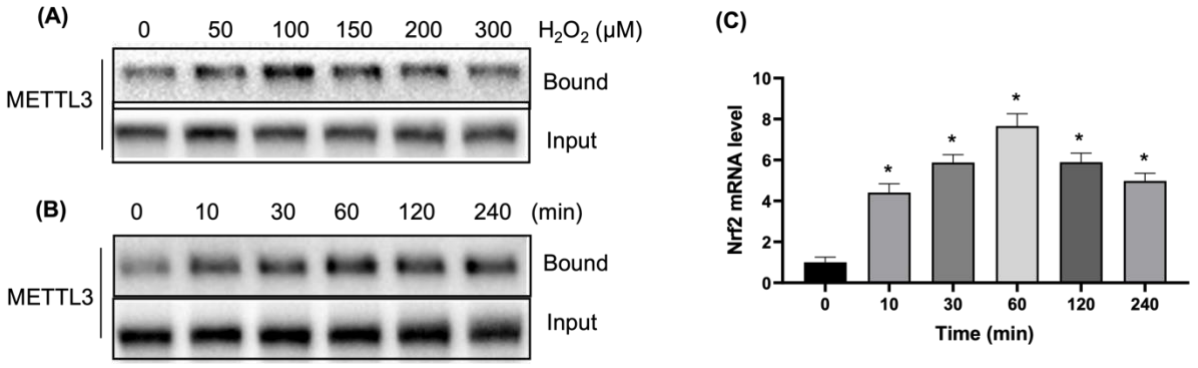

Figure 4. 11. METTL3 Binds to Nrf2 5'UTR and Mediates Nrf2 Induction.

Hela cells were collected at 1 hr after 10 mins H_2O_2 treatment, for in vitro binding to Nrf2 5'UTR. cDNA containing 555 nucleotides Nrf5 5'UTR sequence downstream of a T7 promoter was used to synthesize biotinylated RNA by *in vitro* transcription. The RNA fragment (50 pmol) was incubated overnight with HeLa cell lysates collected after various dose (A) or 100 mM H_2O_2 treatment (B). Streptavidin agarose beads were added to the reaction mixture for isolating the RNA-protein complex for detection of bound METTL3 (pull down) by Western blot, with METTL3 detected from cell lysates as the input (A & B). HeLa cells were treated with 100 μM H_2O_2 (C) and harvested at indicated time point. HeLa cell lysates were incubated overnight with YTHDF2 specific antibodies. The immunoprecipitates were used for RT-PCR to detect Nrf2 mRNA. * indicates statistically different from time 0.

To explore the specific site YTHDF2 binding with 5'UTR, we used biotinylated Nrf2 5'UTR different fragments as baits to isolate binding proteins. The sequence of Nrf2 5'TUR is showed (Fig 4.12A). The baseline YTHDF2 binding decreased with the deduction of Nrf2 5'UTR sequence and H2O2 treatment increased the binding for -555/0

and -555/-225 but not increase for -555/-333 or -555/-450 (Fig 4.12B). This suggests the the YTHDF2 binding site or m6A site should be in -333/-224.

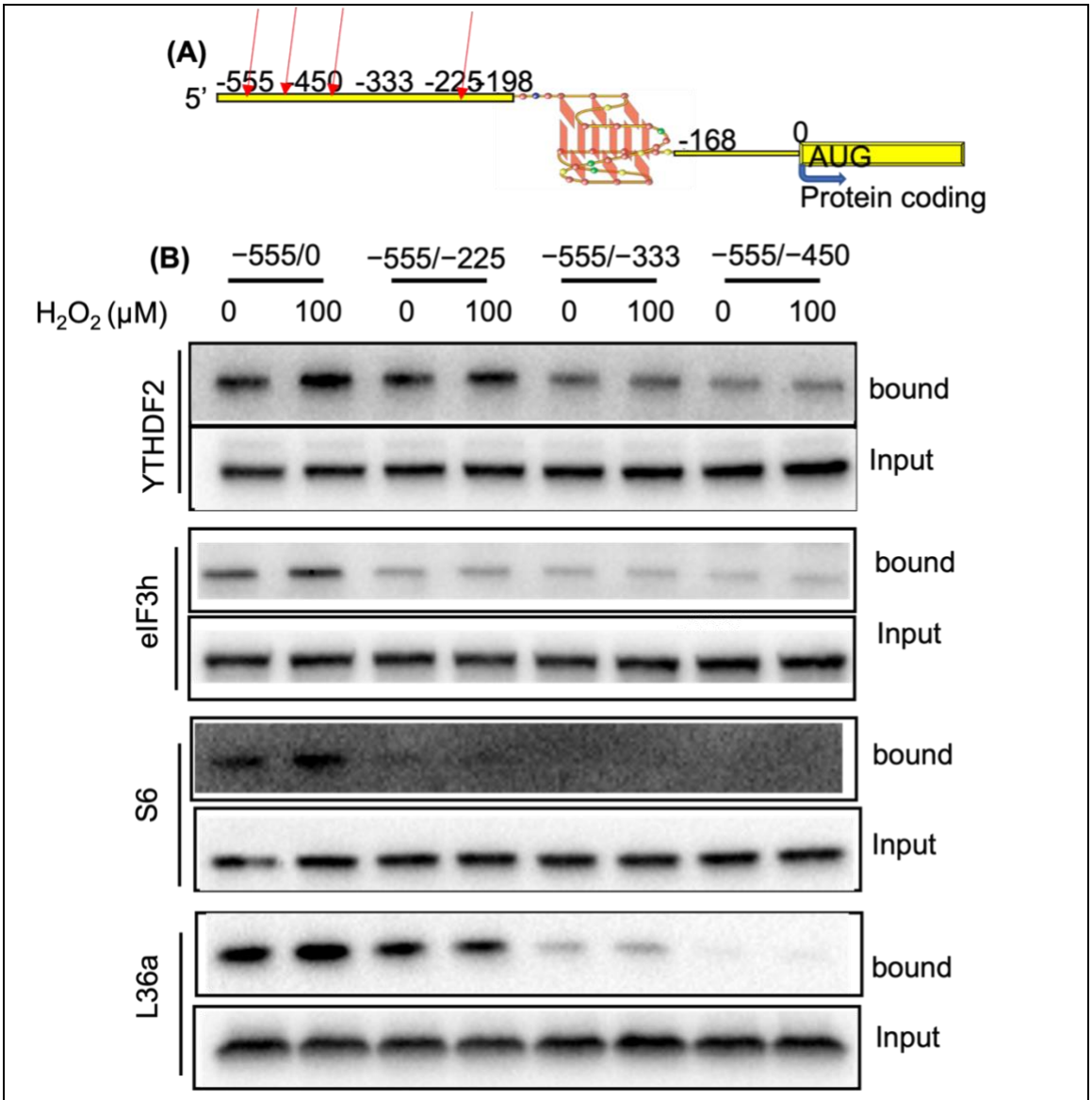

Figure 4. 12. YTHDF2 Binding Site in Nrf2 5'UTR.

Schematic diagram shows Nrf2 5'UTR (A). Full length (-555/0) or fragments of biotinylated Nrf2 5'UTR RNA (50 pmol) were incubated with cytosolic extracts from HeLa cells with or without 100 μM H_2O_2 treatment and harvested at 1 hr.

Biotinylated RNA and its binding proteins were pull down by streptavidin agarose beads for detection of the proteins by Western blot.

Discussion

In this study, we have discovered m6A reader YTHDF2 protein participates in de novo Nrf2 protein translation under oxidative stress. YTHDF2 showed a H2O2 dose- or time- dependent increase in total ribosomal fractions. Although YTHDF2 is present in 40/43/48S, 60S and 80S ribosomal fraction, an increased association was observed in 40/43/48S fractions in H2O2 treated cells. Knocking out YTHDF2 expression using siRNA prevented H2O2 from inducing Nrf2 protein elevation. IP experiments revealed YTHDF2 increased interaction with eIF3h due to H2O2 treatment in an RNA dependent manner. An increase of m6A methylation was discovered in Nrf2 5'UTR as shown by m6A antibody recognition. A role for m6A in Nrf2 5'UTR promoting translation initiation is supported by our discovering that knocking down METTL3 abolished Nrf2 induction by H2O2 treatment. Far-western and RNP-IP results showed an increased binding of METTL3 to Nrf2 mRNA in vitro and in cellular. Our data supports that METTL3 mediated Nrf2 5'UTR methylation recruits YTHDF2 for attachment of 43S PIC to initiate Nrf2 protein translation.

YTHDF2 occupies the full length of 579 amino acids (aa), has the regions localized to mRNA processing bodies (aa 2-384), and targeted the m6A-containing RNA (aa 385-579). Zhu et al. discovered that YTH domain of YTHDF2 was a globular fold with four-stranded β-sheets (β1-β4) surrounded by four α helices (α1-α4) and flanking regions on two sides. Besides, residues K416, R527 on the surface of C-terminal YTH domain are involved in targeting RNA backbone and residues W432 and W486 within the

hydrophobic pocket are participating in the specific recognition of m6A[271]. However, Li et al. has indicated that the YTH domain of YTHDF2 is globularly folded with a central core consisting of eight β-sheets (β1-β8), three α helices (α1-α3), and two 310-helices. Additionally, residues W486 and W491 in the β4-β5 loop, W432 in the β2 strand form an aromatic cage for m6A binding[271]. Wang et al. also revealed that YTHDF2 exhibits a 16-fold higher binding affinity to methylated probe compared[260] to unmethylated one.

Our lab reported that H_2O_2-induced oxidative stress cause Nrf2 de novo translation and the translation initiation starts from the recognition of the IRES in 5'UTR of Nrf2 mRNA with assistance of ITAFs. We have found that 5'UTR of mRNA increases binding to La autoantigen, EF1 and FUBP1 for regulating Nrf2 protein translation against encounter oxidative stress[250, 251] [157, 213]. La and FUBP1 undergo nuclear export, increasing their binding to Nrf2 5'UTR for Nrf2 protein translation regulation. There were evidence that FUBP1 also interacts with eIF3 for translation under stress conditions[213, 250]. Unlike La and FUB1, EF1a does not change subcellular localization but increases the binding to G-quadruplex of Nrf2 5'UTR[157]. Normally, oxidative stress causes methyltransferase (writer) such as METTL3 in nucleus catalyzing the transfering of methyl group to Nrf2 mRNA 5'UTR, leading to the formation of m6A on mRNA. YTHDC1 and YTHDC2 primarily recognize and bind to the site of m6A modification in the nucleus for RNA splicing, nuclear export and increase the translation of target mRNA, respectively[272, 273]. YTHDF2, m6A reader mainly localized in the cytoplasm,

recognized and bind m6A of Nrf2 5'UTR and then recruit eIF3 to initiate translation initiation. This is consistent with our result. We have discovered that YTHDF2 increases its interaction with eIF3 due to H_2O_2 treatment.

Recent studies have uncovered multiple roles of m6A in regulating translation. Importantly, mRNA methylation in different regions may exert different functions. The majority of m6A residues are found in the coding sequence and 3′ UTR influencing RNA for stability, subcellular localization, and translation regulation[274]. However, it has been shown that m6A of mRNA 5'UTR can promote cap-independent heat shock proteins (5'UTR methylated) upon heat shock[261, 275, 276]. In this condition, the YTHDF2 reader translocated in the nucleus preserves mRNAs from FTO-mediated demethylation. Remarkably, the increased 5′ UTR m6A directly binds eukaryotic initiation factor 3 (eIF3), which is sufficient to recruit the 43S complex to initiate translation in the absence of the cap-binding factor eIF4E. Nevertheless, our finding that the binding of YTHDF2 to m6A in Nrf2 mRNA promoting the attachment of 43S pre-initiation complex to Nrf2 mRNA for translation initiation of Nrf2 protein yet protecting against oxidative stress supports their conclusions. m6A modification in the 5′-UTR was also shown to regulate the translation of ATF4 (Activating Transcription Factor 4) during the integrated stress response[187, 277]. In tumors, the regulation of translation by m6A sites in the 5′-UTR promotes the translation of the HIF-1α and Twist1 in hypoxia and facilitates the epithelial–mesenchymal transition (EMT), which plays a relevant role in cancer metastases[278]. But how exactly the methylated adenosine recruits the translation machinery merits further investigation. m6A modification has been shown to alter RNA secondary structures[279]. It is possible

that distinct translation initiation factors are recruited to the methylated 5′UTR, thereby facilitating cap-independent translation.

5’UTR m6A function as a mechanism for mRNA to bypass the cap requirement for translation. Our studies show that cap-independent translation mediated by m^6A requires a m^6A reader, YTHDF2 and its increased interaction with eIF3h. Many eIF3-binding sites in the transcriptome overlap with m^6A sites in 5′ UTRs. By binding eIF3, 5′ UTR m^6A residues can stimulate translation initiation by directly recruiting the 43S preinitiation complex to the 5′ UTR of mRNAs.

The stress-inducible mRNA 5′UTR methylation permits ribosomes to distinguish nascent transcripts from pre-existing messages, thereby achieving selective mRNA translation. The unexpected stress-inducible feature of YTHDF2 offers an elegant mechanism for temporal control of m6A modification on subsets of mRNAs. The mechanistic connection between 5′UTR methylation and cap-independent translation solves the central puzzle of how selective translation is achieved when global translation is suppressed in responding to stress.

Limitation

One limitation of this study is that if the changes in Nrf2 are due to changes in translation, the authors need to show whether Nrf2 mRNA changes with siRNA YTHDF2 in ribosome fractions. Additionally, the data showing binding of a biotinylated Nrf2 5'UTR to YTHDF2 with increasing times and H_2O_2 doses are helpful, but they could simply reflect changes in endogenous YTHDF2. Evidence is needed that endogenous YTHDF2 binds endogenous NRF2 mRNA (including all necessary controls. Finally, the study is conducted in vitro and further research is needed to validate these findings in vivo.

CHAPTER V: SUMMARY STATEMENT

Cardiovascular disease (CVD) represents a significant health and economic burden worldwide. Although improvements of patient care and cardiopulmonary bypass (CPB) technology have revolutionized cardiac surgery and dramatically increased the survival rate of the patients, clinical outcome data suggest that a greater protection strategy is highly in demand. Several lines of evidence point to oxidative stress playing an important role in the onset and progression of postoperative complications. Despite decades of practice with cardioplegia for open heart surgery, there has been little change in the formulation over the past 20 years. Our data using cardiomyocytes in culture supports that DN, HK and LK cardioplegic solutions provide superior myocardia protection via independent mechanisms.

Nrf2 is a master controller of antioxidant defense with well-documented examples in protecting organs from oxidative injury. This dissertation has revealed that Nrf2 activation by DN cardioplegia serves to protect cardiac myocytes from cell injury by oxidative stress. The data presented in this dissertation supports a protective role of Nrf2 in the myocardium. The study presented in Chapter II explored the cardioplegia exhibits cardiac protective effect via Nrf2 induction. In Chapter III, we addressed whether cardioplegic solutions affect the base cellular metabolism and prevent metabolic reprogramming by oxidative stress. Inadequate energy metabolism during CPB can lead to complications such as myocardial, cerebral or renal dysfunction. Preservation of energy metabolism during oxidative stress is important for the protective effects following I/R. Finally, the data presented in Chapter IV points to the role of YTHDF2 and RNA

methylation in Nrf2 induction under oxidative stress. The mechanism of YTHDF2 participation in Nrf2 de novo protein translation by oxidative stress was demonstrated by METTL3 mediated Nrf2 5'UTR methylation and recruitment of YTHDF2 for assembly of 43S PIC to initiate Nrf2 protein translation.

This study has provided three exciting discoveries. First, antegrade perfusion with cardioplegic solutions from the left ventricle to arrest the heart provides a convenient model to study the protective effects of cardioplegic solutions. By incubating cardioplegic solutions with the mouse myocardial tissue or AC16 human cardiomyocytes, we found that high K^+ in DN Cardioplegia induces NRF2 protein, and the expression of antioxidant and detoxification genes, providing a molecular basis for cardiac protection. This study also found that Ca^{2+} plays an important role in K^+ induced Nrf2 protein elevation, and Keap1 mediates Nrf2 protein stability and activity. DN cardioplegia offers a better myocardial preservation compared to other conventional cardioplegia in adult cardiac surgery, as supported by clinical studies[179, 280]. The findings highlight the importance of controlling extracellular Ca^{2+} concentrations in a safe range for induction of NRF2 yet minimizing Ca^{2+} overload and post-operative complications. Optimizing cardioplegia in the future study by adding a non-cytotoxic agent for effective Nrf2 induction may serve well for expanding the potential of Nrf2 mediated cardiac protection.

Second, we evaluated the effects of different cardioplegic solutions on cellular metabolism and metabolic alternations due to oxidative stress. HK and LK cardioplegic

solutions had a minimal impact on the baseline metabolic profile but protected against metabolic changes caused by oxidative stress, suggesting their superiority in clinical settings. NRF2 mediated preservation of mitochondria needs to be confirmed *in vivo* using models of cardiac injury as an underlying mechanism of protection.

Third, we report that RNA methylation m6A reader YTHDF2 protein participates in *de novo* Nrf2 protein translation under oxidative stress. This study showed that knocking down METTL3 or YTHDF2 abolished Nrf2 induction by H_2O_2 treatment, and that METTL3 mediated NRF2 5'UTR methylation recruits YTHDF2 for attachment of 43S PIC to initiate Nrf2 protein translation. We discussed the importance of mRNA methylation in regulating translation and shows that m6A in Nrf2 mRNA 5'UTR can promote cap-independent protein translation, through YTHDF2-medicated recognition and recruitment of 43S pre-initiation complex. Where the m6A occurs within Nrf2 mRNA 5'UTR in response to oxidative stress is an interesting question for follow-up studies.

In conclusion, cardioplegia induces controlled cardiac arrest and provides protection of the myocardium during open-heart surgery. The protective capacity of cardioplegic solutions in cardiac myocytes appears to be multi-faceted, involving the Nrf2 activation for antioxidant system and preservation of energy metabolism. DN cardioplegia protects cardiac myocytes from oxidative injury via activation of Nrf2 whereas HK, LK cardioplegic solutions are superior to other cardioplegia for energy metabolism

preservation during open heart surgery. Nrf2 de novo translation by oxidative stress is YTHDF2 dependent.

References

1. Roth, G.A., et al., *Global Burden of Cardiovascular Diseases and Risk Factors, 1990-2019: Update From the GBD 2019 Study.* J Am Coll Cardiol, 2020. **76**(25): p. 2982-3021.
2. Wittnich, C., et al., *Relative vulnerability of neonatal and adult hearts to ischemic injury.* Circulation, 1987. **76**(5 Pt 2): p. V156-60.
3. Organization, W.H., *Cardiovascular diseases (CVDs).* 11 june 2021.
4. Tsao, C.W., et al., *Heart Disease and Stroke Statistics-2022 Update: A Report From the American Heart Association.* Circulation, 2022. **145**(8): p. e153-e639.
5. Spadaccio, C. and U. Benedetto, *Coronary artery bypass grafting (CABG) vs. percutaneous coronary intervention (PCI) in the treatment of multivessel coronary disease: quo vadis? -a review of the evidences on coronary artery disease.* Ann Cardiothorac Surg, 2018. **7**(4): p. 506-515.
6. Wan, S., et al., *Myocardium is a major source of proinflammatory cytokines in patients undergoing cardiopulmonary bypass.* J Thorac Cardiovasc Surg, 1996. **112**(3): p. 806-11.
7. Zakkar, M., et al., *Cardiopulmonary bypass and oxidative stress.* Oxid Med Cell Longev, 2015. **2015**: p. 189863.
8. Buckberg, G.D., *Left ventricular subendocardial necrosis.* Ann Thorac Surg, 1977. **24**(4): p. 379-93.
9. Dobson, G.P., et al., *Hyperkalemic cardioplegia for adult and pediatric surgery: end of an era?* Front Physiol, 2013. **4**: p. 228.
10. Podesser, B.K. and D.J. Chambers, *New solutions for the heart: an update in advanced perioperative protection*. 2010: Springer Science & Business Media.
11. Chambers, D.J. and H.B. Fallouh, *Cardioplegia and cardiac surgery: pharmacological arrest and cardioprotection during global ischemia and reperfusion.* Pharmacol Ther, 2010. **127**(1): p. 41-52.
12. Wade, J.D., et al., *The Effects of Potassium Citrate Arrest on the Dog's Heart.* Scottish Medical Journal, 1962. **7**(7): p. 306-310.
13. Allen, P., *Some basic features of open-heart surgery using the bubble oxygenator.* Can Med Assoc J, 1957. **77**(12): p. 1125-8.
14. Helmsworth, J.A., et al., *Myocardial injury associated with asystole induced with potassium citrate.* Annals of surgery, 1959. **149**(2): p. 200.
15. Nunn, D.D., et al., *A comparative study of aortic occlusion alone and of potassium citrate arrest during cardiopulmonary bypass.* Surgery, 1959. **45**(5): p. 848-851.
16. Wasserman, F., et al., *Comparative effect of 15 per cent potassium chloride and 30 per cent potassium citrate in resuscitation from ventricular fibrillation following acute myocardial infarction: An Experimental Study.* The Journal of Thoracic and Cardiovascular Surgery, 1959. **38**(1): p. 30-39.
17. Willman, V., et al., *Depression of ventricular function following elective cardiac arrest with potassium citrate.* Surgery, 1959. **46**(4): p. 792-796.
18. Tyers, G.F.O., et al., *The mechanism of myocardial damage following potassium citrate (Melrose) cardioplegia.* Surgery, 1975. **78**(1): p. 45-53.

19. Shumway, N.E., R.R. Lower, and R.C. Stofer, *Selective hypothermia of the heart in anoxic cardiac arrest.* Surg Gynecol Obstet, 1959. **109**: p. 750-4.
20. Kirklin, J.W., V.R. Conti, and E.H. Blackstone, *Prevention of myocardial damage during cardiac operations.* N Engl J Med, 1979. **301**(3): p. 135-41.
21. Cooley, D.A., G.J. Reul, Jr., and D.C. Wukasch, *Ischemic myocardial contracture ("stone heart"). A complication of cardiac surgery.* Isr J Med Sci, 1975. **11**(2-3): p. 203-10.
22. Hoelscher, B., *Studies by electron microscopy on the effects of magnesium chloride-procaine amide or potassium citrate on the myocardium in induced cardiac arrest.* J Cardiovasc Surg (Torino), 1967. **8**(2): p. 163-6.
23. Takahashi, A., et al., *Optimal myocardial protection during crystalloid cardioplegia. Interrelationship between volume and duration of infusion.* J Thorac Cardiovasc Surg, 1988. **96**(5): p. 730-40.
24. Hoyer, E., et al., *Calcium binding to a disordered domain of a type III-secreted protein from a coral pathogen promotes secondary structure formation and catalytic activity.* Scientific Reports, 2019. **9**(1): p. 1-13.
25. Preusse, C.J., *Cardioplegia with an intracellular formulation*, in *Ischemia-reperfusion in cardiac surgery*, H.M. Piper and C.J. Preusse, Editors. 1993, Springer Netherlands: Dordrecht. p. 107-134.
26. Jynge, P., et al., *The St. Thomas' hospital cardioplegic solution: a characterization in two species.* Scand J Thorac Cardiovasc Surg Suppl, 1981. **30**: p. 1-28.
27. Braimbridge, M.V., et al., *Cold cardioplegia or continuous coronary perfusion?: Report on preliminary clinical experience as assessed cytochemically.* The Journal of Thoracic and Cardiovascular Surgery, 1977. **74**(6): p. 900-906.
28. Lolley, D.M., et al., *Reduction of intraoperative myocardial infarction by means of exogenous anaerobic substrate enhancement: prospective randomized study.* The Annals of Thoracic Surgery, 1978. **26**(6): p. 515-524.
29. Conti, V.R., et al., *Cold cardioplegia versus hypothermia for myocardial protection. Randomized clinical study.* J Thorac Cardiovasc Surg, 1978. **76**(5): p. 577-89.
30. Robinson, L.A., et al., *Myocardial protection for acquired heart disease surgery: results of a national survey.* Ann Thorac Surg, 1995. **59**(2): p. 361-72.
31. Follette, D.M., et al., *Advantages of blood cardioplegia over continuous coronary perfusion or intermittent ischemia. Experimental and clinical study.* J Thorac Cardiovasc Surg, 1978. **76**(5): p. 604-19.
32. Barner, H.B., *Blood cardioplegia: a review and comparison with crystalloid cardioplegia.* Ann Thorac Surg, 1991. **52**(6): p. 1354-67.
33. Guru, V., et al., *Is blood superior to crystalloid cardioplegia? A meta-analysis of randomized clinical trials.* Circulation, 2006. **114**(1_supplement): p. I-331-I-338.
34. McMurchie, E.J., J.K. Raison, and K.D. Cairncross, *Temperature-induced phase changes in membranes of heart: a contrast between the thermal response of poikilotherms and homeotherms.* Comp Biochem Physiol B, 1973. **44**(4): p. 1017-26.
35. Rahn, H., R.B. Reeves, and B.J. Howell, *Hydrogen ion regulation, temperature, and evolution.* Am Rev Respir Dis, 1975. **112**(2): p. 165-72.
36. Rosenkranz, E.R., et al., *Warm induction of cardioplegia with glutamate-enriched blood in coronary patients with cardiogenic shock who are dependent on inotropic drugs and*

intra-aortic balloon support: initial experience and operative strategy. The Journal of thoracic and cardiovascular surgery, 1983. **86**(4): p. 507-518.
37. Buckberg, G.D., *Update on current techniques of myocardial protection.* Ann Thorac Surg, 1995. **60**(3): p. 805-14.
38. Robertson, J.M., et al., *Safety of prolonged aortic clamping with blood cardioplegia. I. Glutamate enrichment in normal hearts.* J Thorac Cardiovasc Surg, 1984. **88**(3): p. 395-401.
39. Allen, B.S., *Pediatric myocardial protection: where do we stand?* J Thorac Cardiovasc Surg, 2004. **128**(1): p. 11-3.
40. Magovern, J.A., W.E. Pae, Jr., and J.A. Waldhausen, *Protection of the immature myocardium. An experimental evaluation of topical cooling, single-dose, and multiple-dose administration of St. Thomas' Hospital cardioplegic solution.* J Thorac Cardiovasc Surg, 1988. **96**(3): p. 408-13.
41. Kotani, Y., et al., *Current cardioplegia practice in pediatric cardiac surgery: a North American multiinstitutional survey.* Ann Thorac Surg, 2013. **96**(3): p. 923-9.
42. O'Brien, J.D., et al., *Pediatric cardioplegia strategy results in enhanced calcium metabolism and lower serum troponin T.* Ann Thorac Surg, 2009. **87**(5): p. 1517-23.
43. Talwar, S., et al., *Comparison of del Nido and St Thomas Cardioplegia Solutions in Pediatric Patients: A Prospective Randomized Clinical Trial.* Semin Thorac Cardiovasc Surg, 2017. **29**(3): p. 366-374.
44. Matte, G.S. and P.J. del Nido, *History and use of del Nido cardioplegia solution at Boston Children's Hospital.* J Extra Corpor Technol, 2012. **44**(3): p. 98-103.
45. Ota, T., et al., *Short-term outcomes in adult cardiac surgery in the use of del Nido cardioplegia solution.* Perfusion, 2016. **31**(1): p. 27-33.
46. Sorabella, R.A., et al., *Myocardial protection using del nido cardioplegia solution in adult reoperative aortic valve surgery.* J Card Surg, 2014. **29**(4): p. 445-9.
47. Mongero, L.B., *Del Nido Cardioplegia-Not Just Kids Stuff.* J Extra Corpor Technol, 2016. **48**(2): p. P25-8.
48. O'Donnell, C., et al., *Utilization of Del Nido Cardioplegia in Adult Coronary Artery Bypass Grafting- A Retrospective Analysis.* Circ J, 2019. **83**(2): p. 342-346.
49. Velez, D.A., et al., *All-blood (miniplegia) versus dilute cardioplegia in experimental surgical revascularization of evolving infarction.* Circulation, 2001. **104**(suppl_1): p. I-296-I-302.
50. Kim, W.K., et al., *del Nido cardioplegia in adult cardiac surgery: beyond single-valve surgery.* Interact Cardiovasc Thorac Surg, 2018. **27**(1): p. 81-87.
51. Brown, J.R., et al., *Perioperative increases in serum creatinine are predictive of increased 90-day mortality after coronary artery bypass graft surgery.* Circulation, 2006. **114**(1_supplement): p. I-409-I-413.
52. Scrutinio, D. and P. Giannuzzi, *Comorbidity in patients undergoing coronary artery bypass graft surgery: impact on outcome and implications for cardiac rehabilitation.* European Journal of Preventive Cardiology, 2008. **15**(4): p. 379-385.
53. Berg, K., et al., *Oxidative stress during coronary artery bypass operations: importance of surgical trauma and drug treatment.* Scandinavian Cardiovascular Journal, 2006. **40**(5): p. 291-297.

54. Trachootham, D., et al., *Redox regulation of cell survival.* Antioxidants & redox signaling, 2008. **10**(8): p. 1343-1374.
55. Goodyear-Bruch, C. and J.D. Pierce, *Oxidative stress in critically ill patients.* American Journal of Critical Care, 2002. **11**(6): p. 543-551.
56. Bernstein, J., et al., *PDGF2/c-sis mRNA leader contains a differentiation-linked internal ribosomal entry site (D-IRES).* J Biol Chem, 1997. **272**(14): p. 9356-62.
57. Rahimtoola, S., *The hibernating myocardium in ischaemia and congestive heart failure.* European heart journal, 1993. **14**(suppl_A): p. 22-26.
58. Reimer, K.A., et al., *The wavefront phenomenon of ischemic cell death. 1. Myocardial infarct size vs duration of coronary occlusion in dogs.* Circulation, 1977. **56**(5): p. 786-794.
59. Stanley, W.C. and H.N. Sabbah, *Metabolic therapy for ischemic heart disease: the rationale for inhibition of fatty acid oxidation.* Heart failure reviews, 2005. **10**(4): p. 275.
60. Salem, J.E., et al., *Mechanistic model of myocardial energy metabolism under normal and ischemic conditions.* Annals of Biomedical Engineering, 2002. **30**: p. 202-216.
61. Murphy, E. and C. Steenbergen, *Mechanisms underlying acute protection from cardiac ischemia-reperfusion injury.* Physiological reviews, 2008. **88**(2): p. 581-609.
62. Robergs, R.A., F. Ghiasvand, and D. Parker, *Biochemistry of exercise-induced metabolic acidosis.* American Journal of Physiology-Regulatory, Integrative and Comparative Physiology, 2004.
63. Yokota, A., et al., *TIME LIMIT FOR EARLY CORONARY ARTERY REVASCULARIZATION: Restoration of Contractility in Reperfused Myocardium in Dogs.* japanese Circulation journal, 1981. **45**(12): p. 1355-1363.
64. Kloner, R.A., C.E. Ganote, and R.B. Jennings, *The "no-reflow" phenomenon after temporary coronary occlusion in the dog.* The Journal of clinical investigation, 1974. **54**(6): p. 1496-1508.
65. Imura, H., et al., *Controlled hyperkalemic reperfusion with magnesium rescues ischemic juvenile hearts by reducing calcium loading.* The Journal of thoracic and cardiovascular surgery, 2011. **141**(6): p. 1529-1537.
66. Panconesi, R., et al., *Mitochondria and ischemia reperfusion injury.* Current Opinion in Organ Transplantation, 2022. **27**(5): p. 434-445.
67. Andrienko, T., et al., *27 Monitoring the levels of the reactive oxygen species on the whole heart and in single cardiomyocytes during ischaemia-reperfusion.* Heart, 2011. **97**(24): p. e8-e8.
68. Anedda, A., et al., *The transcription factor Nrf2 promotes survival by enhancing the expression of uncoupling protein 3 under conditions of oxidative stress.* Free radical biology and medicine, 2013. **61**: p. 395-407.
69. Tsutsui, H., S. Kinugawa, and S. Matsushima, *Oxidative stress and heart failure.* American journal of physiology-Heart and circulatory physiology, 2011.
70. Clempus, R.E. and K.K. Griendling, *Reactive oxygen species signaling in vascular smooth muscle cells.* Cardiovascular research, 2006. **71**(2): p. 216-225.
71. Rao, V., et al., *Lactate release during reperfusion predicts low cardiac output syndrome after coronary bypass surgery.* The Annals of thoracic surgery, 2001. **71**(6): p. 1925-1930.

72. Maltesen, R.G., et al., *Metabotyping patients' journeys reveals early predisposition to lung injury after cardiac surgery.* Scientific Reports, 2017. **7**(1): p. 40275.
73. Buggeskov, K.B., et al., *Lung protection strategies during cardiopulmonary bypass affect the composition of blood electrolytes and metabolites—a randomized controlled trial.* Journal of clinical medicine, 2018. **7**(11): p. 462.
74. Merante, F., et al., *Myocardial aerobic metabolism is impaired in a cell culture model of cyanotic heart disease.* American Journal of Physiology-Heart and Circulatory Physiology, 1998. **275**(5): p. H1673-H1681.
75. Lewandowski, E.D. and L.T. White, *Pyruvate dehydrogenase influences postischemic heart function.* Circulation, 1995. **91**(7): p. 2071-2079.
76. Rao, V., et al., *Insulin cardioplegia for elective coronary bypass surgery.* The Journal of Thoracic and Cardiovascular Surgery, 2000. **119**(6): p. 1176-1184.
77. Pearson, T.A., et al., *Markers of inflammation and cardiovascular disease: application to clinical and public health practice: A statement for healthcare professionals from the Centers for Disease Control and Prevention and the American Heart Association.* Circulation, 2003. **107**(3): p. 499-511.
78. Levy, J.H. and K.A. Tanaka, *Inflammatory response to cardiopulmonary bypass.* The Annals of Thoracic Surgery, 2003. **75**(2): p. S715-S720.
79. Olia, S.E., et al., *Mechanical blood trauma in assisted circulation: sublethal RBC damage preceding hemolysis.* Int J Artif Organs, 2016. **39**(4): p. 150-9.
80. Morariu, A.M., et al., *Red blood cell aggregation during cardiopulmonary bypass: a pathogenic cofactor in endothelial cell activation?* European Journal of Cardio-Thoracic Surgery, 2004. **26**(5): p. 939-946.
81. Relevy, H., et al., *Blood banking-induced alteration of red blood cell flow properties.* Transfusion, 2008. **48**(1): p. 136-46.
82. Snyder, J.J., et al., *A comparison of transplant outcomes in peritoneal and hemodialysis patients.* Kidney International, 2002. **62**(4): p. 1423-1430.
83. Callister, M.E., et al., *Extracellular thioredoxin levels are increased in patients with acute lung injury.* Thorax, 2006. **61**(6): p. 521.
84. Gutteridge, J.M., et al., *Pro-oxidant iron is present in human pulmonary epithelial lining fluid: implications for oxidative stress in the lung.* Biochem Biophys Res Commun, 1996. **220**(3): p. 1024-7.
85. Ghorbel, M.T., et al., *Changes in renal medulla gene expression in a pre-clinical model of post cardiopulmonary bypass acute kidney injury.* BMC Genomics, 2014. **15**(1): p. 916.
86. Han, W.K. and J.V. Bonventre, *Biologic markers for the early detection of acute kidney injury.* Current Opinion in Critical Care, 2004. **10**(6).
87. Ercil, H., et al., *Treatment of Moderate Sized Renal Pelvis Calculi: Stone Clearance Time Comparison of Extracorporeal Shock Wave Lithotripsy and Retrograde Intrarenal Surgery.* Urology Journal, 2016. **13**(1): p. 2490-2495.
88. Weijs, B., U. Schotten, and H.J. Crijns, *Pathophysiology of idiopathic atrial fibrillation - prognostic and treatment implications.* Curr Pharm Des, 2015. **21**(5): p. 551-72.
89. Kim Young, M., et al., *Association of Atrial Nicotinamide Adenine Dinucleotide Phosphate Oxidase Activity With the Development of Atrial Fibrillation After Cardiac Surgery.* Journal of the American College of Cardiology, 2008. **51**(1): p. 68-74.

90. Orenes-Piñero, E., et al., *Pre and post-operative treatments for prevention of atrial fibrillation after cardiac surgery.* Mini Rev Med Chem, 2012. **12**(13): p. 1419-31.
91. Kim, Y.M., et al., *A myocardial Nox2 containing NAD(P)H oxidase contributes to oxidative stress in human atrial fibrillation.* Circ Res, 2005. **97**(7): p. 629-36.
92. Montaigne, D., et al., *Mitochondrial dysfunction as an arrhythmogenic substrate: a translational proof-of-concept study in patients with metabolic syndrome in whom post-operative atrial fibrillation develops.* J Am Coll Cardiol, 2013. **62**(16): p. 1466-73.
93. Anderson, E.J., et al., *Monoamine oxidase is a major determinant of redox balance in human atrial myocardium and is associated with postoperative atrial fibrillation.* J Am Heart Assoc, 2014. **3**(1): p. e000713.
94. Pell, V.R., et al., *Succinate metabolism: a new therapeutic target for myocardial reperfusion injury.* Cardiovascular Research, 2016. **111**(2): p. 134-141.
95. Hartmann, M. and U.K.M. Decking, *Blocking Na+–H+Exchange by Cariporide Reduces Na+-overload in Ischemia and is Cardioprotective.* Journal of Molecular and Cellular Cardiology, 1999. **31**(11): p. 1985-1995.
96. Griffiths, E.J., et al., *Mitochondrial calcium transporting pathways during hypoxia and reoxygenation in single rat cardiomyocytes.* Cardiovascular Research, 1998. **39**(2): p. 423-433.
97. Shoshan-Barmatz, V., S. De, and A. Meir, *The Mitochondrial Voltage-Dependent Anion Channel 1, Ca(2+) Transport, Apoptosis, and Their Regulation.* Front Oncol, 2017. **7**: p. 60.
98. Patron, M., et al., *The Mitochondrial Calcium Uniporter (MCU): Molecular Identity and Physiological Roles*.* Journal of Biological Chemistry, 2013. **288**(15): p. 10750-10758.
99. Brown, D.A., et al., *Mitochondrial function as a therapeutic target in heart failure.* Nature Reviews Cardiology, 2017. **14**(4): p. 238-250.
100. Nohl, H., V. Koltover, and K. Stolze, *Ischemia/reperfusion impairs mitochondrial energy conservation and triggers O2.- release as a byproduct of respiration.* Free Radic Res Commun, 1993. **18**(3): p. 127-37.
101. Bulua, A.C., et al., *Mitochondrial reactive oxygen species promote production of proinflammatory cytokines and are elevated in TNFR1-associated periodic syndrome (TRAPS).* J Exp Med, 2011. **208**(3): p. 519-33.
102. Danzeisen, R., et al., *Targeted antioxidative and neuroprotective properties of the dopamine agonist pramipexole and its nondopaminergic enantiomer SND919CL2x [(+)2-amino-4,5,6,7-tetrahydro-6-Lpropylamino-benzathiazole dihydrochloride].* J Pharmacol Exp Ther, 2006. **316**(1): p. 189-99.
103. Quinlan, C.L., et al., *Mitochondrial complex II can generate reactive oxygen species at high rates in both the forward and reverse reactions.* J Biol Chem, 2012. **287**(32): p. 27255-64.
104. Starkov, A.A., et al., *Mitochondrial alpha-ketoglutarate dehydrogenase complex generates reactive oxygen species.* J Neurosci, 2004. **24**(36): p. 7779-88.
105. Marí, M., et al., *Mitochondrial glutathione, a key survival antioxidant.* Antioxid Redox Signal, 2009. **11**(11): p. 2685-700.
106. *Superoxide Dismutases: Role in Redox Signaling, Vascular Function, and Diseases.* Antioxidants & Redox Signaling, 2011. **15**(6): p. 1583-1606.

107. Ribas, V., C. García-Ruiz, and J.C. Fernández-Checa, *Glutathione and mitochondria.* Frontiers in Pharmacology, 2014. **5**.
108. Rodríguez-Manzaneque, M.T., et al., *Grx5 is a mitochondrial glutaredoxin required for the activity of iron/sulfur enzymes.* Mol Biol Cell, 2002. **13**(4): p. 1109-21.
109. Pérez, V.I., et al., *Thioredoxin 2 haploinsufficiency in mice results in impaired mitochondrial function and increased oxidative stress.* Free Radical Biology and Medicine, 2008. **44**(5): p. 882-892.
110. Kiermayer, C., et al., *Heart-Specific Knockout of the Mitochondrial Thioredoxin Reductase (Txnrd2) Induces Metabolic and Contractile Dysfunction in the Aging Myocardium.* J Am Heart Assoc, 2015. **4**(7).
111. Pasdois, P., et al., *The role of oxidized cytochrome c in regulating mitochondrial reactive oxygen species production and its perturbation in ischaemia.* Biochemical Journal, 2011. **436**(2): p. 493-505.
112. Madesh, M. and G. Hajnóczky, *VDAC-dependent permeabilization of the outer mitochondrial membrane by superoxide induces rapid and massive cytochrome c release.* J Cell Biol, 2001. **155**(6): p. 1003-15.
113. Zimmet, J.M. and J.M. Hare, *Nitroso–Redox Interactions in the Cardiovascular System.* Circulation, 2006. **114**(14): p. 1531-1544.
114. Xiang, M., et al., *Role of Oxidative Stress in Reperfusion following Myocardial Ischemia and Its Treatments.* Oxidative Medicine and Cellular Longevity, 2021. **2021**: p. 6614009.
115. Gao, X., et al., *Role of TNF-alpha-induced reactive oxygen species in endothelial dysfunction during reperfusion injury.* Am J Physiol Heart Circ Physiol, 2008. **295**(6): p. H2242-9.
116. Nanduri, J., et al., *Xanthine oxidase mediates hypoxia-inducible factor-2α degradation by intermittent hypoxia.* PLoS One, 2013. **8**(10): p. e75838.
117. Muralikrishna Adibhatla, R. and J.F. Hatcher, *Phospholipase A2, reactive oxygen species, and lipid peroxidation in cerebral ischemia.* Free Radical Biology and Medicine, 2006. **40**(3): p. 376-387.
118. Kelley, E.E., et al., *Moderate hypoxia induces xanthine oxidoreductase activity in arterial endothelial cells.* Free Radical Biology and Medicine, 2006. **40**(6): p. 952-959.
119. Seymour, K.J., et al., *Stress activation of mammary epithelial cell xanthine oxidoreductase is mediated by p38 MAPK and CCAAT/enhancer-binding protein-beta.* J Biol Chem, 2006. **281**(13): p. 8545-58.
120. Zhang, Y.-S., et al., *Allopurinol attenuates oxidative injury in rat hearts suffered ischemia/reperfusion via suppressing the xanthine oxidase/vascular peroxidase 1 pathway.* European Journal of Pharmacology, 2021. **908**: p. 174368.
121. Vickneson, K. and J. George, *Xanthine Oxidoreductase Inhibitors*, in *Reactive Oxygen Species : Network Pharmacology and Therapeutic Applications*, H.H.H.W. Schmidt, P. Ghezzi, and A. Cuadrado, Editors. 2021, Springer International Publishing: Cham. p. 205-228.
122. Cantu-Medellin, N. and E.E. Kelley, *Xanthine oxidoreductase-catalyzed reduction of nitrite to nitric oxide: Insights regarding where, when and how.* Nitric Oxide, 2013. **34**: p. 19-26.

123. De Pascali, F., et al., *Hypoxia and reoxygenation induce endothelial nitric oxide synthase uncoupling in endothelial cells through tetrahydrobiopterin depletion and S-glutathionylation.* Biochemistry, 2014. **53**(22): p. 3679-88.
124. Das, D.K., et al., *Role of xanthine oxidase inhibitor as free radical scavenger: A novel mechanism of action of allopurinol and oxypurinol in myocardial salvage.* Biochemical and Biophysical Research Communications, 1987. **148**(1): p. 314-319.
125. Weidert, E.R., et al., *Inhibition of xanthine oxidase by the aldehyde oxidase inhibitor raloxifene: implications for identifying molybdopterin nitrite reductases.* Nitric Oxide, 2014. **37**: p. 41-5.
126. Battelli, M.G., et al., *Xanthine oxidoreductase in cancer: more than a differentiation marker.* Cancer Med, 2016. **5**(3): p. 546-57.
127. Grill, H.P., et al., *Direct measurement of myocardial free radical generation in an in vivo model: Effects of postischemic reperfusion and treatment with human recombinant superoxide dismutase.* Journal of the American College of Cardiology, 1992. **20**(7): p. 1604-1611.
128. Lambeth, J.D., *NOX enzymes and the biology of reactive oxygen.* Nature Reviews Immunology, 2004. **4**(3): p. 181-189.
129. Barnes, J.L. and Y. Gorin, *Myofibroblast differentiation during fibrosis: role of NAD(P)H oxidases.* Kidney International, 2011. **79**(9): p. 944-956.
130. Santos, C.X.C., et al., *Redox signaling in cardiac myocytes.* Free Radical Biology and Medicine, 2011. **50**(7): p. 777-793.
131. Braunersreuther, V., et al., *Role of NADPH oxidase isoforms NOX1, NOX2 and NOX4 in myocardial ischemia/reperfusion injury.* Journal of Molecular and Cellular Cardiology, 2013. **64**: p. 99-107.
132. Fu, Y., et al., *Regulation of NADPH Oxidase Activity Is Associated with miRNA-25-Mediated NOX4 Expression in Experimental Diabetic Nephropathy.* American Journal of Nephrology, 2010. **32**(6): p. 581-589.
133. Maejima, Y., et al., *Regulation of myocardial growth and death by NADPH oxidase.* Journal of Molecular and Cellular Cardiology, 2011. **50**(3): p. 408-416.
134. Ambasta, R.K., et al., *Direct interaction of the novel Nox proteins with p22phox is required for the formation of a functionally active NADPH oxidase.* J Biol Chem, 2004. **279**(44): p. 45935-41.
135. Siu, K.L., et al., *Netrin-1 abrogates ischemia/reperfusion-induced cardiac mitochondrial dysfunction via nitric oxide-dependent attenuation of NOX4 activation and recoupling of NOS.* Journal of Molecular and Cellular Cardiology, 2015. **78**: p. 174-185.
136. Looi, Y.H., et al., *Involvement of Nox2 NADPH oxidase in adverse cardiac remodeling after myocardial infarction.* Hypertension, 2008. **51**(2): p. 319-25.
137. Doerries, C., et al., *Critical role of the NAD(P)H oxidase subunit p47phox for left ventricular remodeling/dysfunction and survival after myocardial infarction.* Circ Res, 2007. **100**(6): p. 894-903.
138. Matsushima, S., et al., *Broad suppression of NADPH oxidase activity exacerbates ischemia/reperfusion injury through inadvertent downregulation of hypoxia-inducible factor-1α and upregulation of peroxisome proliferator-activated receptor-α.* Circ Res, 2013. **112**(8): p. 1135-49.

139. Takac, I., K. Schröder, and R.P. Brandes, *The Nox Family of NADPH Oxidases: Friend or Foe of the Vascular System?* Current Hypertension Reports, 2012. **14**(1): p. 70-78.
140. Olek, R.A., et al., *Antioxidant activity of NADH and its analogue--an in vitro study.* J Biochem Mol Biol, 2004. **37**(4): p. 416-21.
141. Bedard, K. and K.H. Krause, *The NOX family of ROS-generating NADPH oxidases: physiology and pathophysiology.* Physiol Rev, 2007. **87**(1): p. 245-313.
142. Vásquez-Vivar, J., et al., *Superoxide generation by endothelial nitric oxide synthase: The influence of cofactors.* Proceedings of the National Academy of Sciences, 1998. **95**(16): p. 9220-9225.
143. Landmesser, U., et al., *Oxidation of tetrahydrobiopterin leads to uncoupling of endothelial cell nitric oxide synthase in hypertension.* J Clin Invest, 2003. **111**(8): p. 1201-9.
144. Wang, P. and J.L. Zweier, *Measurement of nitric oxide and peroxynitrite generation in the postischemic heart. Evidence for peroxynitrite-mediated reperfusion injury.* J Biol Chem, 1996. **271**(46): p. 29223-30.
145. Ferdinandy, P. and R. Schulz, *Nitric oxide, superoxide, and peroxynitrite in myocardial ischaemia-reperfusion injury and preconditioning.* Br J Pharmacol, 2003. **138**(4): p. 532-43.
146. Moi, P., et al., *Isolation of NF-E2-related factor 2 (Nrf2), a NF-E2-like basic leucine zipper transcriptional activator that binds to the tandem NF-E2/AP1 repeat of the beta-globin locus control region.* Proceedings of the National Academy of Sciences, 1994. **91**(21): p. 9926-9930.
147. Ma, Q., *Role of nrf2 in oxidative stress and toxicity.* Annu Rev Pharmacol Toxicol, 2013. **53**: p. 401-26.
148. He, F., et al., *NRF2 activates growth factor genes and downstream AKT signaling to induce mouse and human hepatomegaly.* J Hepatol, 2020. **72**(6): p. 1182-1195.
149. Chen, Q.M. and A.J. Maltagliati, *Nrf2 at the heart of oxidative stress and cardiac protection.* Physiol Genomics, 2018. **50**(2): p. 77-97.
150. Zhang, Y. and G.B. Gordon, *A strategy for cancer prevention: Stimulation of the Nrf2-ARE signaling pathway.* Molecular Cancer Therapeutics, 2004. **3**(7): p. 885-893.
151. Cullinan, S.B., et al., *Nrf2 is a direct PERK substrate and effector of PERK-dependent cell survival.* Mol Cell Biol, 2003. **23**(20): p. 7198-209.
152. Baird, L., et al., *Regulatory flexibility in the Nrf2-mediated stress response is conferred by conformational cycling of the Keap1-Nrf2 protein complex.* Proceedings of the National Academy of Sciences, 2013. **110**(38): p. 15259-15264.
153. Komatsu, M., et al., *The selective autophagy substrate p62 activates the stress responsive transcription factor Nrf2 through inactivation of Keap1.* Nature Cell Biology, 2010. **12**(3): p. 213-223.
154. Ichimura, Y., et al., *Phosphorylation of p62 Activates the Keap1-Nrf2 Pathway during Selective Autophagy.* Molecular Cell, 2013. **51**(5): p. 618-631.
155. Purdom-Dickinson, S.E., et al., *Translational control of nrf2 protein in activation of antioxidant response by oxidants.* Molecular pharmacology, 2007. **72**(4): p. 1074-1081.
156. Li, W., et al., *An internal ribosomal entry site mediates redox-sensitive translation of Nrf2.* Nucleic Acids Research, 2009. **38**(3): p. 778-788.

157. Lee, S.C., et al., *G-Quadruplex in the NRF2 mRNA 5' Untranslated Region Regulates De Novo NRF2 Protein Translation under Oxidative Stress.* Mol Cell Biol, 2017. **37**(1).
158. Shenton, D., et al., *Global Translational Responses to Oxidative Stress Impact upon Multiple Levels of Protein Synthesis*.* Journal of Biological Chemistry, 2006. **281**(39): p. 29011-29021.
159. Edmunds, L.H., Jr., *The evolution of cardiopulmonary bypass: lessons to be learned.* Perfusion, 2002. **17**(4): p. 243-51.
160. Stoney, W.S., *Evolution of cardiopulmonary bypass.* Circulation, 2009. **119**(21): p. 2844-53.
161. Hessel, E.A., 2nd, *A Brief History of Cardiopulmonary Bypass.* Semin Cardiothorac Vasc Anesth, 2014. **18**(2): p. 87-100.
162. Nicolini, F., et al., *The evolution of cardiovascular surgery in elderly patient: a review of current options and outcomes.* Biomed Res Int, 2014. **2014**: p. 736298.
163. Loberman, D., et al., *Myocardial preservation methods in isolated minimal invasive mitral valve surgery: Society of Thoracic Surgeons (STS) database outcomes.* J Card Surg, 2020. **35**(1): p. 163-173.
164. Oliveira, M.A., et al., *Modes of induced cardiac arrest: hyperkalemia and hypocalcemia--literature review.* Rev Bras Cir Cardiovasc, 2014. **29**(3): p. 432-6.
165. Fallouh, H.B., et al., *Esmolol cardioplegia: the cellular mechanism of diastolic arrest.* Cardiovascular Research, 2010. **87**(3): p. 552-560.
166. Suleiman, M.S., A.P. Halestrap, and E.J. Griffiths, *Mitochondria: a target for myocardial protection.* Pharmacol Ther, 2001. **89**(1): p. 29-46.
167. Becker, L.B., et al., *Generation of superoxide in cardiomyocytes during ischemia before reperfusion.* Am J Physiol, 1999. **277**(6): p. H2240-6.
168. Murphy, M.P., *How mitochondria produce reactive oxygen species.* Biochem J, 2009. **417**(1): p. 1-13.
169. Raedschelders, K., D.M. Ansley, and D.D. Chen, *The cellular and molecular origin of reactive oxygen species generation during myocardial ischemia and reperfusion.* Pharmacol Ther, 2012. **133**(2): p. 230-55.
170. Chen, Q.M., *Nrf2 for protection against oxidant generation and mitochondrial damage in cardiac injury.* Free Radic Biol Med, 2022. **179**: p. 133-143.
171. Chen, Q.M., *Nrf2 for cardiac protection: pharmacological options against oxidative stress.* Trends Pharmacol Sci, 2021. **42**(9): p. 729-744.
172. Cock, P.J.A., et al., *The Sanger FASTQ file format for sequences with quality scores, and the Solexa/Illumina FASTQ variants.* Nucleic Acids Research, 2009. **38**(6): p. 1767-1771.
173. Kim, D., B. Langmead, and S.L. Salzberg, *HISAT: a fast spliced aligner with low memory requirements.* Nat Methods, 2015. **12**(4): p. 357-60.
174. Langmead, B. and S.L. Salzberg, *Fast gapped-read alignment with Bowtie 2.* Nat Methods, 2012. **9**(4): p. 357-9.
175. Li, B. and C.N. Dewey, *RSEM: accurate transcript quantification from RNA-Seq data with or without a reference genome.* BMC Bioinformatics, 2011. **12**(1): p. 323.
176. Ziazadeh, D., et al., *Single-dose del Nido Cardioplegia in Minimally Invasive Aortic Valve Surgery.* Semin Thorac Cardiovasc Surg, 2017.

177. Vistarini, N., et al., *Del Nido cardioplegia in the setting of minimally invasive aortic valve surgery.* Perfusion, 2017. **32**(2): p. 112-117.
178. An, K.R., et al., *A Systematic Review and Meta-Analysis of del Nido Versus Conventional Cardioplegia in Adult Cardiac Surgery.* Innovations (Phila), 2019. **14**(5): p. 385-393.
179. Li, Y., et al., *Del Nido Cardioplegia for Myocardial Protection in Adult Cardiac Surgery: A Systematic Review and Meta-Analysis.* ASAIO J, 2018. **64**(3): p. 360-367.
180. Reidy, M.R., et al., *Single-Dose del Nido Cardioplegia Compared With Standard Cardioplegia During Coronary Artery Bypass Grafting at a Veterans Affairs Hospital.* Tex Heart Inst J, 2021. **48**(1).
181. Ball, L., F. Costantino, and P. Pelosi, *Postoperative complications of patients undergoing cardiac surgery.* Curr Opin Crit Care, 2016. **22**(4): p. 386-92.
182. Peretto, G., et al., *Postoperative Arrhythmias after Cardiac Surgery: Incidence, Risk Factors, and Therapeutic Management.* Cardiology Research and Practice, 2014. **2014**: p. 615987.
183. Shu, C., et al., *Effect of Del Nido cardioplegia on ventricular arrhythmias after cardiovascular surgery.* BMC Cardiovasc Disord, 2021. **21**(1): p. 32.
184. Lin, X., et al., *The application of del Nido cardioplegia for myocardial protection in adult coronary artery bypass grafting: a cohort study.* J Thorac Dis, 2022. **14**(1): p. 177-184.
185. Ler, A., et al., *Comparison of outcomes of the use of Del Nido and St. Thomas cardioplegia in adult and paediatric cardiac surgery: a systematic review and meta-analysis.* Perfusion, 2020. **35**(8): p. 724-735.
186. Zhai, K., et al., *Del Nido cardioplegia for myocardial protection in adult cardiac surgery: a systematic review and update meta-analysis.* Perfusion, 2021: p. 2676591211031095.
187. Misra, S., et al., *Myocardial Protection in Adult Cardiac Surgery With del Nido Versus Blood Cardioplegia: A Systematic Review and Meta-Analysis.* Heart Lung Circ, 2021. **30**(5): p. 642-655.
188. Chan, J., et al., *Network meta-analysis comparing blood cardioplegia, Del Nido cardioplegia and custodiol cardioplegia in minimally invasive cardiac surgery.* Perfusion, 2022: p. 2676591221075522.
189. Yamamoto, F., M.V. Braimbridge, and D.J. Hearse, *Calcium and cardioplegia. The optimal calcium content for the St. Thomas' Hospital cardioplegic solution.* J Thorac Cardiovasc Surg, 1984. **87**(6): p. 908-12.
190. Takemoto, N., et al., *Effects of calcium in continuous cardioplegia on myocardial protection.* Surg Today, 1996. **26**(3): p. 179-83.
191. Nakamura, Y., et al., *The advantages of normocalcemic continuous warm cardioplegia over low calcemic cardioplegia in myocardial protection.* Surg Today, 1999. **29**(9): p. 884-9.
192. Cyran, S.E., et al., *Developmental differences in cardiac myocyte calcium homeostasis after steady-state potassium depolarization: mechanisms and implications for cardioplegia.* J Pediatr, 1993. **122**(6): p. S77-83.
193. Pridjian, A.K., et al., *Intracellular sodium and calcium in the postischemic myocardium.* Ann Thorac Surg, 1987. **43**(4): p. 416-9.
194. Jimenez, E., et al., *Effects of low extracellular calcium on cytosolic calcium and ischemic contracture.* J Surg Res, 1990. **49**(3): p. 252-5.

195. Jimenez, E., et al., *Redistribution of myocardial calcium during ischemia. Relationship to onset of contracture.* J Thorac Cardiovasc Surg, 1993. **105**(6): p. 988-94.
196. Rebeyka, I.M., et al., *Calcium paradox in an in vivo model of multidose cardioplegia and moderate hypothermia. Prevention with diltiazem or trace calcium levels.* J Thorac Cardiovasc Surg, 1990. **99**(3): p. 475-83.
197. Yamamoto, M., T.W. Kensler, and H. Motohashi, *The KEAP1-NRF2 System: a Thiol-Based Sensor-Effector Apparatus for Maintaining Redox Homeostasis.* Physiol Rev, 2018. **98**(3): p. 1169-1203.
198. Cuadrado, A., et al., *Therapeutic targeting of the NRF2 and KEAP1 partnership in chronic diseases.* Nat Rev Drug Discov, 2019. **18**(4): p. 295-317.
199. Baird, L. and M. Yamamoto, *The Molecular Mechanisms Regulating the KEAP1-NRF2 Pathway.* Mol Cell Biol, 2020. **40**(13).
200. Villeneuve, N.F., A. Lau, and D.D. Zhang, *Regulation of the Nrf2-Keap1 antioxidant response by the ubiquitin proteasome system: an insight into cullin-ring ubiquitin ligases.* Antioxid Redox Signal, 2010. **13**(11): p. 1699-712.
201. Goldman, S.G., H. Tao, and S.V. Jin, *Autophagy in White Adipose Tissue*, in *Adipose Tissue and Adipokines in Health and Disease*, G. Fantuzzi and C. Braunschweig, Editors. 2014, Humana Press: Totowa, NJ. p. 115-127.
202. Bootman, M.D., et al., *The regulation of autophagy by calcium signals: Do we have a consensus?* Cell Calcium, 2018. **70**: p. 32-46.
203. Pahwa, S., et al., *Impact of postoperative complications after cardiac surgery on long-term survival.* J Card Surg, 2021. **36**(6): p. 2045-2052.
204. Lazzarino, G., et al., *Myocardial release of malondialdehyde and purine compounds during coronary bypass surgery.* Circulation, 1994. **90**(1): p. 291-7.
205. Habertheuer, A., et al., *Cardioprotection: A Review of Current Practice in Global Ischemia and Future Translational Perspective.* BioMed Research International, 2014. **2014**: p. 325725.
206. Ji, M.J. and J.H. Hong, *A Cardioplegic Solution with an Understanding of a Cardiochannelopathy.* Antioxidants, 2021. **10**(12): p. 1878.
207. Francica, A., et al., *Cardioplegia between Evolution and Revolution: From Depolarized to Polarized Cardiac Arrest in Adult Cardiac Surgery.* Journal of Clinical Medicine, 2021. **10**(19): p. 4485.
208. Llosa, J.C., et al., *Celsior, a novel cardioplegic solution for arrest and storage in heart transplantation.* Transplant Proc, 2000. **32**(8): p. 2589-90.
209. Turer, A.T., *Using metabolomics to assess myocardial metabolism and energetics in heart failure.* Journal of Molecular and Cellular Cardiology, 2013. **55**: p. 12-18.
210. Liu, A., et al., *Quantitative bioanalysis of antibody-conjugated payload in monkey plasma using a hybrid immuno-capture LC–MS/MS approach: Assay development, validation, and a case study.* Journal of Chromatography B, 2015. **1002**: p. 54-62.
211. Zhu, C., et al., *Metabolomics of oxidative stress: Nrf2 independent depletion of NAD or increases of sugar alcohols.* Toxicology and Applied Pharmacology, 2022. **442**: p. 115949.
212. Zhu, C., et al., *Metabolomics of oxidative stress: Nrf2 independent depletion of NAD or increases of sugar alcohols.* Toxicol Appl Pharmacol, 2022. **442**: p. 115949.

213. Dai, W., et al., *Far Upstream Binding Protein 1 (FUBP1) participates in translational regulation of Nrf2 protein under oxidative stress.* Redox Biol, 2021. **41**: p. 101906.
214. Sies, H., *Hydrogen peroxide as a central redox signaling molecule in physiological oxidative stress: Oxidative eustress.* Redox Biology, 2017. **11**: p. 613-619.
215. Jacob, S., et al., *Is blood cardioplegia superior to crystalloid cardioplegia?* Interact Cardiovasc Thorac Surg, 2008. **7**(3): p. 491-8.
216. Ribeiro, R.V.P., et al., *Supplemental Cardioplegia During Donor Heart Implantation: A Systematic Review and Meta-Analysis.* Ann Thorac Surg, 2020. **110**(2): p. 545-552.
217. Karduz, G., et al., *St. Thomas and del Nido cardioplegia are superior to Custodiol cardioplegia in a rat model of donor heart.* Scand Cardiovasc J, 2021. **55**(2): p. 122-128.
218. Sharma, A., et al., *DelNido cardioplegia versus St Thomas cardioplegia solution in double valve replacement: a single centre experience.* Perfusion, 2021. **36**(5): p. 476-481.
219. Lenoir, M., et al., *Del Nido cardioplegia versus blood cardioplegia in adult aortic root surgery.* J Thorac Cardiovasc Surg, 2021. **162**(2): p. 514-522 e2.
220. Velez, D.A., et al., *All-blood (miniplegia) versus dilute cardioplegia in experimental surgical revascularization of evolving infarction.* Circulation, 2001. **104**(12 Suppl 1): p. I296-302.
221. Fang, Y., et al., *Blood versus crystalloid cardioplegia for pediatric cardiac surgery: a meta-analysis.* Perfusion, 2015. **30**(7): p. 529-36.
222. Carlucci, F., et al., *Cardiac surgery: myocardial energy balance, antioxidant status and endothelial function after ischemia–reperfusion.* Biomedicine & Pharmacotherapy, 2002. **56**(10): p. 483-491.
223. Nguyen, B.A., et al., *Metabolic derangement and cardiac injury early after reperfusion following intermittent cross-clamp fibrillation in patients undergoing coronary artery bypass graft surgery using conventional or miniaturized cardiopulmonary bypass.* Mol Cell Biochem, 2014. **395**(1-2): p. 167-75.
224. Maltesen, R.G., et al., *Metabotyping Patients' Journeys Reveals Early Predisposition to Lung Injury after Cardiac Surgery.* Sci Rep, 2017. **7**: p. 40275.
225. Galvez, A.S., et al., *Aldose reductase induced by hyperosmotic stress mediates cardiomyocyte apoptosis: differential effects of sorbitol and mannitol.* J Biol Chem, 2003. **278**(40): p. 38484-94.
226. Chiong, M., et al., *Parallel activation of Ca(2+)-induced survival and death pathways in cardiomyocytes by sorbitol-induced hyperosmotic stress.* Apoptosis, 2010. **15**(8): p. 887-903.
227. Son, N.H., et al., *Cardiomyocyte aldose reductase causes heart failure and impairs recovery from ischemia.* PLoS One, 2012. **7**(9): p. e46549.
228. Wu, J., et al., *Sources and implications of NADH/NAD(+) redox imbalance in diabetes and its complications.* Diabetes Metab Syndr Obes, 2016. **9**: p. 145-53.
229. Ojuka, E., et al., *Measurement of beta-oxidation capacity of biological samples by respirometry: a review of principles and substrates.* Am J Physiol Endocrinol Metab, 2016. **310**(9): p. E715-23.
230. Jaswal, J.S., et al., *Targeting fatty acid and carbohydrate oxidation--a novel therapeutic intervention in the ischemic and failing heart.* Biochim Biophys Acta, 2011. **1813**(7): p. 1333-50.

231. Aitken-Buck, H.M., et al., *Long-Chain Acylcarnitines and Cardiac Excitation-Contraction Coupling: Links to Arrhythmias.* Front Physiol, 2020. **11**: p. 577856.
232. Marsh, J.D. and T.S. Smith, *Calcium overload and ischemic myocardial injury.* Circulation, 1991. **83**(2): p. 709-11.
233. Kubrova, E., et al., *Differences in Cytotoxicity of Lidocaine, Ropivacaine, and Bupivacaine on the Viability and Metabolic Activity of Human Adipose-Derived Mesenchymal Stem Cells.* Am J Phys Med Rehabil, 2021. **100**(1): p. 82-91.
234. Nishimura, Y., et al., *Cytometric analysis of lidocaine-induced cytotoxicity: a model experiment using rat thymocytes.* Toxicology, 2006. **218**(1): p. 48-57.
235. Jin, H. and J. Yu, *Lidocaine protects H9c2 cells from hypoxia-induced injury through regulation of the MAPK/ERK/NF-κB signaling pathway.* Exp Ther Med, 2019. **18**(5): p. 4125-4131.
236. Kaczmarek, Dominik J., et al., *Lidocaine Protects from Myocardial Damage due to Ischemia and Reperfusion in Mice by Its Antiapoptotic Effects.* Anesthesiology, 2009. **110**(5): p. 1041-1049.
237. Canyon, S.J. and G.P. Dobson, *Protection against ventricular arrhythmias and cardiac death using adenosine and lidocaine during regional ischemia in the in vivo rat.* Am J Physiol Heart Circ Physiol, 2004. **287**(3): p. H1286-95.
238. Dias, R.R., et al., *Inclusion of lidocaine in cardioplegic solutions provides additional myocardial protection.* J Cardiovasc Surg (Torino), 2004. **45**(6): p. 551-5.
239. Lesnefsky, E.J., et al., *Lidocaine reduces canine infarct size and decreases release of a lipid peroxidation product.* J Cardiovasc Pharmacol, 1989. **13**(6): p. 895-901.
240. Lee, R., et al., *Retrograde infusion of lidocaine or L-arginine before reperfusion reduces myocardial infarct size.* Ann Thorac Surg, 1998. **65**(5): p. 1353-9.
241. STEFENELLI, T., et al., *Effects of propafenone on pacing-induced ventricular fibrillation and intracellular calcium in rat hearts.* European Heart Journal, 1992. **13**(11): p. 1556-1561.
242. Guo, J.-L., et al., *Transient Receptor Potential Melastatin 7 (TRPM7) Contributes to H2O2-Induced Cardiac Fibrosis via Mediating Ca2+ Influx and Extracellular Signal–Regulated Kinase 1/2 (ERK1/2) Activation in Cardiac Fibroblasts.* Journal of Pharmacological Sciences, 2014. **125**(2): p. 184-192.
243. Baron, D.W., M. Sunamori, and C.E. Harrison, *Preservation of Oxidative Phosphorylation by Lidocaine in Ischemic and Reperfused Myocardium*, in *Advances in Myocardiology: Volume 4*, E. Chazov, V. Saks, and G. Rona, Editors. 1983, Springer US: Boston, MA. p. 567-573.
244. Egar, J., et al., *The Na+/Ca2+ exchange inhibitor SEA0400 limits intracellular Ca2+ accumulation and improves recovery of ventricular function when added to cardioplegia.* J Cardiothorac Surg, 2014. **9**: p. 11.
245. Namekata, I., et al., *Reduction by SEA0400 of myocardial ischemia-induced cytoplasmic and mitochondrial Ca2+ overload.* Eur J Pharmacol, 2006. **543**(1-3): p. 108-15.
246. Antonio, C., et al., *Transcription Factor NRF2 as a Therapeutic Target for Chronic Diseases: A Systems Medicine Approach.* Pharmacological Reviews, 2018. **70**(2): p. 348.

247. Katsuoka, F., et al., *Genetic evidence that small maf proteins are essential for the activation of antioxidant response element-dependent genes.* Mol Cell Biol, 2005. **25**(18): p. 8044-51.
248. Homma, S., et al., *Nrf2 Enhances Cell Proliferation and Resistance to Anticancer Drugs in Human Lung Cancer.* Clinical Cancer Research, 2009. **15**(10): p. 3423-3432.
249. Shen, K., et al., *Exosomes from adipose-derived stem cells alleviate the inflammation and oxidative stress via regulating Nrf2/HO-1 axis in macrophages.* Free Radical Biology and Medicine, 2021. **165**: p. 54-66.
250. Zhang, J., et al., *La autoantigen mediates oxidant induced de novo Nrf2 protein translation.* Molecular & Cellular Proteomics, 2012. **11**(6).
251. Xu, B., et al., *Myocardial ischemic reperfusion induces de novo Nrf2 protein translation.* Biochimica et Biophysica Acta (BBA) - Molecular Basis of Disease, 2014. **1842**(9): p. 1638-1647.
252. Faye, M.D. and M. Holcik, *The role of IRES trans-acting factors in carcinogenesis.* Biochimica et Biophysica Acta (BBA) - Gene Regulatory Mechanisms, 2015. **1849**(7): p. 887-897.
253. Preiss, T. and W.H. M, *Starting the protein synthesis machine: eukaryotic translation initiation.* Bioessays, 2003. **25**(12): p. 1201-11.
254. Jackson, R.J., C.U.T. Hellen, and T.V. Pestova, *The mechanism of eukaryotic translation initiation and principles of its regulation.* Nature Reviews Molecular Cell Biology, 2010. **11**(2): p. 113-127.
255. Holcik, M., N. Sonenberg, and R.G. Korneluk, *Internal ribosome initiation of translation and the control of cell death.* Trends in Genetics, 2000. **16**(10): p. 469-473.
256. Spriggs, K.A., et al., *Internal ribosome entry segment-mediated translation during apoptosis: the role of IRES-trans-acting factors.* Cell Death & Differentiation, 2005. **12**(6): p. 585-591.
257. Hazra, D., C. Chapat, and M. Graille, *m6A mRNA Destiny: Chained to the rhYTHm by the YTH-Containing Proteins.* Genes, 2019. **10**(1): p. 49.
258. Du, H., et al., *YTHDF2 destabilizes m6A-containing RNA through direct recruitment of the CCR4–NOT deadenylase complex.* Nature Communications, 2016. **7**(1): p. 12626.
259. Fu, Y., et al., *Gene expression regulation mediated through reversible m6A RNA methylation.* Nature Reviews Genetics, 2014. **15**(5): p. 293-306.
260. Wang, X., et al., *N6-methyladenosine-dependent regulation of messenger RNA stability.* Nature, 2014. **505**(7481): p. 117-120.
261. Zhou, J., et al., *Dynamic m6A mRNA methylation directs translational control of heat shock response.* Nature, 2015. **526**(7574): p. 591-594.
262. Batista, Pedro J., et al., *m6A RNA Modification Controls Cell Fate Transition in Mammalian Embryonic Stem Cells.* Cell Stem Cell, 2014. **15**(6): p. 707-719.
263. Zaccara, S., R.J. Ries, and S.R. Jaffrey, *Reading, writing and erasing mRNA methylation.* Nature Reviews Molecular Cell Biology, 2019. **20**(10): p. 608-624.
264. Ianniello, Z., A. Paiardini, and A. Fatica, *N(6)-Methyladenosine (m(6)A): A Promising New Molecular Target in Acute Myeloid Leukemia.* Front Oncol, 2019. **9**: p. 251.
265. Yue, Y., et al., *VIRMA mediates preferential m(6)A mRNA methylation in 3'UTR and near stop codon and associates with alternative polyadenylation.* Cell Discov, 2018. **4**: p. 10.

266. Huang, H., H. Weng, and J. Chen, *m(6)A Modification in Coding and Non-coding RNAs: Roles and Therapeutic Implications in Cancer.* Cancer Cell, 2020. **37**(3): p. 270-288.
267. Patil, D.P., et al., *m(6)A RNA methylation promotes XIST-mediated transcriptional repression.* Nature, 2016. **537**(7620): p. 369-373.
268. Shi, H., et al., *YTHDF3 facilitates translation and decay of N(6)-methyladenosine-modified RNA.* Cell Res, 2017. **27**(3): p. 315-328.
269. Purdom-Dickinson, S.E., et al., *Translational control of nrf2 protein in activation of antioxidant response by oxidants.* Mol Pharmacol, 2007. **72**(4): p. 1074-81.
270. Montero, H., R. García-Román, and S.I. Mora, *eIF4E as a Control Target for Viruses.* Viruses, 2015. **7**(2): p. 739-750.
271. Zhu, T., et al., *Crystal structure of the YTH domain of YTHDF2 reveals mechanism for recognition of N6-methyladenosine.* Cell Research, 2014. **24**(12): p. 1493-1496.
272. Liu, Z.X., et al., *Link Between m6A Modification and Cancers.* Front Bioeng Biotechnol, 2018. **6**: p. 89.
273. Zhou, B., et al., *N(6) -Methyladenosine Reader Protein YT521-B Homology Domain-Containing 2 Suppresses Liver Steatosis by Regulation of mRNA Stability of Lipogenic Genes.* Hepatology, 2021. **73**(1): p. 91-103.
274. Meyer, Kate D., et al., *Comprehensive Analysis of mRNA Methylation Reveals Enrichment in 3′ UTRs and near Stop Codons.* Cell, 2012. **149**(7): p. 1635-1646.
275. Zhou, J., K.A. Rode, and S.B. Qian, *m(6)A: A novel hallmark of translation.* Cell Cycle, 2016. **15**(3): p. 309-10.
276. Coots, R.A., et al., *m6A Facilitates eIF4F-Independent mRNA Translation.* Molecular Cell, 2017. **68**(3): p. 504-514.e7.
277. Zhou, J., et al., *N6-Methyladenosine Guides mRNA Alternative Translation during Integrated Stress Response.* Molecular Cell, 2018. **69**(4): p. 636-647.e7.
278. Tanabe, A., et al., *RNA helicase YTHDC2 promotes cancer metastasis via the enhancement of the efficiency by which HIF-1α mRNA is translated.* Cancer Letters, 2016. **376**(1): p. 34-42.
279. Liu, N. and T. Pan, *N6-methyladenosine–encoded epitranscriptomics.* Nature Structural & Molecular Biology, 2016. **23**(2): p. 98-102.
280. Rizvi, M.F.A., et al., *Prospective randomized study comparing outcome of myocardial protection with Del-Nido Cardioplegia versus Saint Thomas Cardioplegia in adult cardiac surgical patients.* Pak J Med Sci, 2022. **38**(3Part-I): p. 699-704.